nature portfolio

https://doi.org/10.1038/s41593-022-01042-4

Supplementary information

Genetic variants associated with longitudinal changes in brain structure across the lifespan

In the format provided by the authors and unedited

Supplementary Note and Supplementary Figures associated with *"Genetic variants associated with longitudinal changes in brain structure across the lifespan"* by Brouwer et al., 2022

Correction for intracranial volume

It is common practice in studies of (cross-sectional) brain volumes to correct for intracranial volume or total brain volume: either to be sure that the differences that are found are region specific and not caused by a difference in overall brain size, or to be able to distinguish developmental effects (maximal brain size, approximated by the intracranial volume) from effects that occur later in life. When considering longitudinal changes over time, the choice of whether one has to correct translates into the question whether one wants to investigate absolute change (in e.g. ml/year, no correction) versus relative change (in %/year, correcting for baseline volume). However, neither total brain volume nor intracranial volume[95] are stable across the lifespan, which complicates interpretation when these are used as correction factors[96], especially when one combines data from across the lifespan. Therefore, we chose not to include overall brain volume in our main GWAS.

As a post-hoc analysis, we assessed the influence of adding intracranial volume to our analysis in the replication cohorts. To this end, we calculated relative annual change by subtracting baseline volume from follow-up volume, and dividing by follow-up duration in years times intracranial volume at baseline. We excluded the phenotypes mean cortical thickness and total surface area from these analyses, since these are global measures themselves and a one- or two- dimensional brain measure should not be corrected by a three-dimensional volume. The association between relative and absolute annual change was very high in all three cohorts (all correlations > 0.97), which can be explained by intracranial volume having a much lower standard deviation compared to the mean than annual rates of change. This implies that applying a correction for ICV to annual rates of change is approximately a scaling factor which should not influence the GWAS findings. As expected, the effect estimates and p-values from the GWAS for relative and absolute annual change were also highly correlated (> 0.96; Supplementary Figure 8).

Potential scanner effects

Combining imaging data from multiple sources could be subject to biases driven by the scanner manufacturer of scanning sequence, which could be a problem if data included in the study is not well distributed across different acquisitions with respect to the contrast of interest. Different approaches for pooling of imaging data have been proposed, including pre-acquisition harmonization of protocols, or post-acquisition methods (e.g. COMBAT[97]). The latter requires access to individual data which was not feasible for our study. However, through our design of meta-analysis of rates of change, several potential scanner effects are already accounted for. First, we would like to mention that all results are based on the effect of a genetic variant *within a cohort* and the mean of a change rate in a cohort is therefore not influencing our genetic findings. That is, a potential within-cohort offset between baseline and follow-up measurement does influence the average change rate, but not the GWAS output, as the latter is essentially based on the ranking between subjects.
We further argue that potential additive and multiplicative scanner effects (as are assumed in COMBAT) will not bias our meta-analytic findings: additive scanner effects (an offset) is already accounted by computation of the annual rate of change, since there we subtract the follow-up from the baseline volume. Any multiplicative factors would not influence the Z-

scores (or p-values) within a cohort as those are present in both the SNP-effect and the associated standard error. This implies that a potential scanner effect will only affect the weights in our meta-analyses, and this will not change the null distribution. Therefore, if anything, potential scanner effects will introduce noise, but should not introduce bias.

For our top-findings, we ran simulation analyses incorporating potential multiplicative scanner effects which indeed show that our main findings are robust to relatively large perturbations: we assumed a multiplicative effect on the beta-SNP estimates for each cohort/scanner, by simulating a multiplicative factor from a standard normal distribution with mean 1 and a standard deviation ranging from 0.01 to 0.05. This multiplication factor should be interpreted as a deviation from the true volume, i.e. a factor of 0.95 suggests that brain volume is underestimated in all subjects (more so for larger brains than for smaller brains in absolute terms). Hence, also the change rate and associated SNP-beta obtained from GWAS is underestimated. The upper bound of 0.05 corresponds to the extreme case where relatively large perturbations occur regularly (in 5% of cases, the error will be larger than 10% of the volume). After simulating the multiplication factor for each cohort, we multiplied mean and standard error by this factor and repeated the meta-analysis or meta-regression 1000 times. This analysis was done for all our genome-wide significant findings. Supplementary Figure 9 shows the percentage of cases where the top-findings were still significant, as a function of the variation of simulated multiplicative scanner effects. Power to detect our findings was generally high, indicating that our findings are robust under such modest perturbations.

References (Supplementary Note and Supplementary Figures)

95. Caspi, Y. *et al.* Changes in the intracranial volume from early adulthood to the sixth decade of life: A longitudinal study. *NeuroImage* **220**, 116842 (2020).

96. Mills, K. L. & Tamnes, C. K. Methods and considerations for longitudinal structural brain imaging analysis across development. *Dev. Cogn. Neurosci.* **9**, 172–190 (2014).

97. Beer, J. C. *et al.* Longitudinal ComBat: A method for harmonizing longitudinal multi-scanner imaging data. *NeuroImage* **220**, (2020).

98. Pruim, R. J. *et al.* LocusZoom: Regional visualization of genome-wide association scan results. *Bioinformatics* **27**, 2336–2337 (2011).

Consortium information and authors

ADNI: Data used in the preparation of this article were obtained from the Alzheimer's Disease Neuroimaging Initiative (ADNI) database (adni.loni.usc.edu). The ADNI was launched in 2003 as a public-private partnership, led by Principal Investigator Michael W. Weiner, MD.
ADNI Infrastructure Investigators: Michael Weiner (UC San Francisco), Paul Aisen (University of Southern California), Ronald Petersen (Mayo Clinic, Rochester), Clifford R. Jack, Jr. (Mayo Clinic, Rochester), William Jagust (UC Berkeley), John Q. Trojanowki (U Pennsylvania), Arthur W. Toga (USC), Laurel Beckett (UC), Davis Robert C. Green (Brigham and Women's Hospital/Harvard Medical School), Andrew J. Saykin (Indiana University), John Morris (Washington University St. Louis), Leslie M. Shaw (University of Pennsylvania). ADNI External Advisory Board (ESAB): Zaven Khachaturian (Prevent Alzheimer's Disease 2020 (Chair)), Greg Sorensen (Siemens), Maria Carrillo (Alzheimer's Association), Lew Kuller (University of Pittsburgh), Marc Raichle (Washington University St. Louis), Steven Paul (Cornell University), Peter Davies (Albert Einstein College of Medicine of Yeshiva University), Howard Fillit (AD Drug Discovery Foundation), Franz Hefti (Acumen Pharmaceuticals), David Holtzman (Washington University St. Louis), M. Marcel Mesulam (Northwestern University), William Potter (National Institute of Mental Health), Peter Snyder (Brown University). ADNI 3 Private Partner Scientific Board (PPSB): Veronika Logovinsky, (Eli Lilly (Chair)). Data and Publications Committee: Robert C. Green (BWH/HMS (Chair)). Resource Allocation Review Committee: Tom Montine (University of Washington (Chair)). Clinical Core Leaders: Ronald Petersen (Mayo Clinic, Rochester (Core PI)), Paul Aisen (University of Southern California). Clinical Informatics and Operations: Gustavo Jimenez (USC), Michael Donohue (USC), Devon Gessert (USC), Kelly Harless (USC), Jennifer Salazar (USC), Yuliana Cabrera (USC), Sarah Walter (USC), Lindsey Hergesheimer (USC). Biostatistics Core Leaders and Key Personnel: Laurel Beckett (UC Davis (Core PI)), Danielle Harvey (UC Davis), Michael Donohue (UC San Diego). MRI Core Leaders and Key Personnel: Clifford R. Jack, Jr. (Mayo Clinic, Rochester (Core PI)), Matthew Bernstein (Mayo Clinic, Rochester), Nick Fox (University of London), Paul Thompson (UCLA School of Medicine), Norbert Schuff (UCSF MRI), Charles DeCarli (UC Davis), Bret Borowski (RT Mayo Clinic), Jeff Gunter (Mayo Clinic), Matt Senjem (Mayo Clinic), Prashanthi Vemuri (Mayo Clinic), David Jones (Mayo Clinic), Kejal Kantarci (Mayo Clinic), Chad Ward (Mayo Clinic). PET Core Leaders and Key Personnel: William Jagust (UC Berkeley (Core PI)), Robert A. Koeppe (University of Michigan), Norm Foster (University of Utah), Eric M. Reiman (Banner Alzheimer's Institute), Kewei Chen (Banner Alzheimer's Institute), Chet Mathis (University of Pittsburgh), Susan Landau (UC Berkeley). Neuropathology Core Leaders: John C. Morris (Washington University St. Louis), Nigel J. Cairns (Washington University St. Louis), Erin Franklin (Washington University St. Louis), Lisa Taylor-Reinwald (Washington University St. Louis – Past Investigator). Biomarkers Core Leaders and Key Personnel: Leslie M. Shaw (UPenn School of Medicine), John Q. Trojanowki (UPenn School of Medicine), Virginia Lee (UPenn School of Medicine), Magdalena Korecka (UPenn School of Medicine), Michal Figurski (UPenn School of Medicine). Informatics Core Leaders and Key Personnel: Arthur W. Toga (USC (Core PI)), Karen Crawford (USC), Scott Neu (USC). Genetics Core Leaders and Key Personnel: Andrew J. Saykin (Indiana University), Tatiana M. Foroud (Indiana University), Steven Potkin (UC Irvine), Li Shen (Indiana University), Kelley Faber (Indiana University), Sungeun Kim (Indiana University), Kwangsik Nho (Indiana University). Initial Concept Planning & Development: Michael W. Weiner (UC San Francisco), Leon Thal (UC San Diego), Zaven Khachaturian (Prevent Alzheimer's Disease 2020). Early Project Proposal

Development: Leon Thal (UC San Diego), Neil Buckholtz (National Institute on Aging), Michael W. Weiner (UC San Francisco), Peter J. Snyder (Brown University), William Potter (National Institute of Mental Health), Steven Paul (Cornell University), Marilyn Albert (Johns Hopkins University), Richard Frank (Richard Frank Consulting), Zaven Khachaturian (Prevent Alzheimer's Disease 2020). NIA: John Hsiao (National Institute on Aging). ADNI Investigators by Site: Oregon Health & Science University: Joseph Quinn, Lisa C. Silbert, Betty Lind, Jeffrey A. Kaye – Past Investigator, Raina Carter – Past Investigator, Sara Dolen – Past Investigator. University of Southern California: Lon S. Schneider, Sonia Pawluczyk, Mauricio Becerra, Liberty Teodoro, Bryan M. Spann – Past Investigator. University of California – San Diego: James Brewer, Helen Vanderswag, Adam Fleisher – Past Investigator. University of Michigan: Jaimie Ziolkowski, Judith L. Heidebrink, Joanne L. Lord – Past Investigator. Mayo Clinic, Rochester: Ronald Petersen, Sara S. Mason, Colleen S. Albers, David Knopman, Kris Johnson – Past Investigator. Baylor College of Medicine: Javier Villanueva-Meyer, Valory Pavlik, Nathaniel Pacini, Ashley Lamb, Joseph S. Kass, Rachelle S. Doody – Past Investigator, Victoria Shibley – Past Investigator, Munir Chowdhury – Past Investigator, Susan Rountree – Past Investigator, Mimi Dang – Past Investigator. Columbia University Medical Center: Yaakov Stern, Lawrence S. Honig, Karen L. Bell, Randy Yeh. Washington University, St. Louis: Beau Ances, John C. Morris, David Winkfield, Maria Carroll, Angela Oliver, Mary L. Creech – Past Investigator, Mark A. Mintun – Past Investigator, Stacy Schneider – Past Investigator. University of Alabama - Birmingham: Daniel Marson, David Geldmacher, Marissa Natelson Love, Randall Griffith – Past Investigator, David Clark – Past Investigator, John Brockington – Past Investigator. Mount Sinai School of Medicine: Hillel Grossman, Effie Mitsis – Past Investigator. Rush University Medical Center: Raj C. Shah, Melissa Lamar, Patricia Samuels. Wien Center: Ranjan Duara, Maria T. Greig-Custo, Rosemarie Rodriguez. Johns Hopkins University: Marilyn Albert, Chiadi Onyike, Daniel D'Agostino II, Stephanie Kielb – Past Investigator. New York University: Martin Sadowski, Mohammed O. Sheikh, Jamika Singleton-Garvin, Anaztasia Ulysse, Mrunalini Gaikwad. Duke University Medical Center: P. Murali Doraiswamy, Jeffrey R. Petrella, Olga James, Salvador Borges-Neto, Terence Z. Wong – Past Investigator, Edward Coleman – Past Investigator. University of Pennsylvania: Jason H. Karlawish, David A. Wolk, Sanjeev Vaishnavi, Christopher M. Clark – Past Investigator, Steven E. Arnold – Past Investigator. University of Kentucky: Charles D. Smith, Greg Jicha, Peter Hardy, Riham El Khouli, Elizabeth Oates, Gary Conrad. University of Pittsburgh: Oscar L. Lopez, MaryAnn Oakley, Donna M. Simpson. University of Rochester Medical Center: Anton P. Porsteinsson, Kim Martin, Nancy Kowalksi, Melanie Keltz, Bonnie S. Goldstein – Past Investigator, Kelly M. Makino – Past Investigator, M. Saleem Ismail – Past Investigator, Connie Brand – Past Investigator. University of California Irvine IMIND: Gaby Thai, Aimee Pierce, Beatriz Yanez, Elizabeth Sosa, Megan Witbracht. University of Texas Southwestern Medical School: Kyle Womack, Dana Mathews, Mary Quiceno. Emory University: Allan I. Levey, James J. Lah, Janet S. Cellar. University of Kansas, Medical Center: Jeffrey M. Burns, Russell H. Swerdlow, William M. Brooks. University of California, Los Angeles: Ellen Woo, Daniel H.S. Silverman, Edmond Teng, Sarah Kremen, Liana Apostolova – Past Investigator, Kathleen Tingus – Past Investigator, Po H. Lu – Past Investigator, George Bartzokis – Past Investigator. Mayo Clinic, Jacksonville: Neill R Graff-Radford (London), Francine Parfitt, Kim Poki-Walker. Indiana University: Martin R. Farlow, Ann Marie Hake, Brandy R. Matthews – Past Investigator, Jared R. Brosch, Scott Herring. Yale University School of Medicine: Christopher H. van Dyck, Richard E. Carson, Pradeep Varma. McGill Univ., Montreal-Jewish General Hospital: Howard Chertkow, Howard Bergman, Chris Hosein. Sunnybrook Health Sciences, Ontario: Sandra Black, Bojana Stefanovic, Chris (Chinthaka) Heyn. U.B.C. Clinic for AD & Related Disorders: Ging-Yuek

Robin Hsiung, Benita Mudge, Vesna Sossi, Howard Feldman – Past Investigator, Michele Assaly – Past Investigator. Cognitive Neurology - St. Joseph's, Ontario: Elizabeth Finger, Stephen Pasternak, William Pavlosky, Irina Rachinsky – Past Investigator, Dick Drost – Past Investigator, Andrew Kertesz – Past Investigator. Cleveland Clinic Lou Ruvo Center for Brain Health: Charles Bernick, Donna Muni. Northwestern University: Marek-Marsel Mesulam, Emily Rogalski, Kristine Lipowski, Sandra Weintraub, Borna Bonakdarpour, Diana Kerwin – Past Investigator, Chuang-Kuo Wu – Past Investigator, Nancy Johnson – Past Investigator. Premiere Research Inst (Palm Beach Neurology): Carl Sadowsky, Teresa Villena. Georgetown University Medical Center: Raymond Scott Turner, Kathleen Johnson, Brigid Reynolds. Brigham and Women's Hospital: Reisa A. Sperling, Keith A. Johnson, Gad A. Marshall. Stanford University: Jerome Yesavage, Joy L. Taylor, Steven Chao, Barton Lane – Past Investigator, Allyson Rosen – Past Investigator, Jared Tinklenberg – Past Investigator. Banner Sun Health Research Institute: Edward Zamrini, Christine M. Belden, Sherye A. Sirrel. Boston University: Neil Kowall, Ronald Killiany, Andrew E. Budson, Alexander Norbash – Past Investigator, Patricia Lynn Johnson – Past Investigator. Howard University: Thomas O. Obisesan, Ntekim E. Oyonumo, Joanne Allard, Olu Ogunlana. Case Western Reserve University: Alan Lerner, Paula Ogrocki, Curtis Tatsuoka, Parianne Fatica. University of California, Davis – Sacramento: Evan Fletcher, Pauline Maillard, John Olichney, Charles DeCarli, Owen Carmichael – Past Investigator. Neurological Care of CNY: Smita Kittur – Past Investigator. Parkwood Institute: Michael Borrie, T-Y Lee, Dr Rob Bartha. University of Wisconsin: Sterling Johnson, Sanjay Asthana, Cynthia M. Carlsson. Banner Alzheimer's Institute: Pierre Tariot, Anna Burke, Joel Hetelle, Kathryn DeMarco, Nadira Trncic – Past Investigator, Adam Fleisher – Past Investigator, Stephanie Reeder – Past Investigator. Dent Neurologic Institute: Vernice Bates, Horacio Capote, Michelle Rainka. Ohio State University: Douglas W. Scharre, Maria Kataki, Rawan Tarawneh. Albany Medical College: Earl A. Zimmerman, Dzintra Celmins, David Hart. Hartford Hospital, Olin Neuropsychiatry Research Center: Godfrey D. Pearlson, Karen Blank, Karen Anderson. Dartmouth-Hitchcock Medical Center: Laura A. Flashman, Marc Seltzer, Mary L. Hynes, Robert B. Santulli – Past Investigator. Wake Forest University Health Sciences: Kaycee M. Sink, Mia Yang, Akiva Mintz. Rhode Island Hospital: Brian R. Ott, Geoffrey Tremont, Lori A. Daiello. Butler Hospital: Courtney Bodge, Stephen Salloway, Paul Malloy, Stephen Correia, Athena Lee. UC San Francisco: Howard J. Rosen, Bruce L. Miller, David Perry. Medical University South Carolina: Jacobo Mintzer, Kenneth Spicer, David Bachman. St. Joseph's Health Care: Elizabeth Finger, Stephen Pasternak, Irina Rachinsky, John Rogers, Andrew Kertesz – Past Investigator, Dick Drost – Past Investigator. Nathan Kline Institute: Nunzio Pomara, Raymundo Hernando, Antero Sarrael. University of Iowa College of Medicine: Delwyn D. Miller, Karen Ekstam Smith, Hristina Koleva, Ki Won Nam, Hyungsub Shim, Susan K. Schultz – Past Investigator. Cornell University: Norman Relkin, Gloria Chiang, Michael Lin, Lisa Ravdin. University of South Florida: USF Health Byrd Alzheimer's Institute: Amanda Smith, Christi Leach, Balebail Ashok Raj – Past Investigator, Kristin Fargher – Past Investigator.

IMAGEN: Cambridge University: Trevor Robbins, Jeffrey Dalley, Naresh Subramaniam, David Theobald. Central Institute of Mental Health: Karl Mann, Christiane Bach,Maren Struve, Tobias Banaschewski, Herta Flor, Marcella Rietschel, Rainer Spanagel, Frauke Nees, Mira Fauth-Bühler, Sabina Millenet, Yvonne Grimmer. Central Institute of Mental Health/Medical University of Vienna,Luise Poustka. Centre National de Génotypage,Mark Lathrop. Charité,Andreas Heinz, Lisa Albrecht, Nikolay Ivanov, Nicole Strache, Michael Rapp, Andreas Ströhle , Jan Reuter, Jürgen Gallinat, Henrik Walter, Isabel Gemmeke,

Alexander Genauck, Caroline Parchetka, Katharina Weiß, Johann Kruschwitz, Bianca Raffaelli, Alev Isci, Laura Daedelow. Comissariat à l'Energie Atomique: Alexis Barbot, Benjamin Thyreau, Yannick Schwartz , Christophe Lalanne , Vincent Frouin , Dimitri Papadopoulos Orfanos, Antoine Grigis. Delosis: John Rogers, James Ireland. Deutsches Referenzzentrum für Ethik: Dirk Lanzerath. Fudan University/Warwick University: Jianfeng Feng. INSERM: Jean-Luc Martinot, Zuleima Bricaud, Fanny Gollier Briand, Herve Lemaitre, Ruben Miranda,Eric Artiges, Jessica Massicotte, Marie- Laure Paillère Martinot, Helene Vulser, Jani Pentillä, Irina Filippi, André Galinowski, Pauline Bezivin. IoP: Gunter Schumann, Anna Cattrell, Sylvane Desrivières, Tianye Jia, Helen Werts, Lauren Topper, Laurence Reed, Chris Andrew, Catherine Mallik, Barbara Ruggeri, Charlotte Nymberg, Gareth Barker, Patricia J Conrod, Lindsay Smith, Eva Loth, Stephanie Havatzias , Sheyda Shekarrizi , Emily Kitson, Alice Robinson, Deborah Hall, Chiara Rubino, Hannah Wright, Kerstin Stueber, Eanna Hanratty, Eleanor Kennedy, Fabiana Mesquita de Carvahlo, Argyris Stringaris, Gabriel Robert, Alex Ing, Christine Macare, Bing Xu,Tao Yu, Erin Burke Quinlan. PERTIMM: Patrick Constant. PTB: Semiha Aydin, Ruediger Brühl, Albrecht Ihlenfeld, Bernadeta Walaszek, Bernd Ittermann. Technische Universität Dresden: Michael Smolka, Thomas Hübner, Kathrin Müller, Stephan Ripke, Sarah Jurk, Eva Mennigen, Dirk Schmidt, Nora Vetter, Veronika Ziesch, Juliane H. Froehner. Trinity College Dublin: Hugh Garavan, Arun Bokde, Robert Whelan, Daniel Carter, Emily Walsh, Susanne O'Driscoll, Maria Leonora Fatimah Agan, Mairead McMorrow, Sinead Nugent, Colm Connolly, Eoin Dooley, Clodagh Cremen. University College Dublin: Jennifer Jones, John O'Keefe, Martin O'Connor. McGill University; University of California, Berkeley: Jean-Baptiste Poline. University of Hamburg: Christian Büchel, Uli Bromberg, Tahmine Fadai, Juliana Yacubian, Sophia Schneider, Maria Lobatchewa. University of Nottingham: Claire Lawrence, Craig Newman, Kay Head, Nadja Heym, Penny Gowland, Alicia Stedman, Mehri Kaviani, Susannah Taplin. University of Sussex: Dai Stephens. University of Toronto: Tomáš Paus, Zdenka Pausova, Amir Tahmasebi

List of Supplementary Figures:

1A: change rate amygdala volume

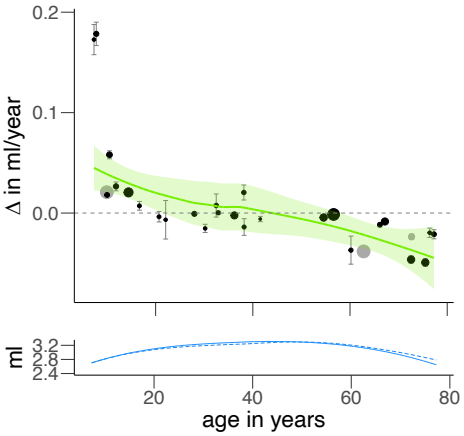

age independent

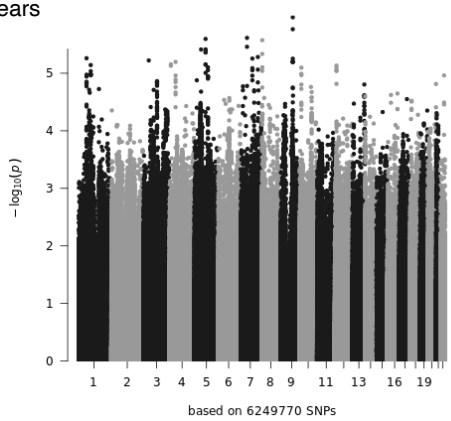

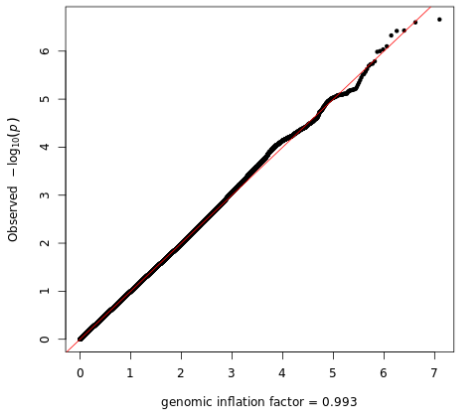

linear age-dependent

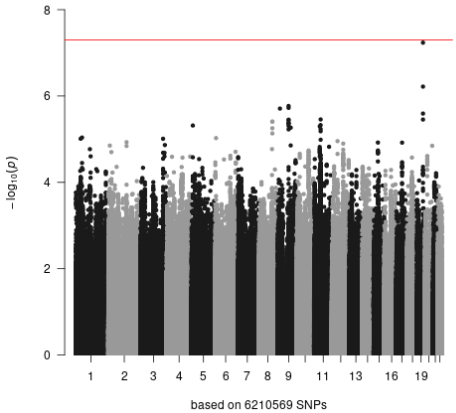

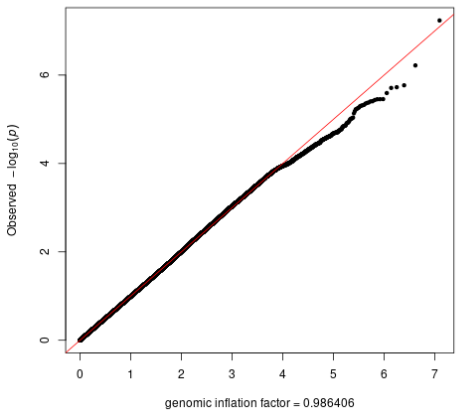

quadratic age-dependent

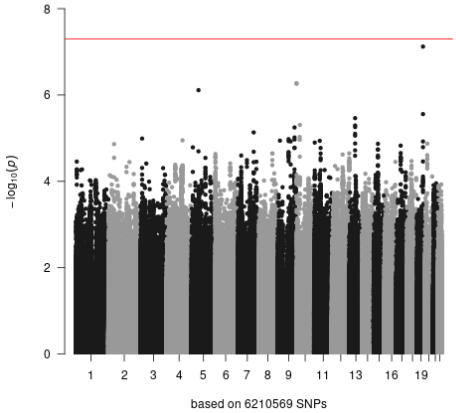

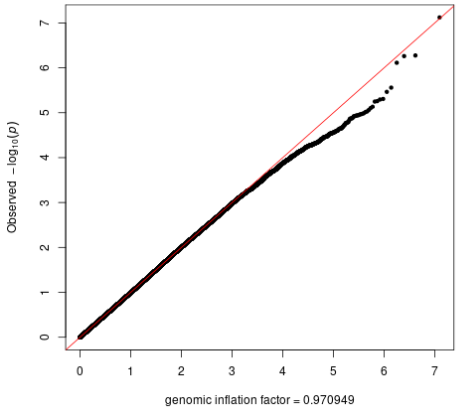

Supplementary Figure 1A: change rate amygdala volume. Top: Change rates per cohort and estimated trajectories of the change rate with confidence intervals (in green) are displayed above. Mean values of individual cohorts are displayed as points, with error bars representing standard errors displayed in grey. The size of the points represents the relative size of the cohorts, total sample size N=15640. Cohorts that were added in phase 2 are displayed in grey. Only cohorts that satisfy N>75 are shown. The estimated trajectories of the volumes themselves are displayed below, for all subjects (solid line) and healthy subjects only (dashed line). Bottom rows contain Manhattan plots and QQ-plots for age-independent, age linear and age quadratic GWASs for rate of change.

1B: change rate caudate volume

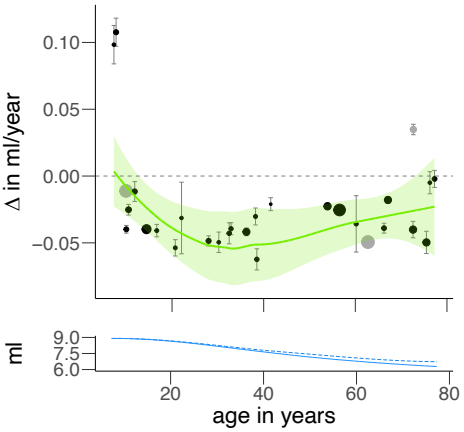

age independent

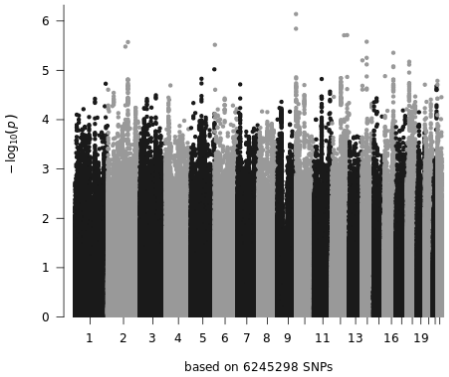

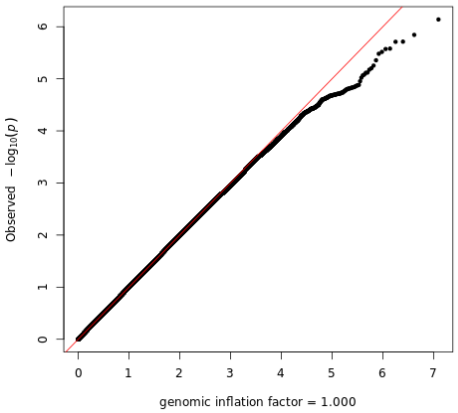

linear age-dependent

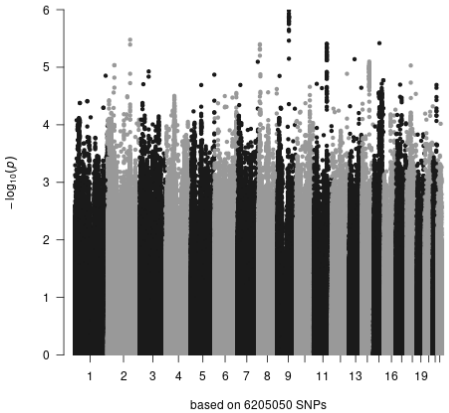

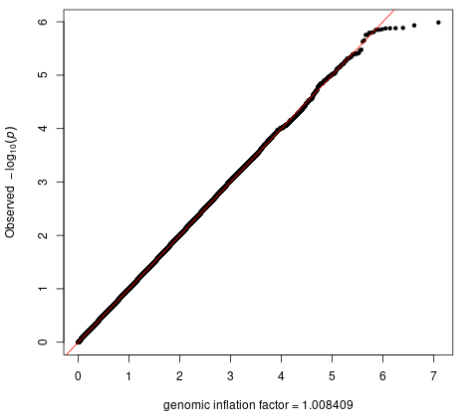

quadratic age-dependent

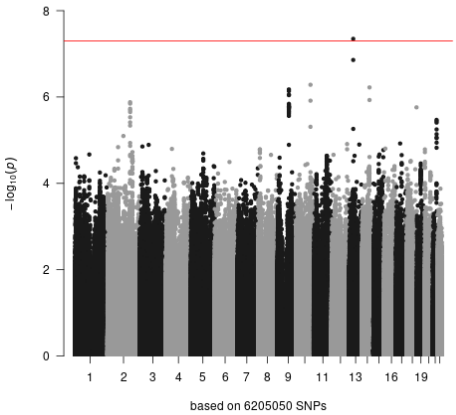

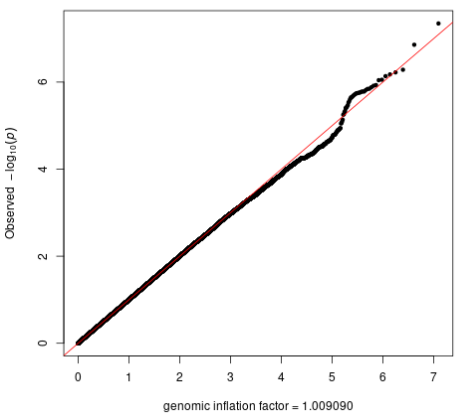

Supplementary Figure 1B: change rate caudate volume.Top: Change rates per cohort and estimated trajectories of the change rate with confidence intervals (in green) are displayed above. Mean values of individual cohorts are displayed as points, with error bars representing standard errors displayed in grey. The size of the points represents the relative size of the cohorts, total sample size N=15640. Cohorts that were added in phase 2 are displayed in grey. Only cohorts that satisfy N>75 are shown. The estimated trajectories of the volumes themselves are displayed below, for all subjects (solid line) and healthy subjects only (dashed line). Bottom rows contain Manhattan plots and QQ-plots for age-independent, age linear and age quadratic GWASs for rate of change.

1C: change rate cerebellum white matter volume

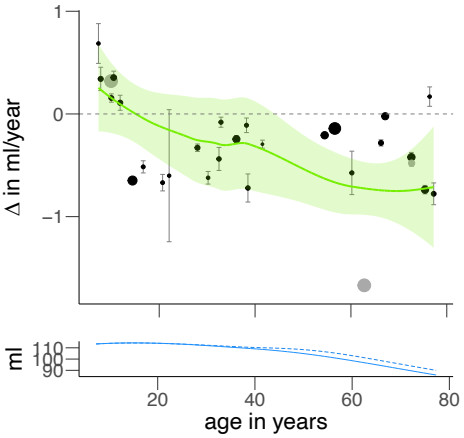

age independent

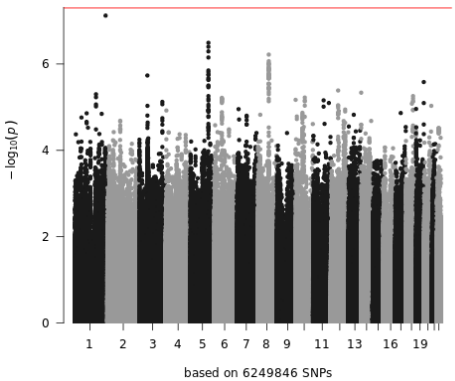

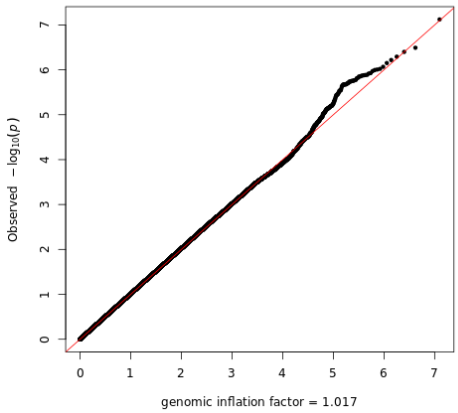

linear age-dependent

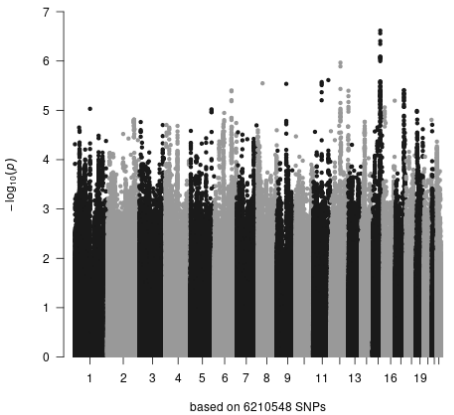

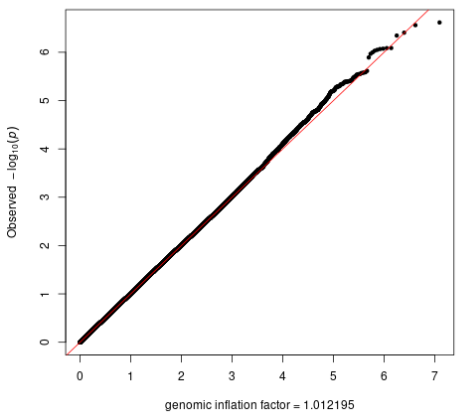

quadratic age-dependent

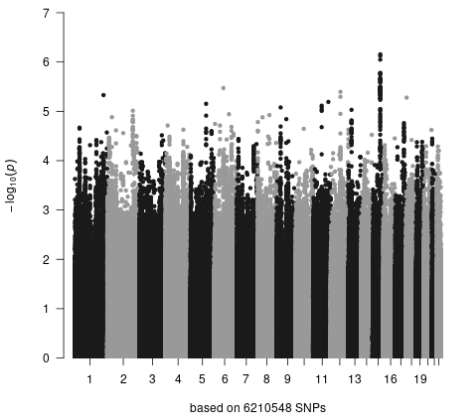

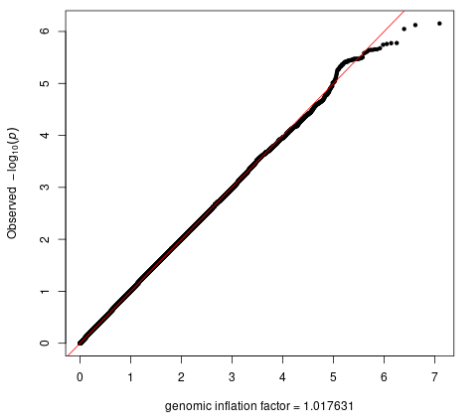

Supplementary Figure 1C: change rate cerebellum white matter volume.Top: Change rates per cohort and estimated trajectories of the change rate with confidence intervals (in green) are displayed above. Mean values of individual cohorts are displayed as points, with error bars representing standard errors displayed in grey. The size of the points represents the relative size of the cohorts, total sample size N=15640. Cohorts that were added in phase 2 are displayed in grey. Only cohorts that satisfy N>75 are shown. The estimated trajectories of the volumes themselves are displayed below, for all subjects (solid line) and healthy subjects only (dashed line). Bottom rows contain Manhattan plots and QQ-plots for age-independent, age linear and age quadratic GWASs for rate of change.

1D: change rate cerebellum gray matter volume

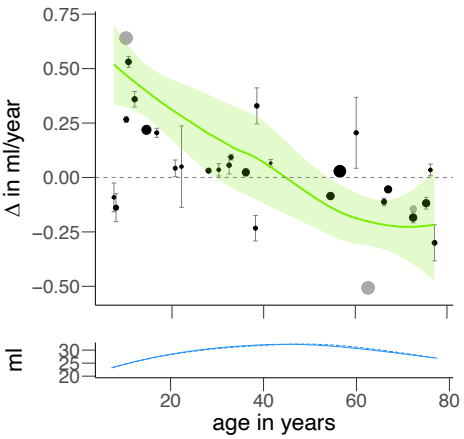

age independent

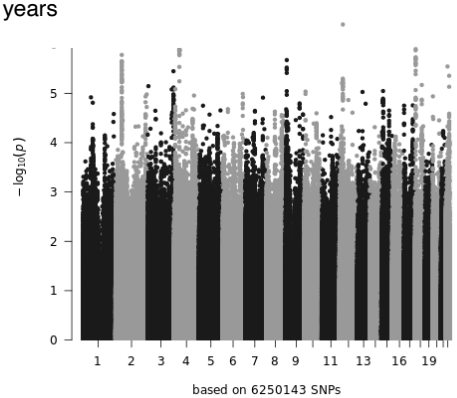

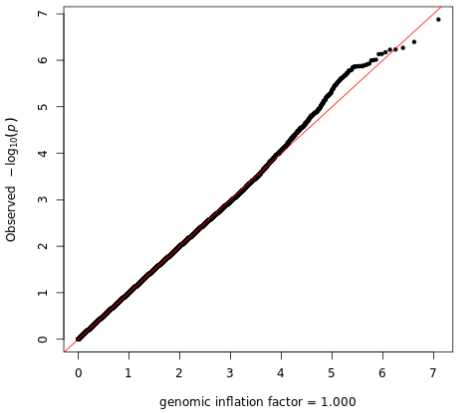

linear age-dependent

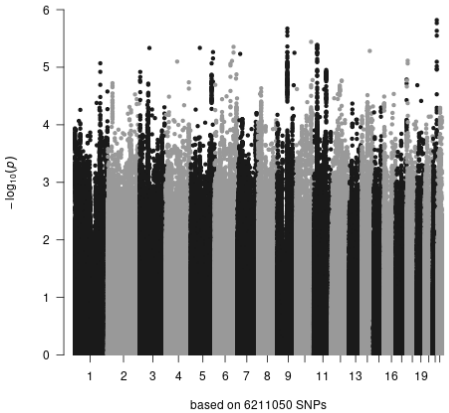

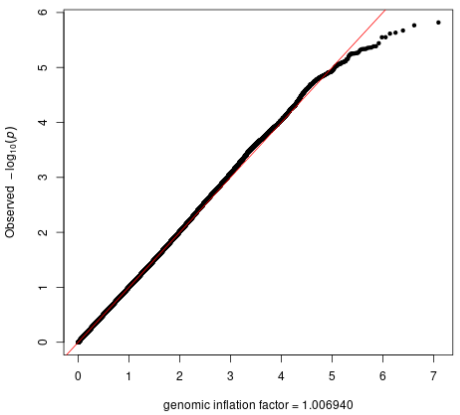

quadratic age-dependent

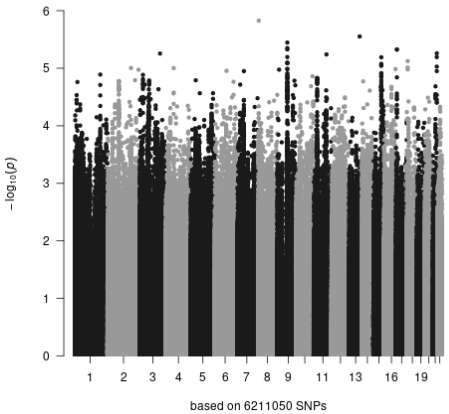

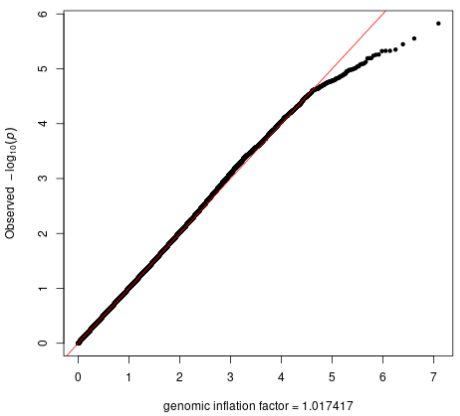

Supplementary Figure 1D: change rate cerebellum gray matter volume. Top: Change rates per cohort and estimated trajectories of the change rate with confidence intervals (in green) are displayed above. Mean values of individual cohorts are displayed as points, with error bars representing standard errors displayed in grey. The size of the points represents the relative size of the cohorts, total sample size N=15640. Cohorts that were added in phase 2 are displayed in grey. Only cohorts that satisfy N>75 are shown. The estimated trajectories of the volumes themselves are displayed below, for all subjects (solid line) and healthy subjects only (dashed line). Bottom rows contain Manhattan plots and QQ-plots for age-independent, age linear and age quadratic GWASs for rate of change.

1E: change rate cerebral white matter volume

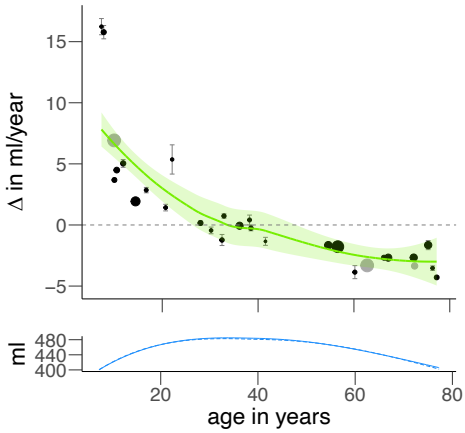

age independent

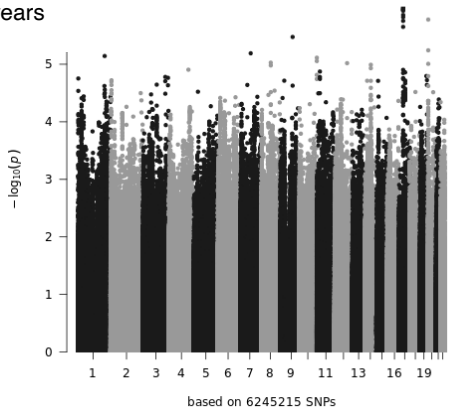

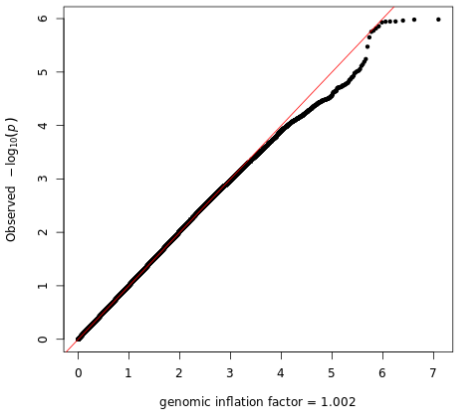

linear age-dependent

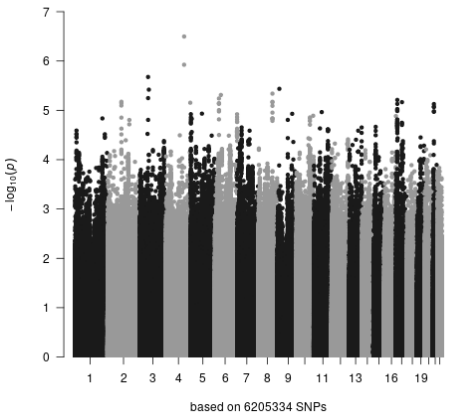

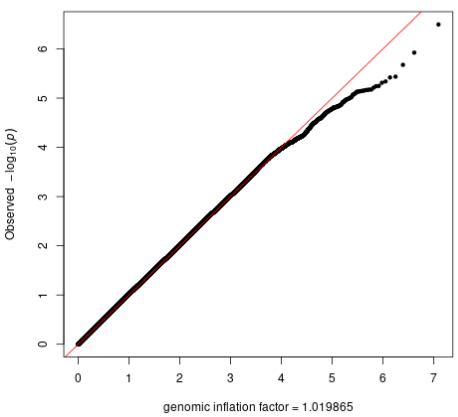

quadratic age-dependent

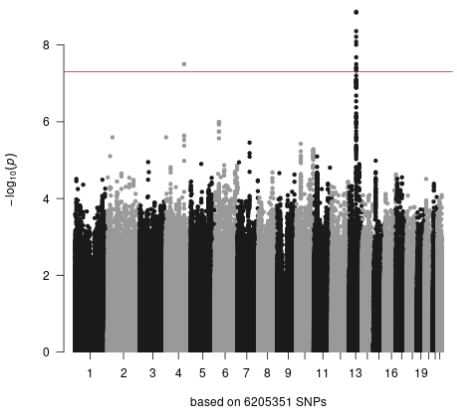

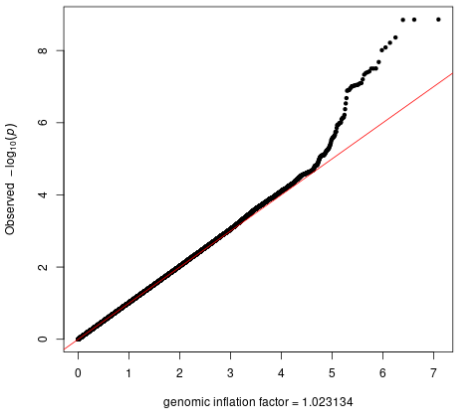

Supplementary Figure 1E: change rate cerebral white matter volume. Top: Change rates per cohort and estimated trajectories of the change rate with confidence intervals (in green) are displayed above. Mean values of individual cohorts are displayed as points, with error bars representing standard errors displayed in grey. The size of the points represents the relative size of the cohorts, total sample size N=15640. Cohorts that were added in phase 2 are displayed in grey. Only cohorts that satisfy N>75 are shown. The estimated trajectories of the volumes themselves are displayed below, for all subjects (solid line) and healthy subjects only (dashed line). Bottom rows contain Manhattan plots and QQ-plots for age-independent, age linear and age quadratic GWASs for rate of change.

1F: change rate cortex volume

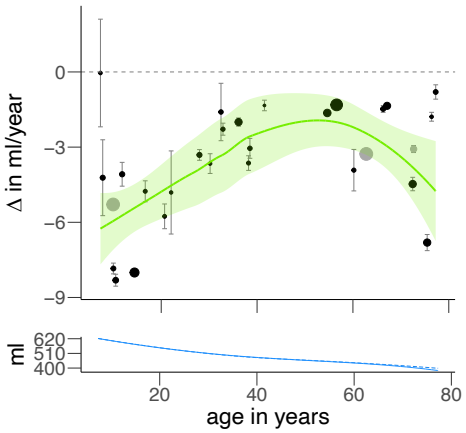

age independent

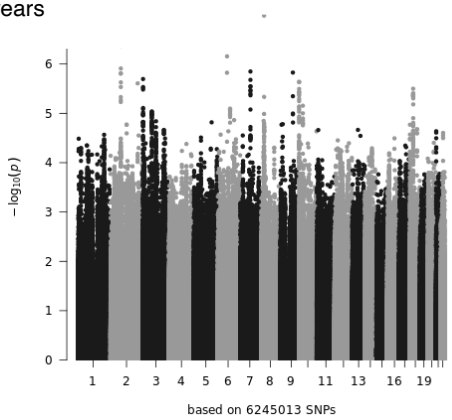

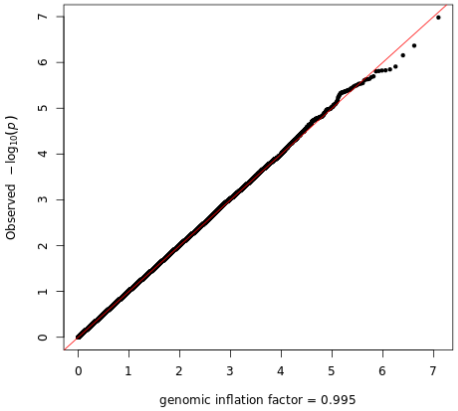

linear age-dependent

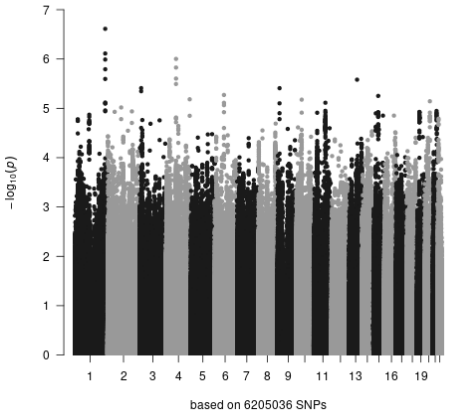

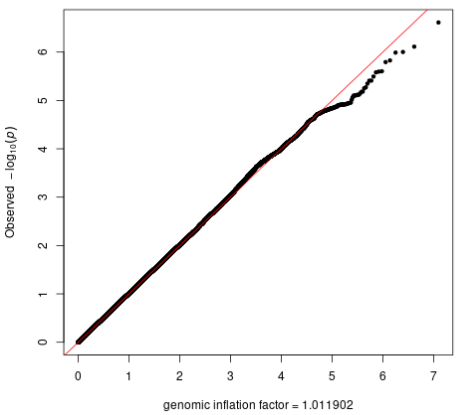

quadratic age-dependent

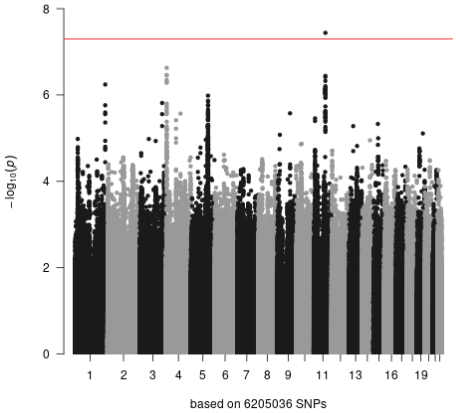

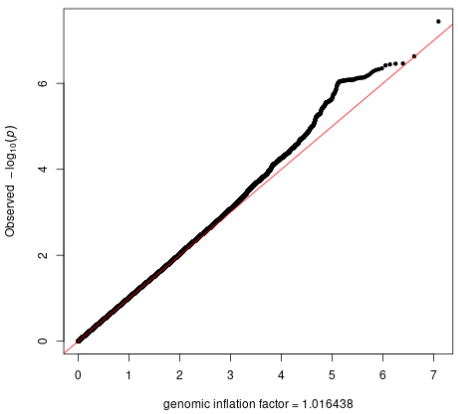

Supplementary Figure 1F: change rate cortex volume. Top: Change rates per cohort and estimated trajectories of the change rate with confidence intervals (in green) are displayed above. Mean values of individual cohorts are displayed as points, with error bars representing standard errors displayed in grey. The size of the points represents the relative size of the cohorts, total sample size N=15640. Cohorts that were added in phase 2 are displayed in grey. Only cohorts that satisfy N>75 are shown. The estimated trajectories of the volumes themselves are displayed below, for all subjects (solid line) and healthy subjects only (dashed line). Bottom rows contain Manhattan plots and QQ-plots for age-independent, age linear and age quadratic GWASs for rate of change.

1G: change rate cortical thickness

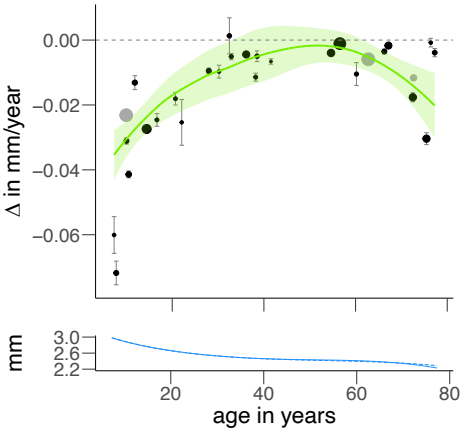

age independent

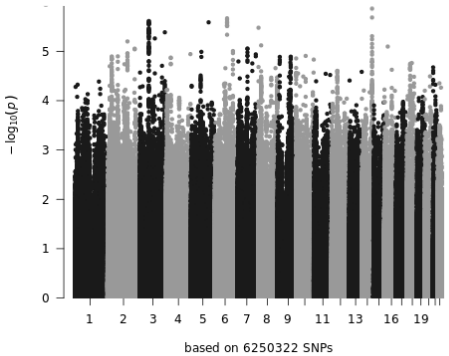

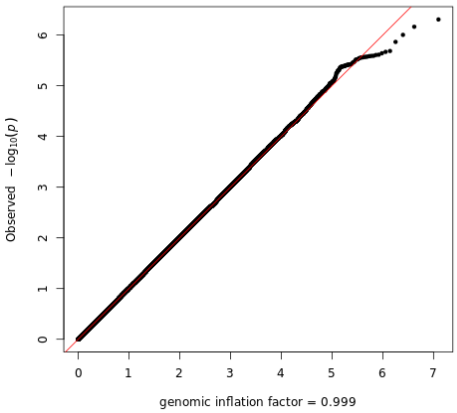

linear age-dependent

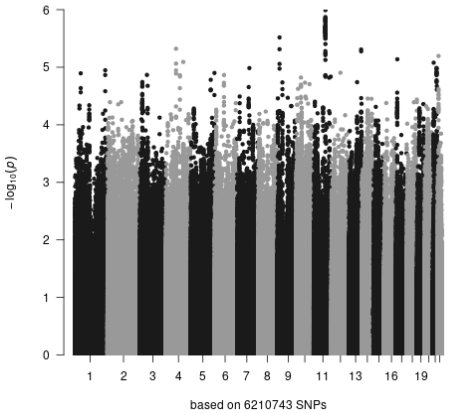

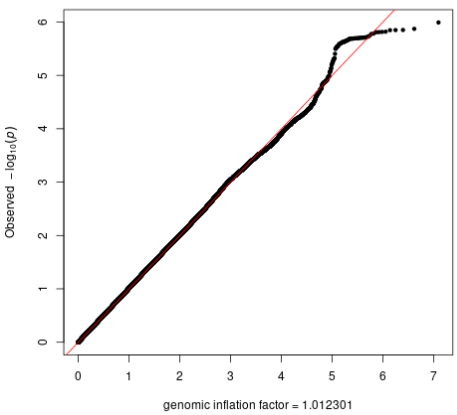

quadratic age-dependent

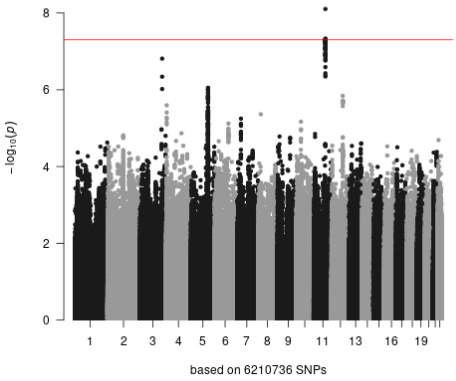

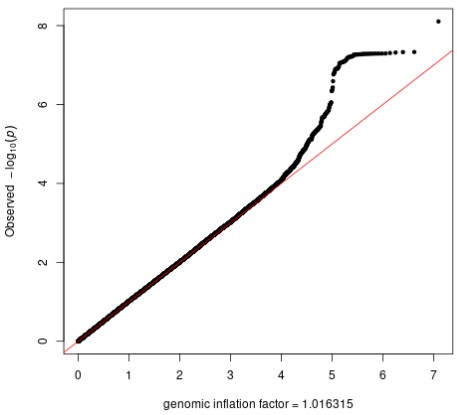

Supplementary Figure 1G: change rate cortical thickness. Top: Change rates per cohort and estimated trajectories of the change rate with confidence intervals (in green) are displayed above. Mean values of individual cohorts are displayed as points, with error bars representing standard errors displayed in grey. The size of the points represents the relative size of the cohorts, total sample size N=15640. Cohorts that were added in phase 2 are displayed in grey. Only cohorts that satisfy N>75 are shown. The estimated trajectories of the volumes themselves are displayed below, for all subjects (solid line) and healthy subjects only (dashed line). Bottom rows contain Manhattan plots and QQ-plots for age-independent, age linear and age quadratic GWASs for rate of change.

1H: change rate hippocampus volume

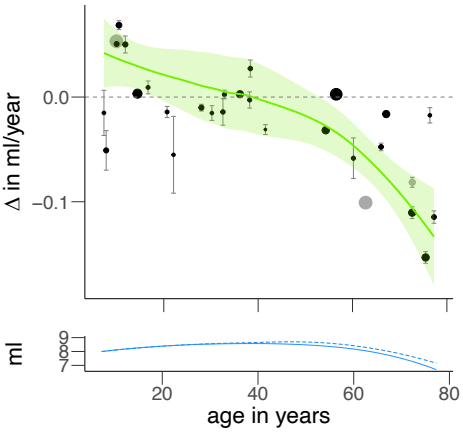

age independent

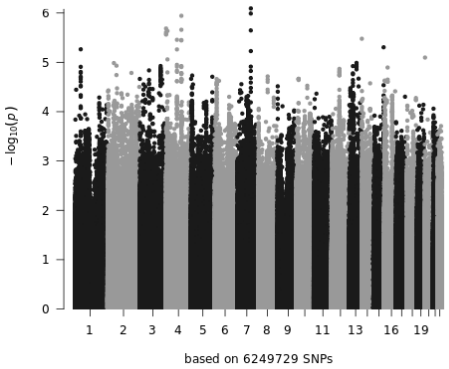

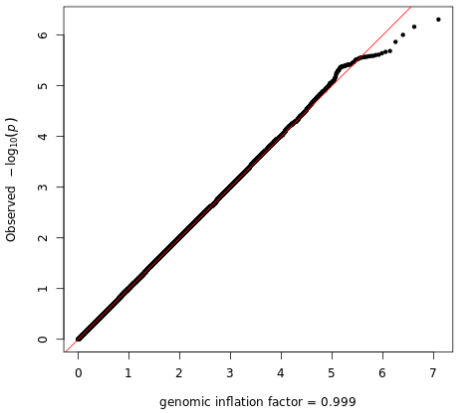

linear age-dependent

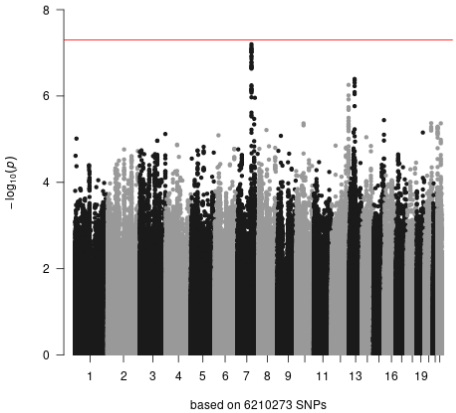

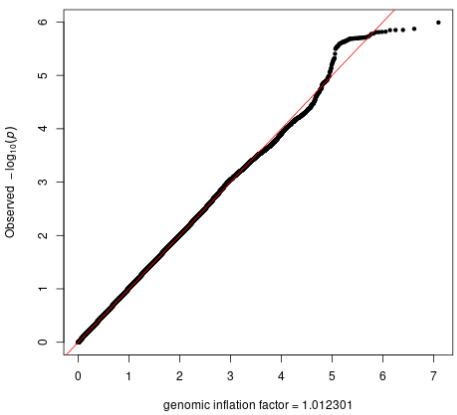

quadratic age-dependent

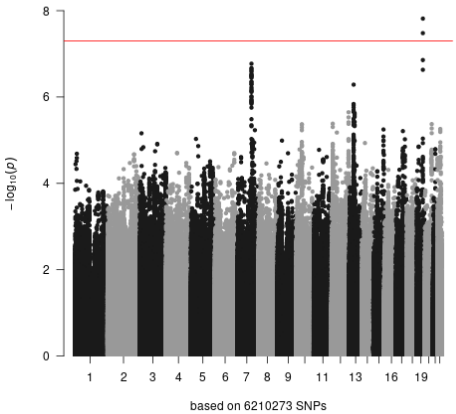

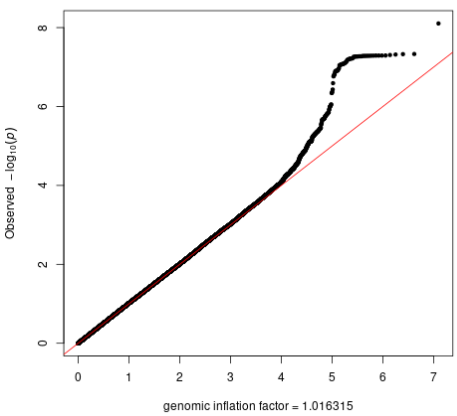

Supplementary Figure 1H: change rate hippocampus volume. Top: Change rates per cohort and estimated trajectories of the change rate with confidence intervals (in green) are displayed above. Mean values of individual cohorts are displayed as points, with error bars representing standard errors displayed in grey. The size of the points represents the relative size of the cohorts, total sample size N=15640. Cohorts that were added in phase 2 are displayed in grey. Only cohorts that satisfy N>75 are shown. The estimated trajectories of the volumes themselves are displayed below, for all subjects (solid line) and healthy subjects only (dashed line). Bottom rows contain Manhattan plots and QQ-plots for age-independent, age linear and age quadratic GWASs for rate of change.

1l: change rate lateral ventricle volume

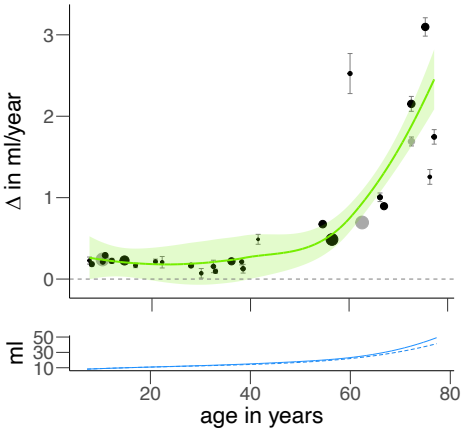

age independent

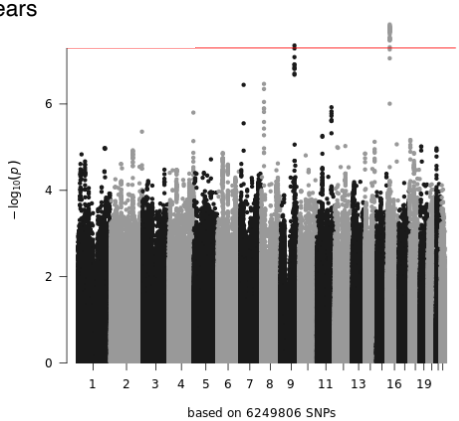

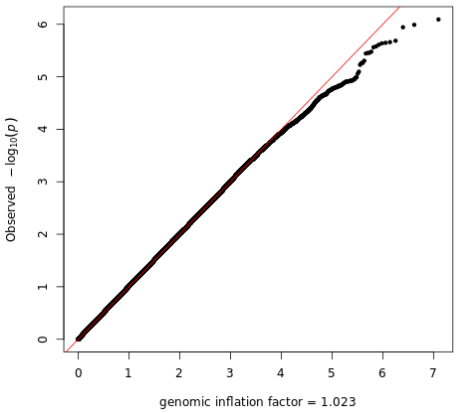

linear age-dependent

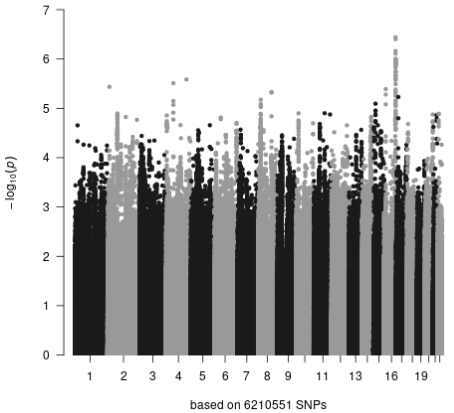

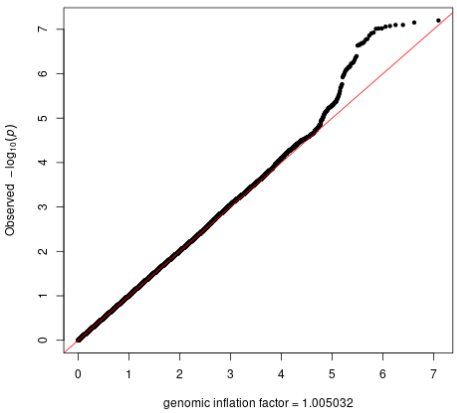

quadratic age-dependent

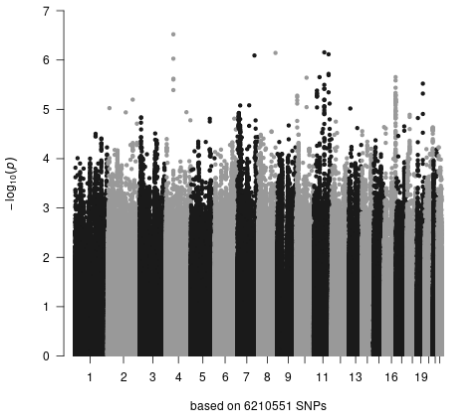

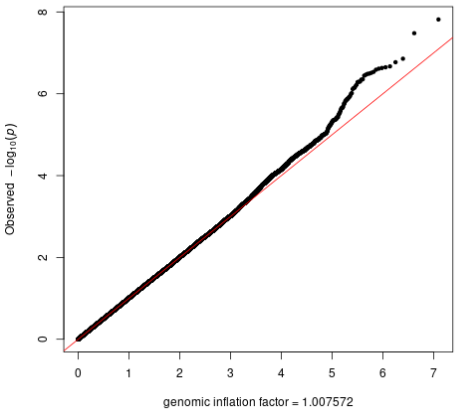

Supplementary Figure 1l: change rate lateral ventricle volume.Top: Change rates per cohort and estimated trajectories of the change rate with confidence intervals (in green) are displayed above. Mean values of individual cohorts are displayed as points, with error bars representing standard errors displayed in grey. The size of the points represents the relative size of the cohorts, total sample size N=15640. Cohorts that were added in phase 2 are displayed in grey. Only cohorts that satisfy N>75 are shown. The estimated trajectories of the volumes themselves are displayed below, for all subjects (solid line) and healthy subjects only (dashed line). Bottom rows contain Manhattan plots and QQ-plots for age-independent, age linear and age quadratic GWASs for rate of change.

1J: change rate nucleus accumbens volume

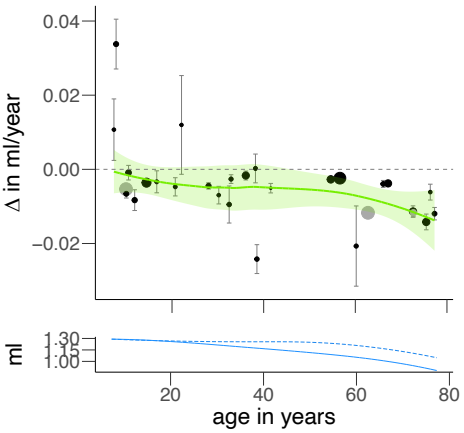

age independent

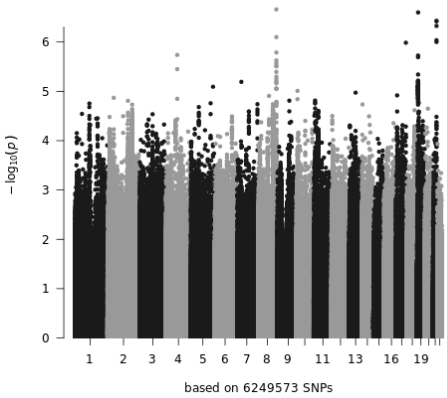

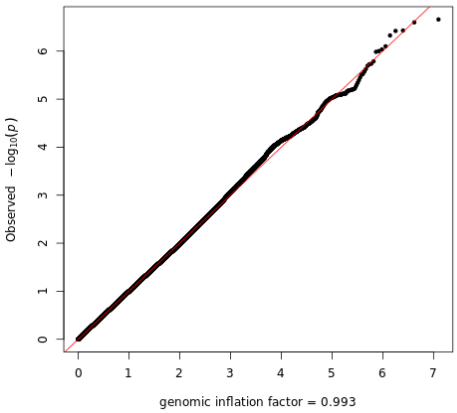

linear age-dependent

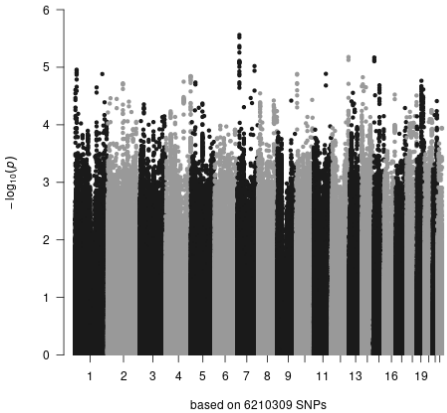

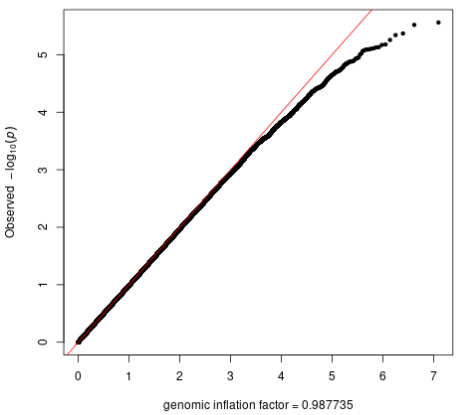

quadratic age-dependent

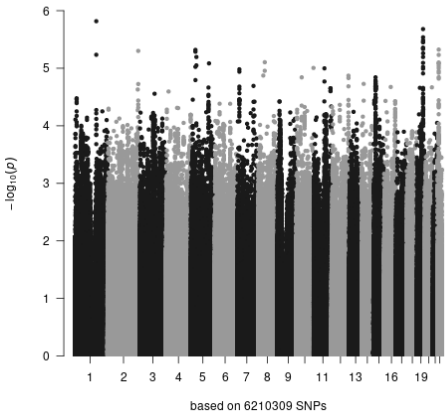

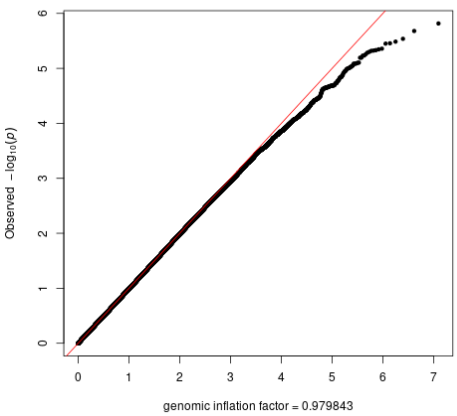

Supplementary Figure 1J: change rate nucleus accumbens volume. Top: Change rates per cohort and estimated trajectories of the change rate with confidence intervals (in green) are displayed above. Mean values of individual cohorts are displayed as points, with error bars representing standard errors displayed in grey. The size of the points represents the relative size of the cohorts, total sample size N=15640. Cohorts that were added in phase 2 are displayed in grey. Only cohorts that satisfy N>75 are shown. The estimated trajectories of the volumes themselves are displayed below, for all subjects (solid line) and healthy subjects only (dashed line). Bottom rows contain Manhattan plots and QQ-plots for age-independent, age linear and age quadratic GWASs for rate of change.

1K: change rate pallidum volume

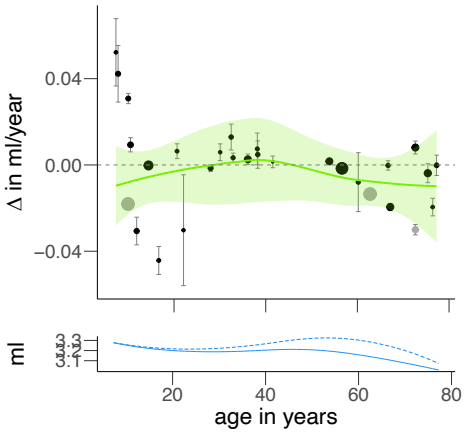

age independent

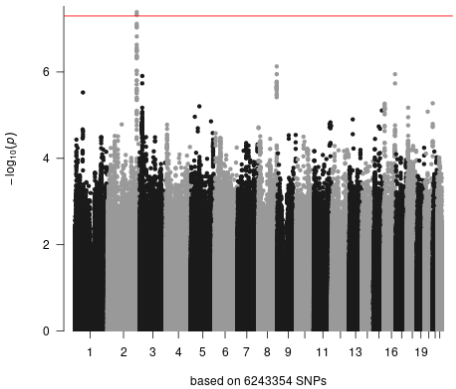

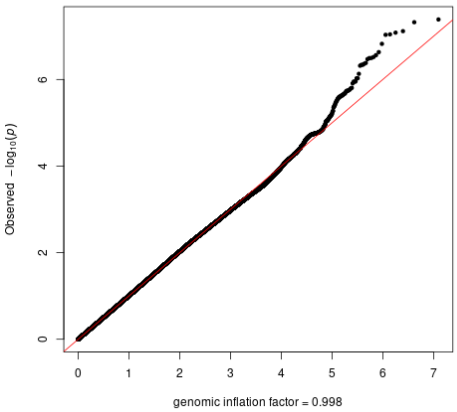

linear age-dependent

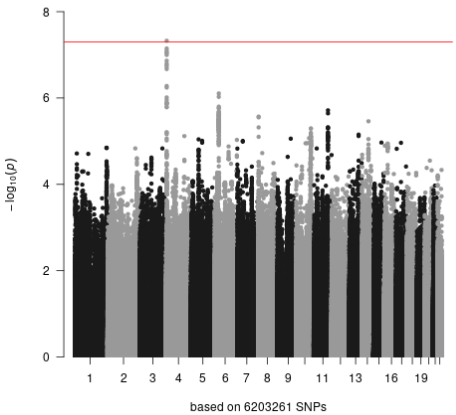

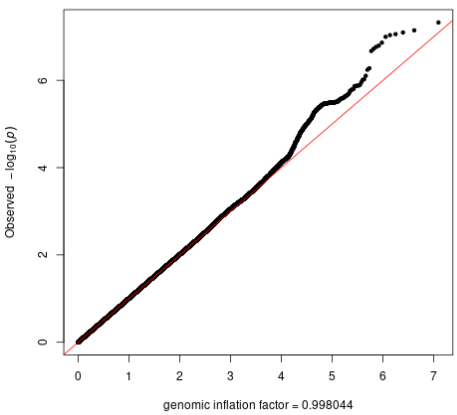

quadratic age-dependent

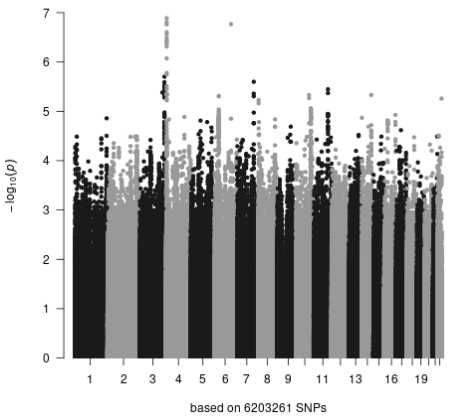

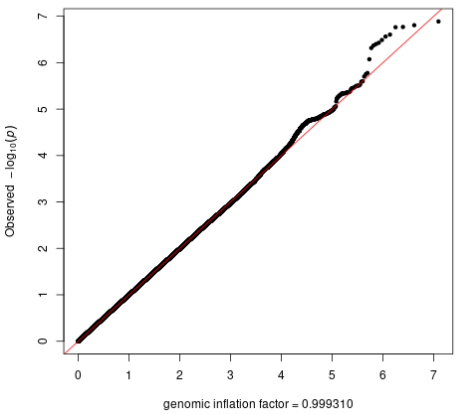

Supplementary Figure 1K: change rate pallidum volume. Top: Change rates per cohort and estimated trajectories of the change rate with confidence intervals (in green) are displayed above. Mean values of individual cohorts are displayed as points, with error bars representing standard errors displayed in grey. The size of the points represents the relative size of the cohorts, total sample size N=15640. Cohorts that were added in phase 2 are displayed in grey. Only cohorts that satisfy N>75 are shown. The estimated trajectories of the volumes themselves are displayed below, for all subjects (solid line) and healthy subjects only (dashed line). Bottom rows contain Manhattan plots and QQ-plots for age-independent, age linear and age quadratic GWASs for rate of change.

1L: change rate putamen volume

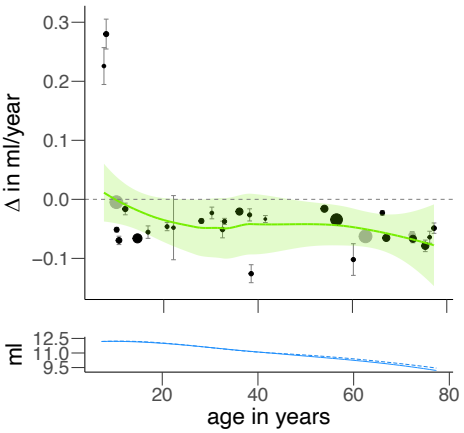

age independent

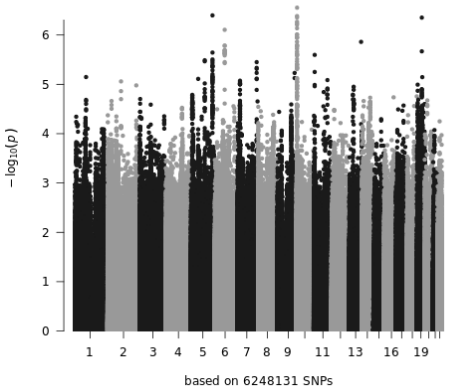

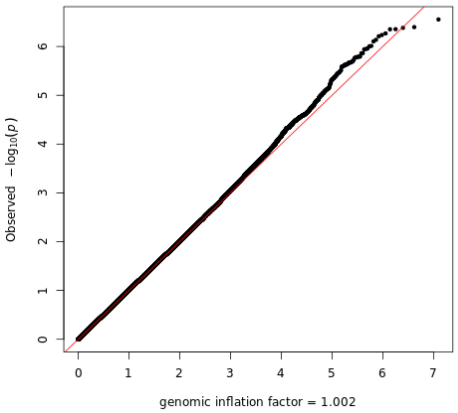

linear age-dependent

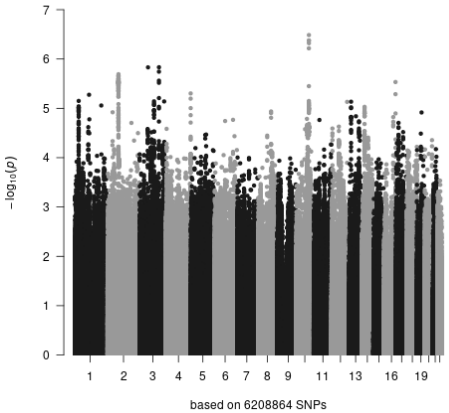

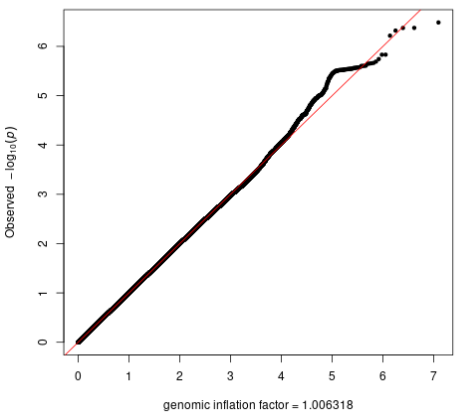

quadratic age-dependent

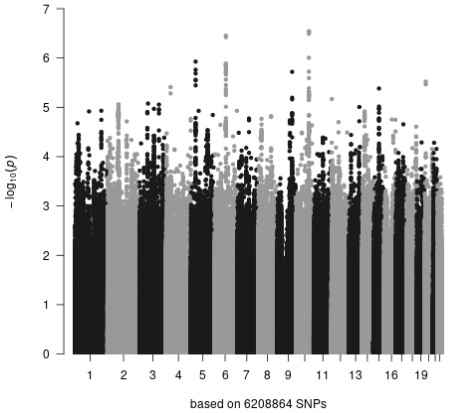

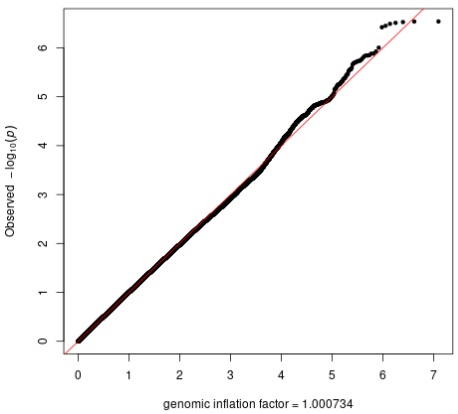

Supplementary Figure 1L: change rate putamen volume.Top: Change rates per cohort and estimated trajectories of the change rate with confidence intervals (in green) are displayed above. Mean values of individual cohorts are displayed as points, with error bars representing standard errors displayed in grey. The size of the points represents the relative size of the cohorts, total sample size N=15640. Cohorts that were added in phase 2 are displayed in grey. Only cohorts that satisfy N>75 are shown. The estimated trajectories of the volumes themselves are displayed below, for all subjects (solid line) and healthy subjects only (dashed line). Bottom rows contain Manhattan plots and QQ-plots for age-independent, age linear and age quadratic GWASs for rate of change.

1M: change rate surface area

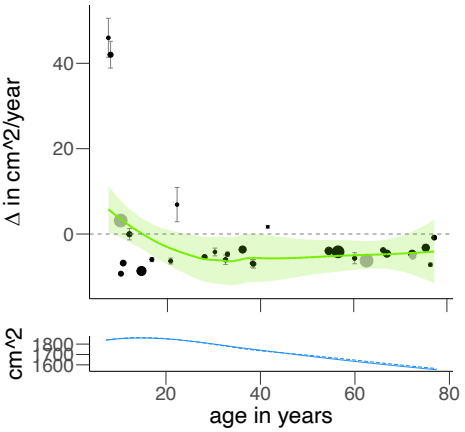

age independent

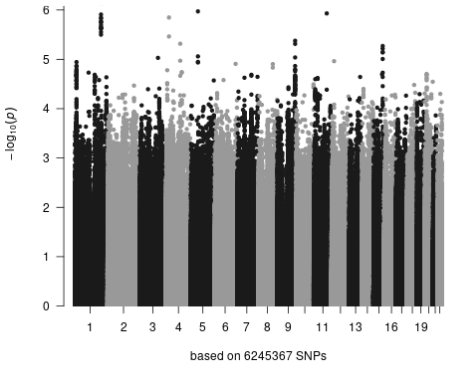

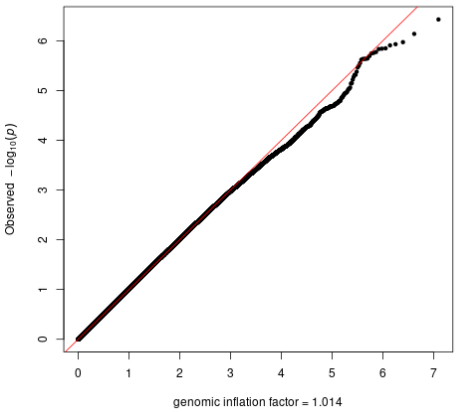

linear age-dependent

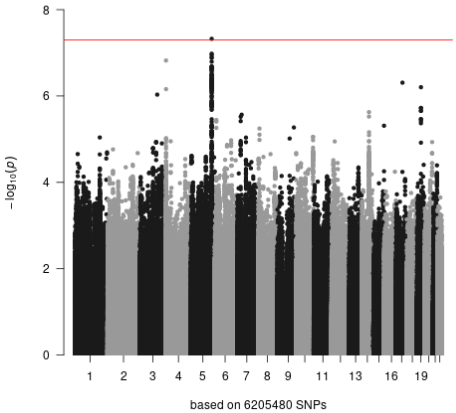

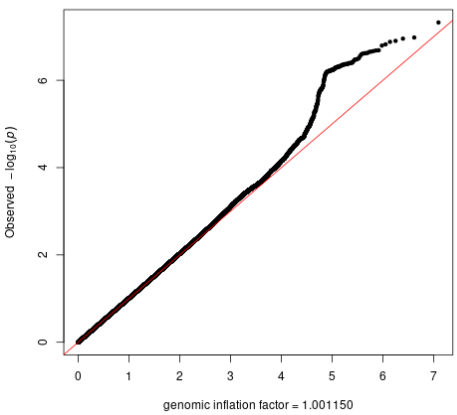

quadratic age-dependent

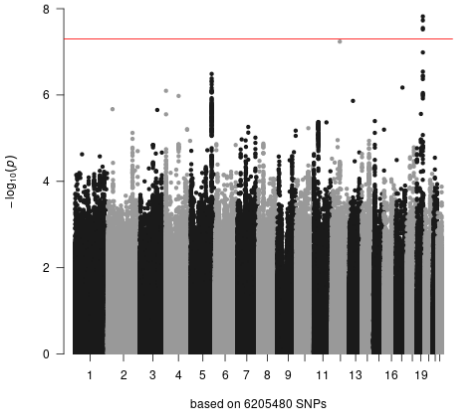

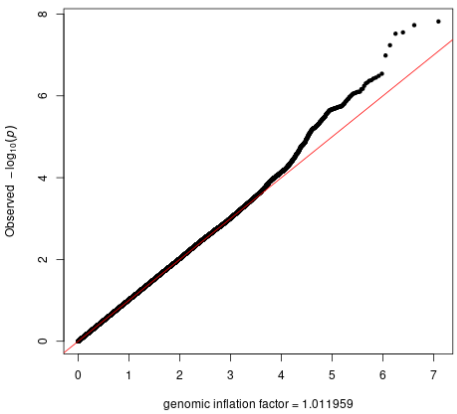

Supplementary Figure 1M: change rate surface area. Top: Change rates per cohort and estimated trajectories of the change rate with confidence intervals (in green) are displayed above. Mean values of individual cohorts are displayed as points, with error bars representing standard errors displayed in grey. The size of the points represents the relative size of the cohorts, total sample size N=15640. Cohorts that were added in phase 2 are displayed in grey. Only cohorts that satisfy N>75 are shown. The estimated trajectories of the volumes themselves are displayed below, for all subjects (solid line) and healthy subjects only (dashed line). Bottom rows contain Manhattan plots and QQ-plots for age-independent, age linear and age quadratic GWASs for rate of change.

1N: change rate thalamus volume

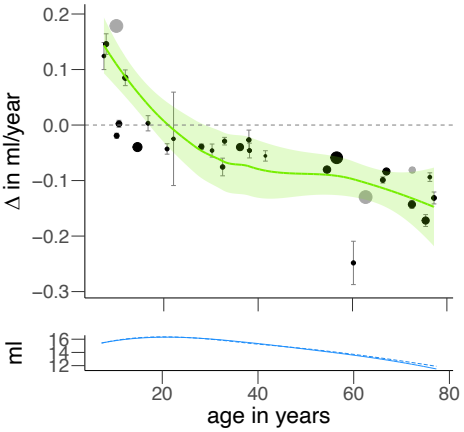

age independent

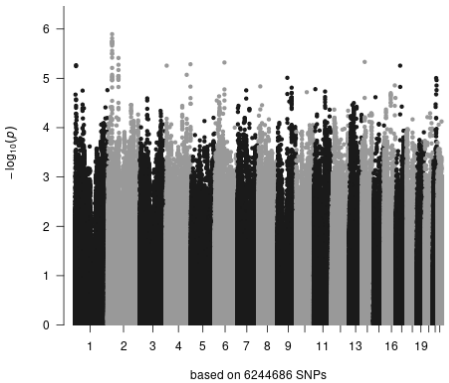

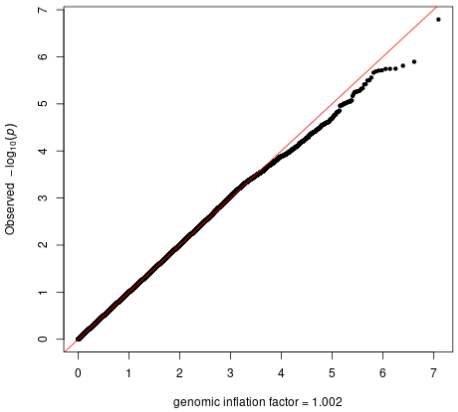

linear age-dependent

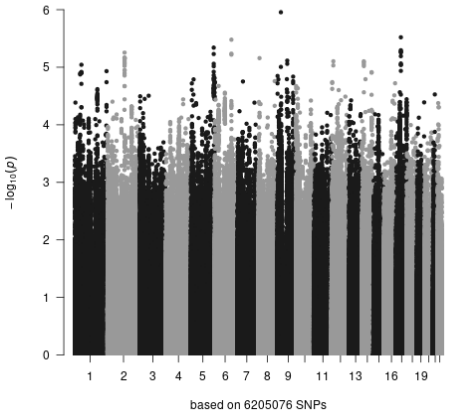

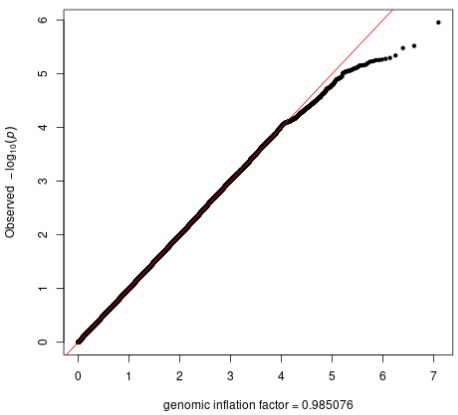

quadratic age-dependent

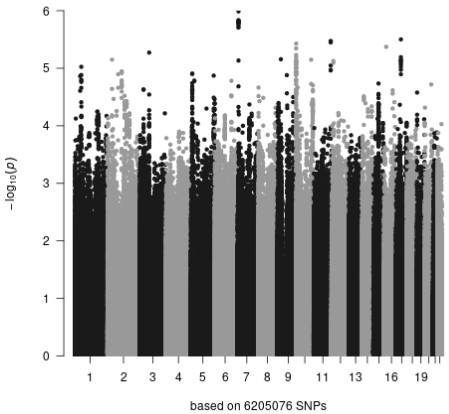

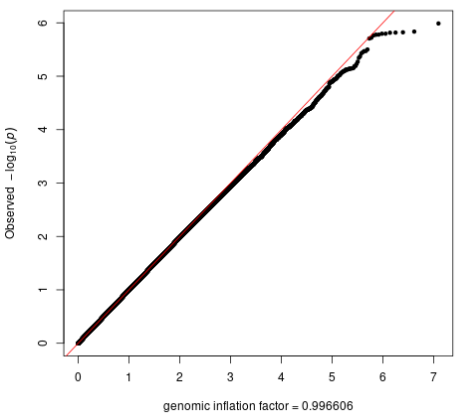

Supplementary Figure 1N: change rate thalamus volume. Top: Change rates per cohort and estimated trajectories of the change rate with confidence intervals (in green) are displayed above. Mean values of individual cohorts are displayed as points, with error bars representing standard errors displayed in grey. The size of the points represents the relative size of the cohorts, total sample size N=15640. Cohorts that were added in phase 2 are displayed in grey. Only cohorts that satisfy N>75 are shown. The estimated trajectories of the volumes themselves are displayed below, for all subjects (solid line) and healthy subjects only (dashed line). Bottom rows contain Manhattan plots and QQ-plots for age-independent, age linear and age quadratic GWASs for rate of change.

1O: change rate total brain volume

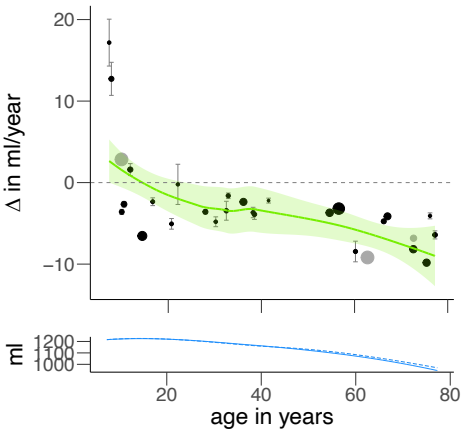

age independent

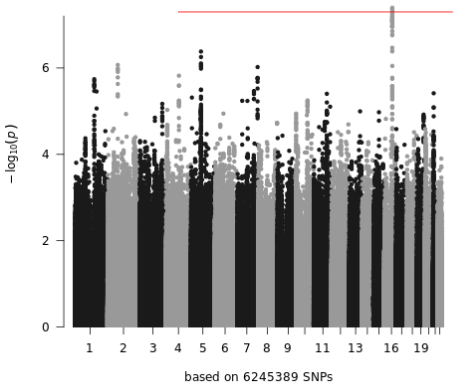

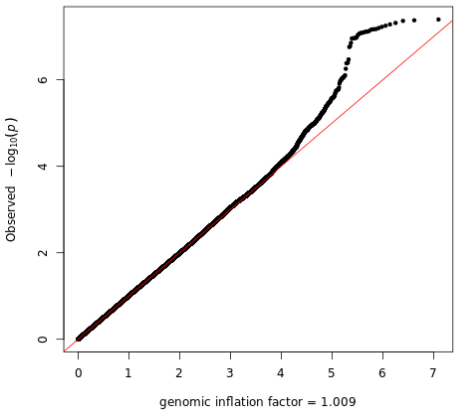

linear age-dependent

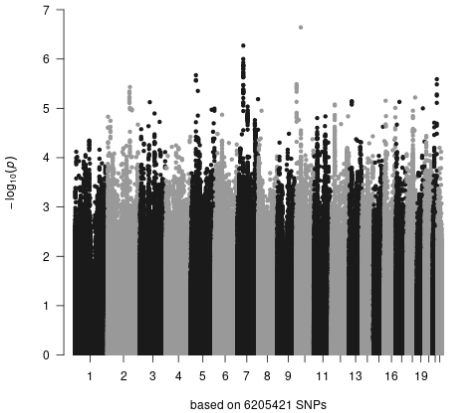

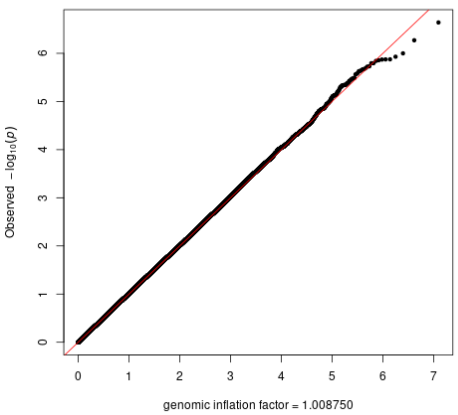

quadratic age-dependent

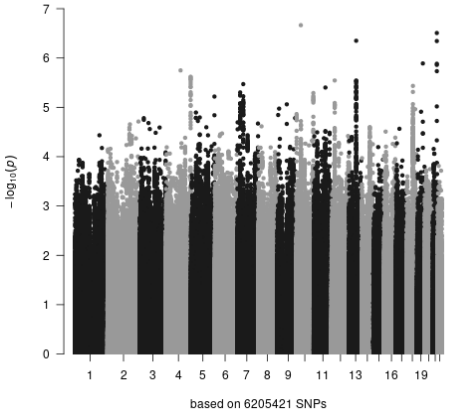

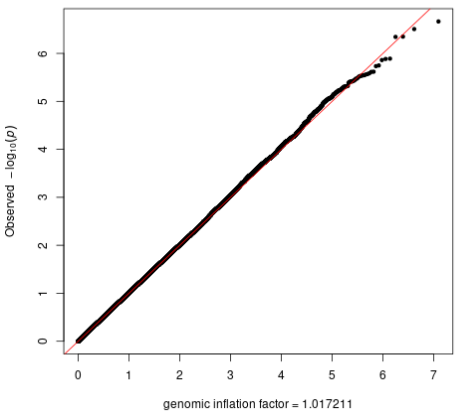

Supplementary Figure 1O: change rate total brain volume.Top: Change rates per cohort and estimated trajectories of the change rate with confidence intervals (in green) are displayed above. Mean values of individual cohorts are displayed as points, with error bars representing standard errors displayed in grey. The size of the points represents the relative size of the cohorts, total sample size N=15640. Cohorts that were added in phase 2 are displayed in grey. Only cohorts that satisfy N>75 are shown. The estimated trajectories of the volumes themselves are displayed below, for all subjects (solid line) and healthy subjects only (dashed line). Bottom rows contain Manhattan plots and QQ-plots for age-independent, age linear and age quadratic GWASs for rate of change.

2A

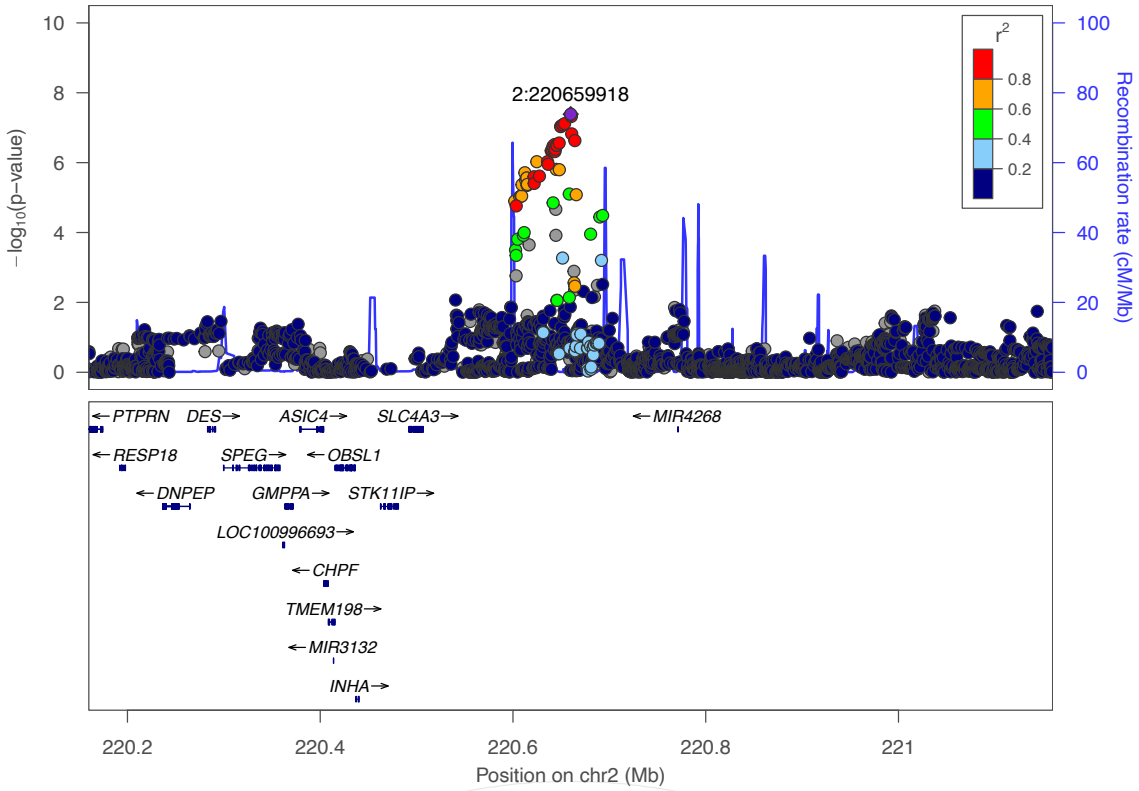

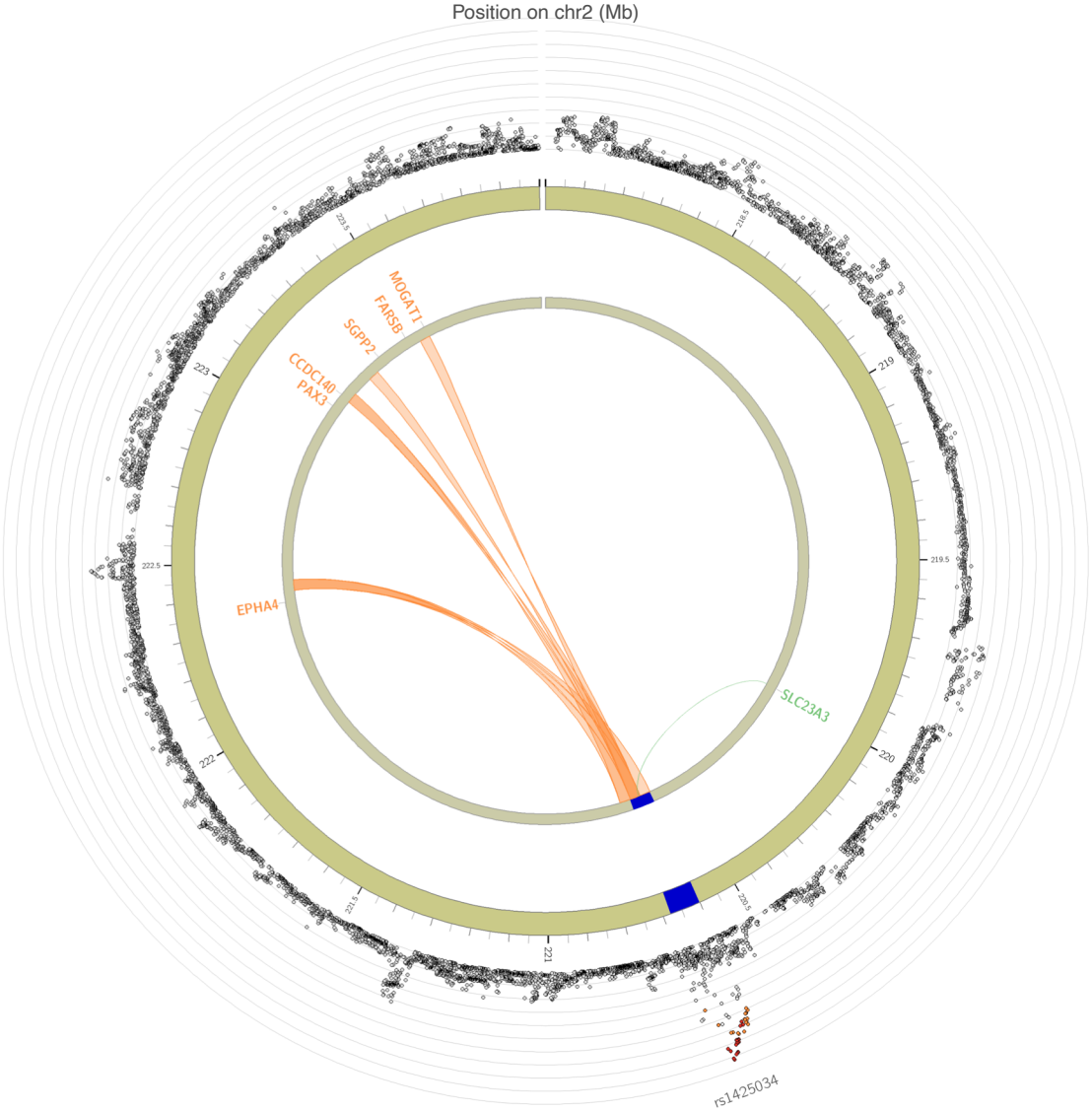

Supplementary Figure 2A: Locusplots (top), eQTL and chromatin interaction mapping (bottom) for genome-wide significant SNP rs1425034; change rate pallidum; independent of age. Locus plots were created with locus zoom[98]. Circos plots were created with FUMA[66].

2B

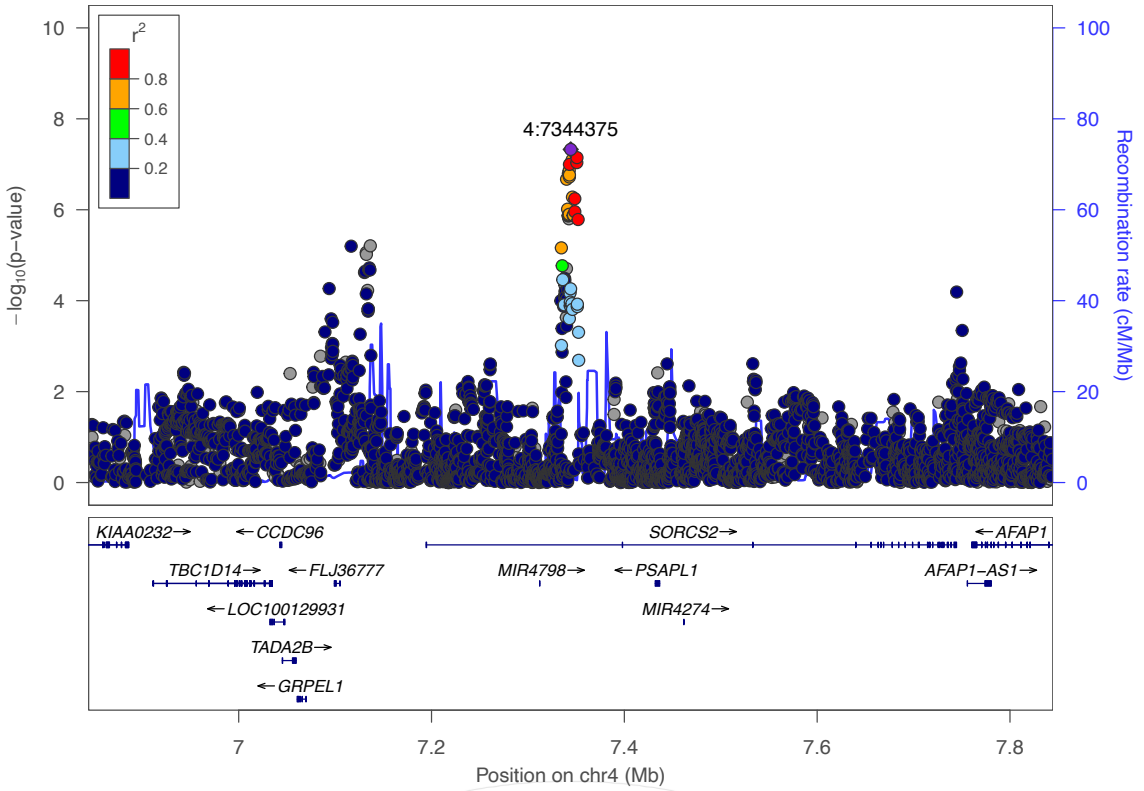

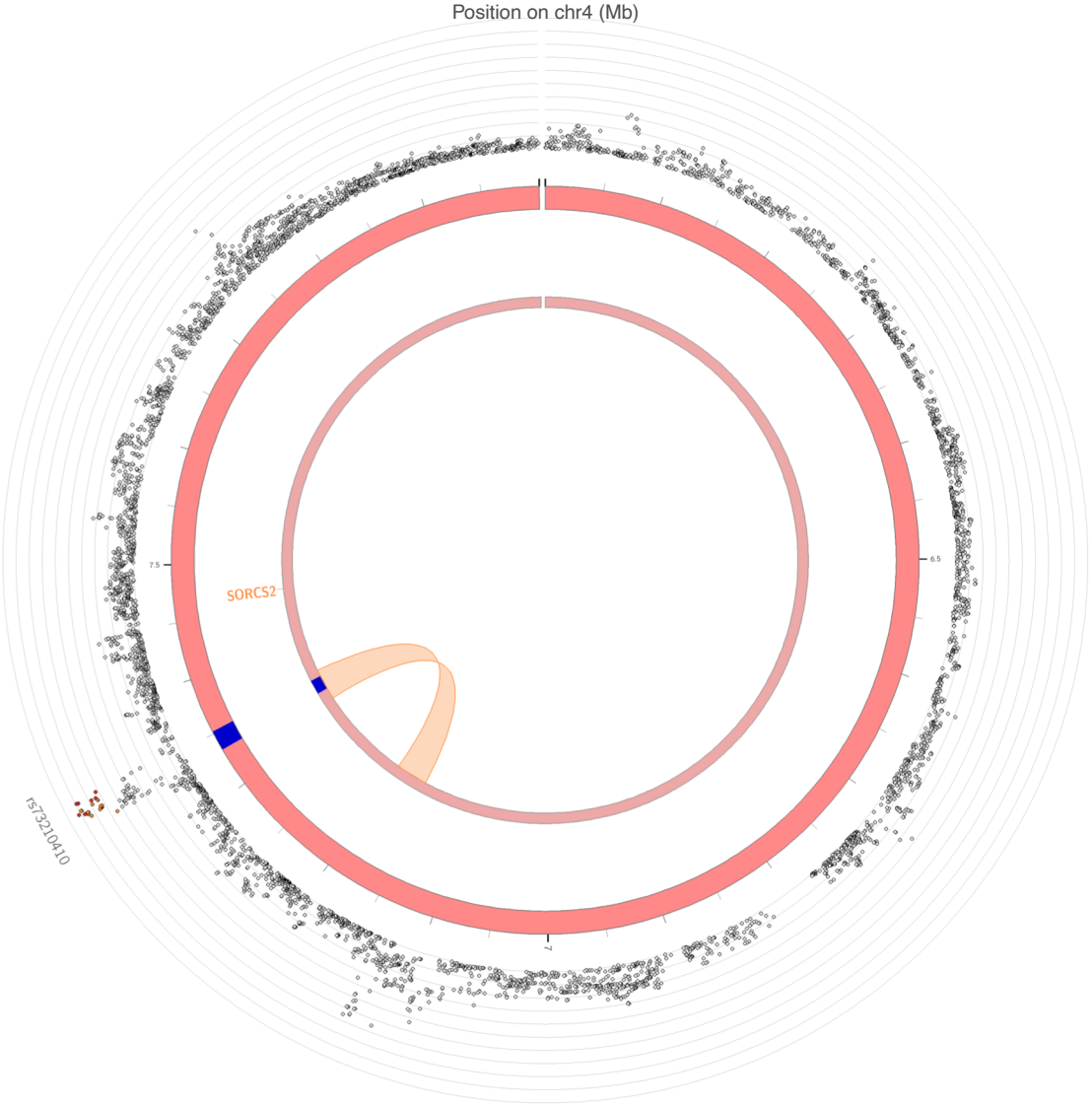

Supplementary Figure 2B: Locusplots (top), eQTL and chromatin interaction mapping (bottom) for genome-wide significant SNP rs73210410; change rate pallidum; linear age dependency. Locus plots were created with locus zoom[98]. Circos plots were created with FUMA[66].

2C

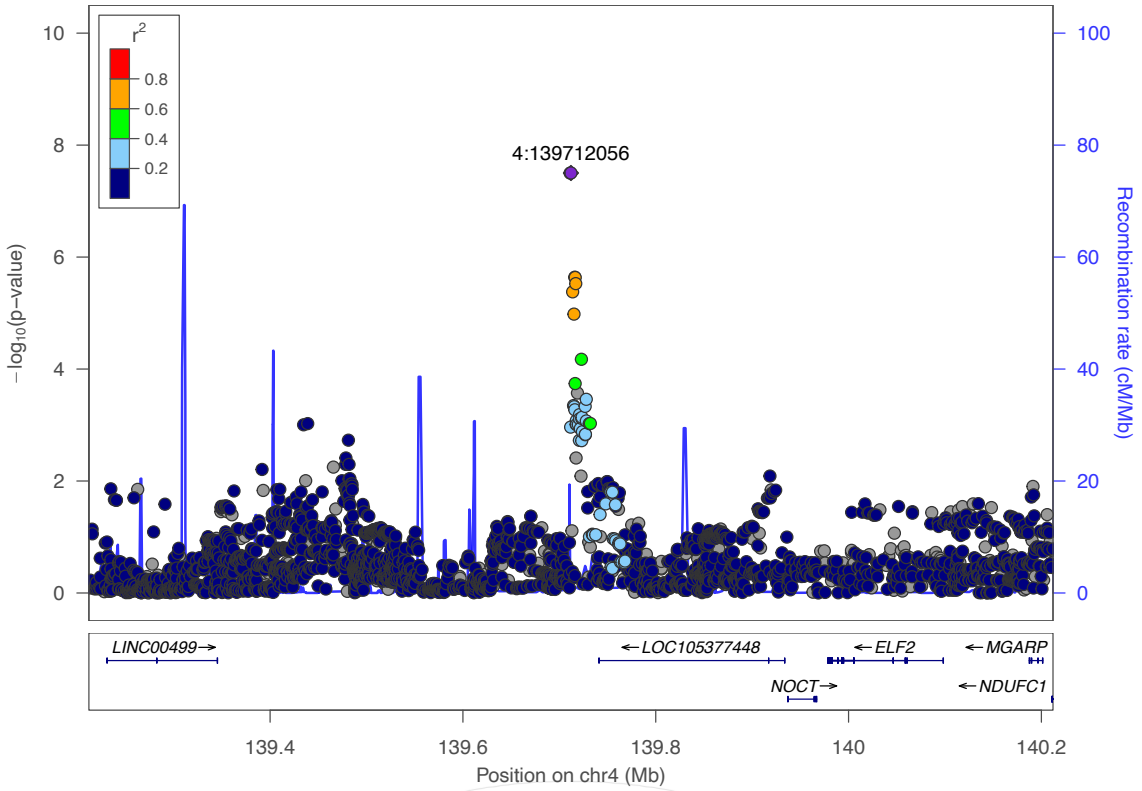

Supplementary Figure 2C: Locusplots (top), eQTL and chromatin interaction mapping (bottom) for genome-wide significant SNP rs11726181; change rate cerebral white matter; quadratic age dependency. Locus plots were created with locus zoom[98]. Circos plots were created with FUMA[66].

2D

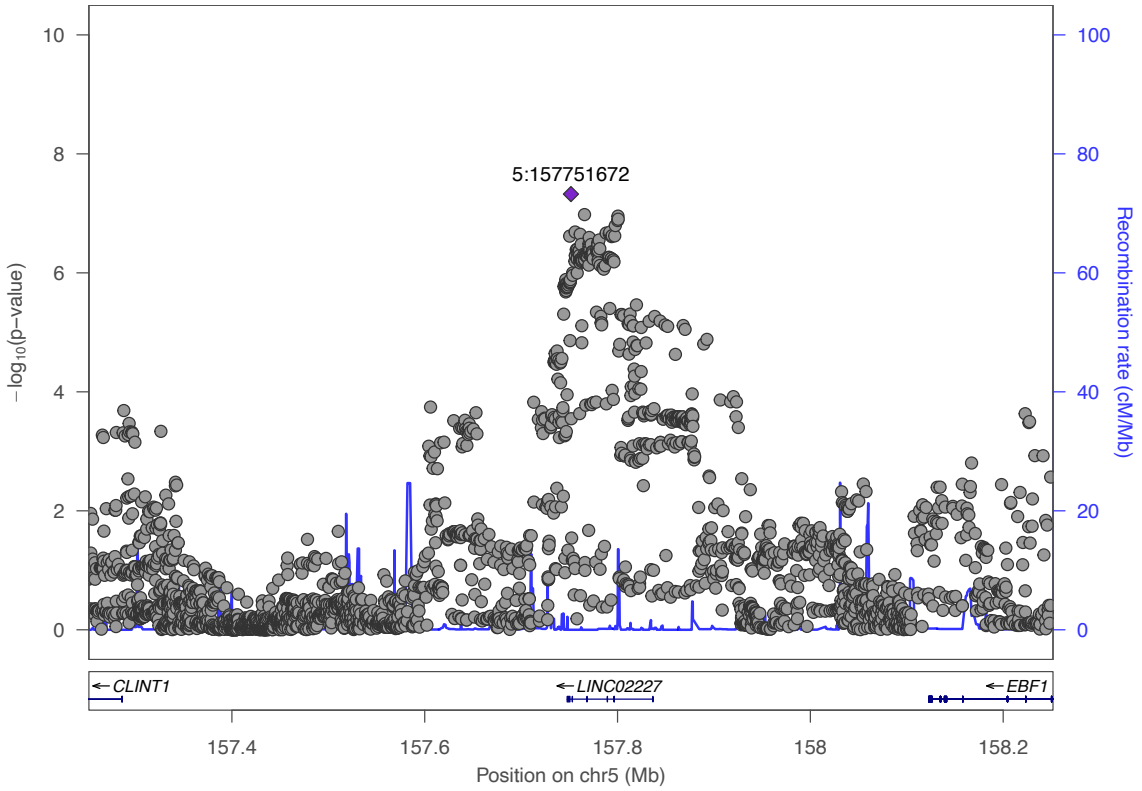

Supplementary Figure 2D: Locusplots (top), eQTL and chromatin interaction mapping (bottom) for genome-wide significant SNP 5:157751672; change rate surface area; linear age dependency. Locus plots were created with locus zoom[98]. This SNP was not present in 1000G reference file and no SNP in high LD could be identified, no LD information or circos plot available.

2E

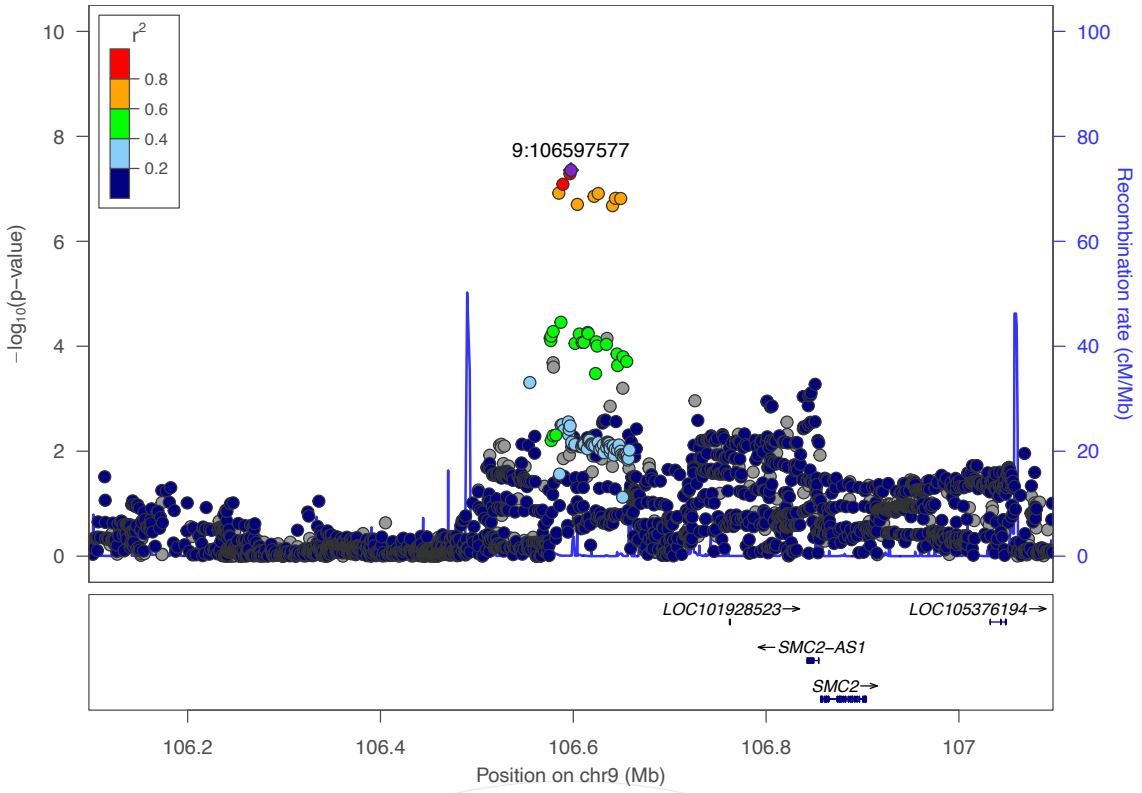

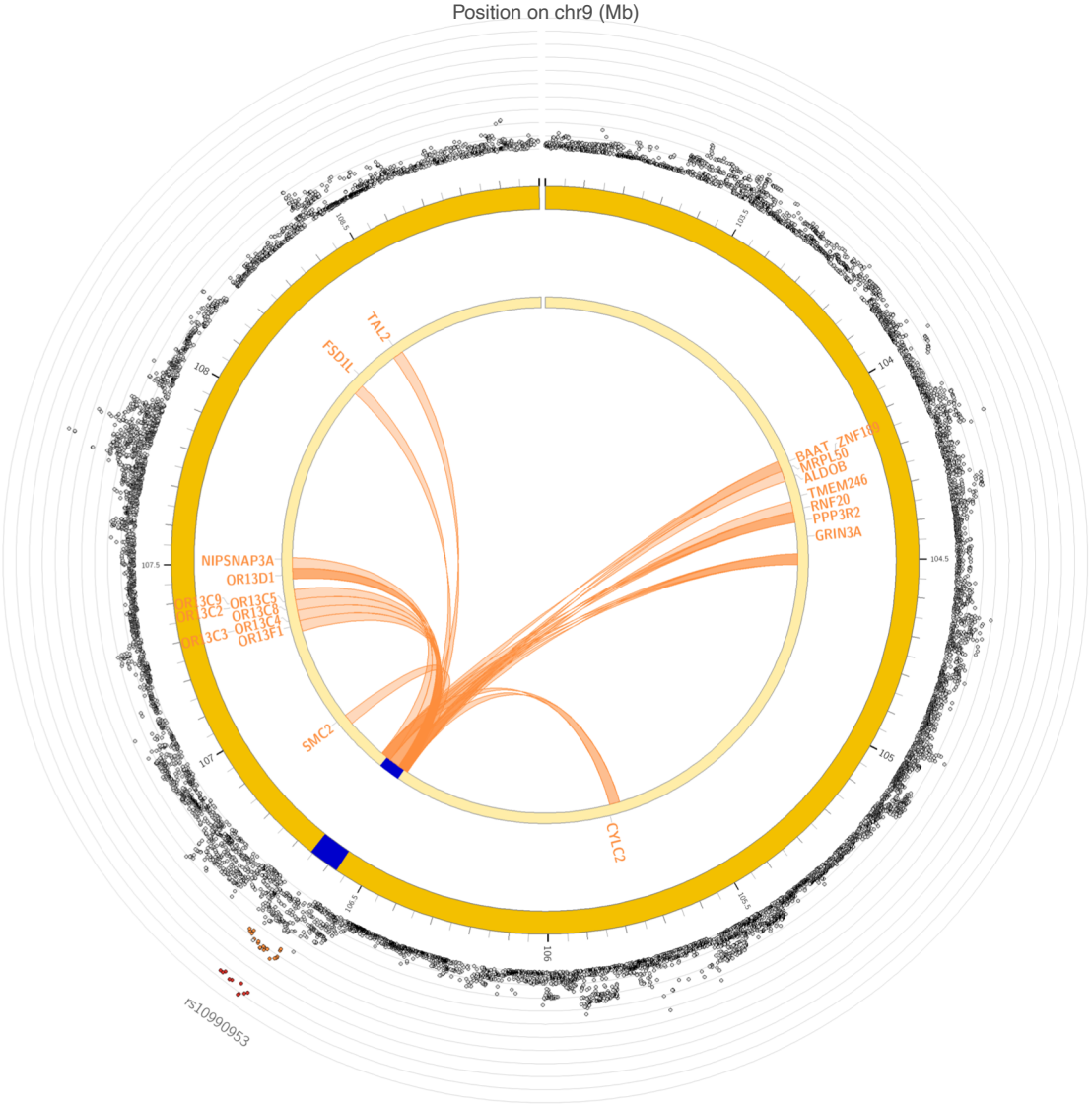

Supplementary Figure 2E: Locusplots (top), eQTL and chromatin interaction mapping (bottom) for genome-wide significant SNP rs10990953; change rate ventricles; independent of age. Locus plots were created with locus zoom[98]. Circos plots were created with FUMA[66].

2F

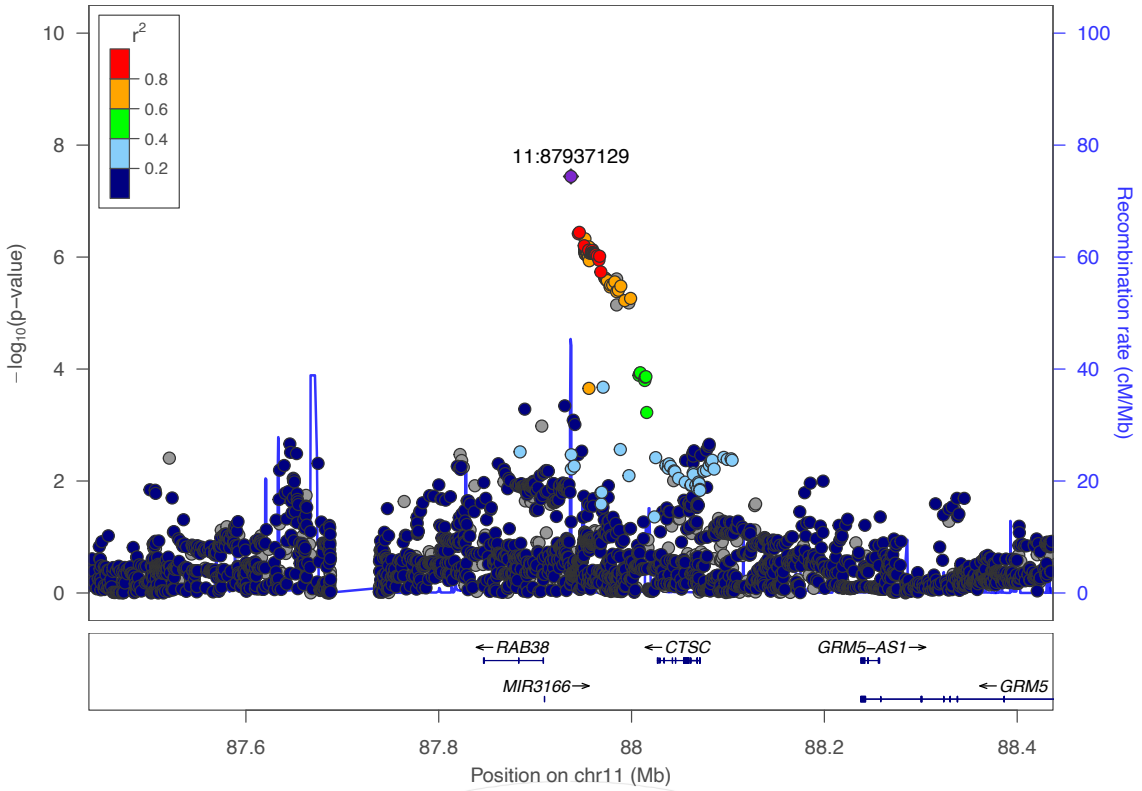

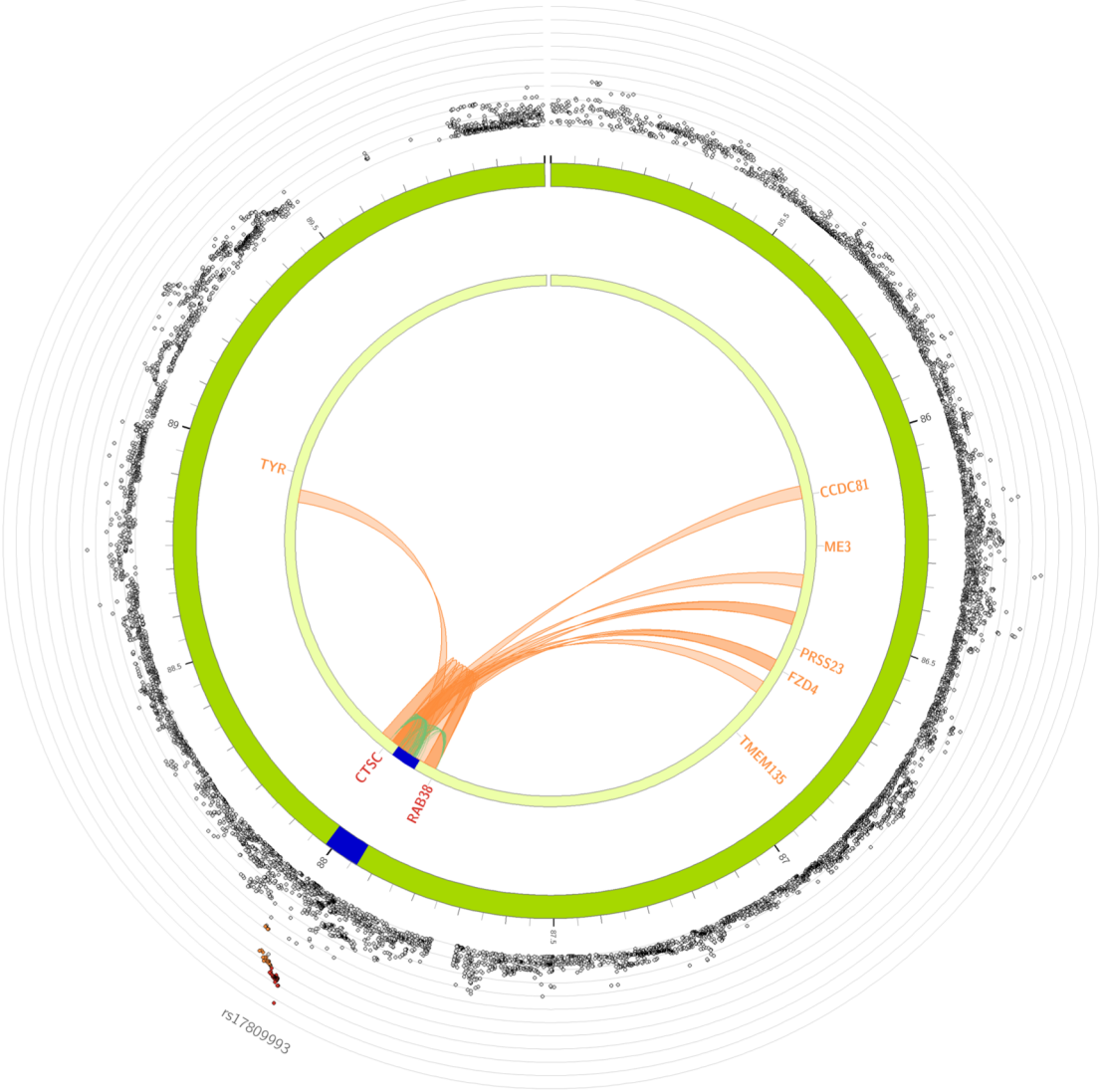

Supplementary Figure 2F: Locusplots (top), eQTL and chromatin interaction mapping (bottom) for genome-wide significant SNP rs17809993; change rate cortex volume quadratic age dependency. Locus plots were created with locus zoom[98]. Circos plots were created with FUMA[66].

2G

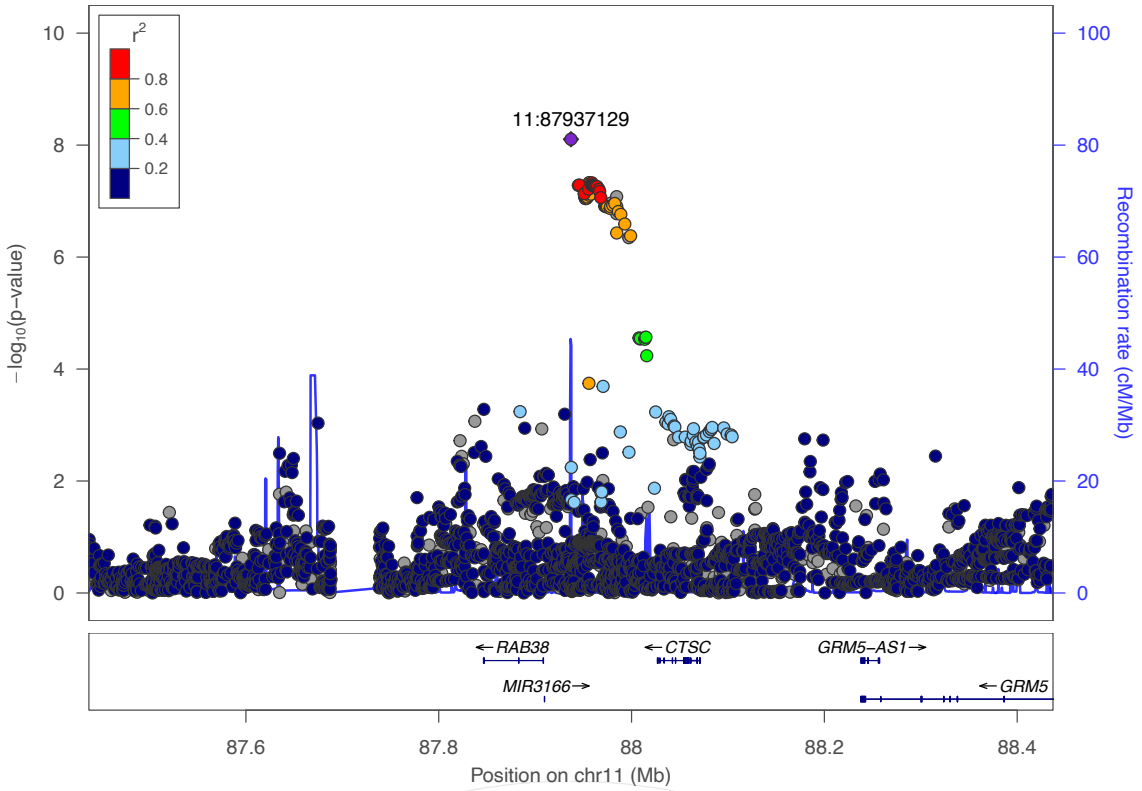

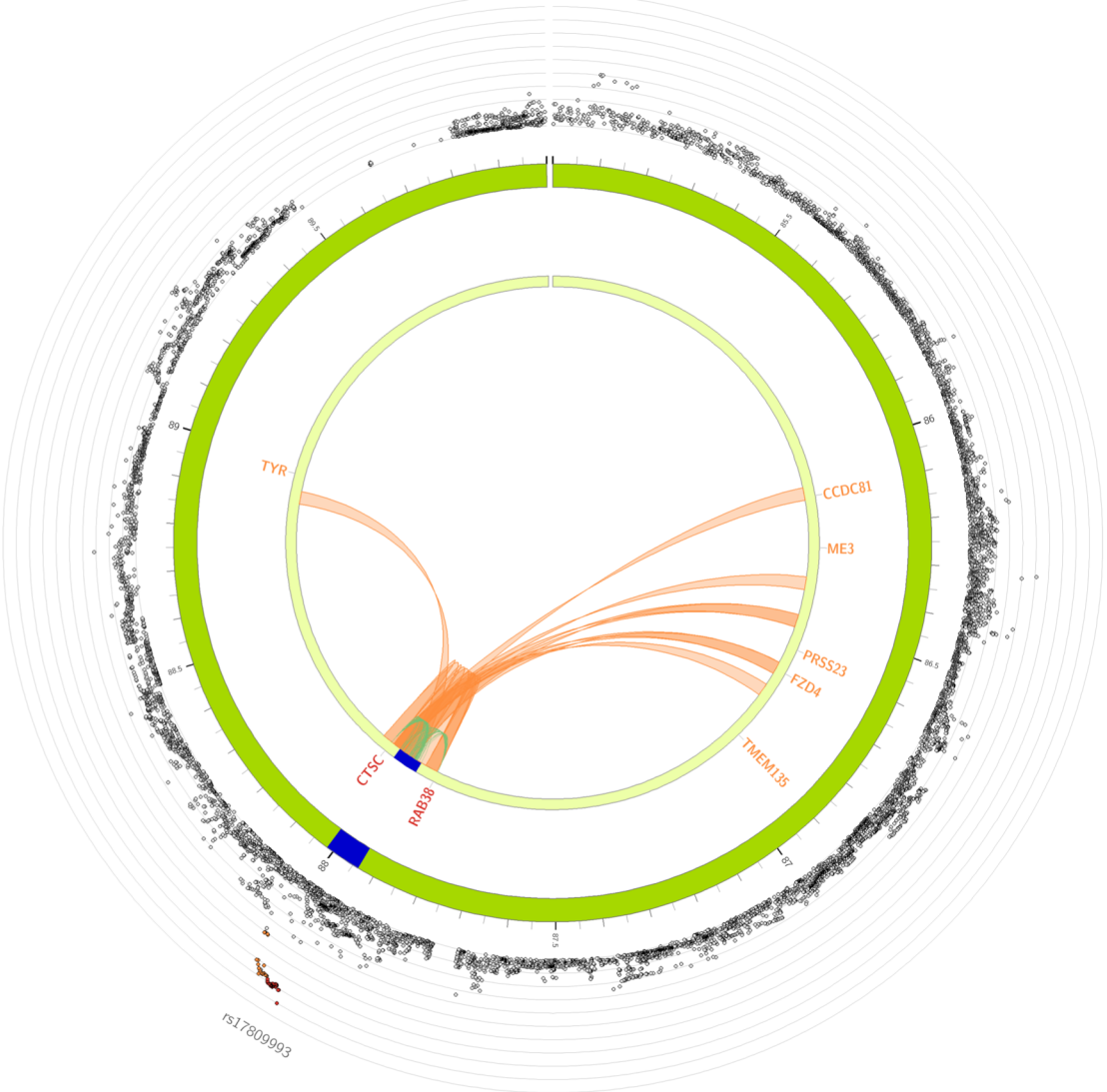

Supplementary Figure 2G: Locusplots (top), eQTL and chromatin interaction mapping (bottom) for genome-wide significant SNP rs17809993; change rate cortical thickness quadratic age dependency. Locus plots were created with locus zoom[98]. Circos plots were created with FUMA[66].

2H

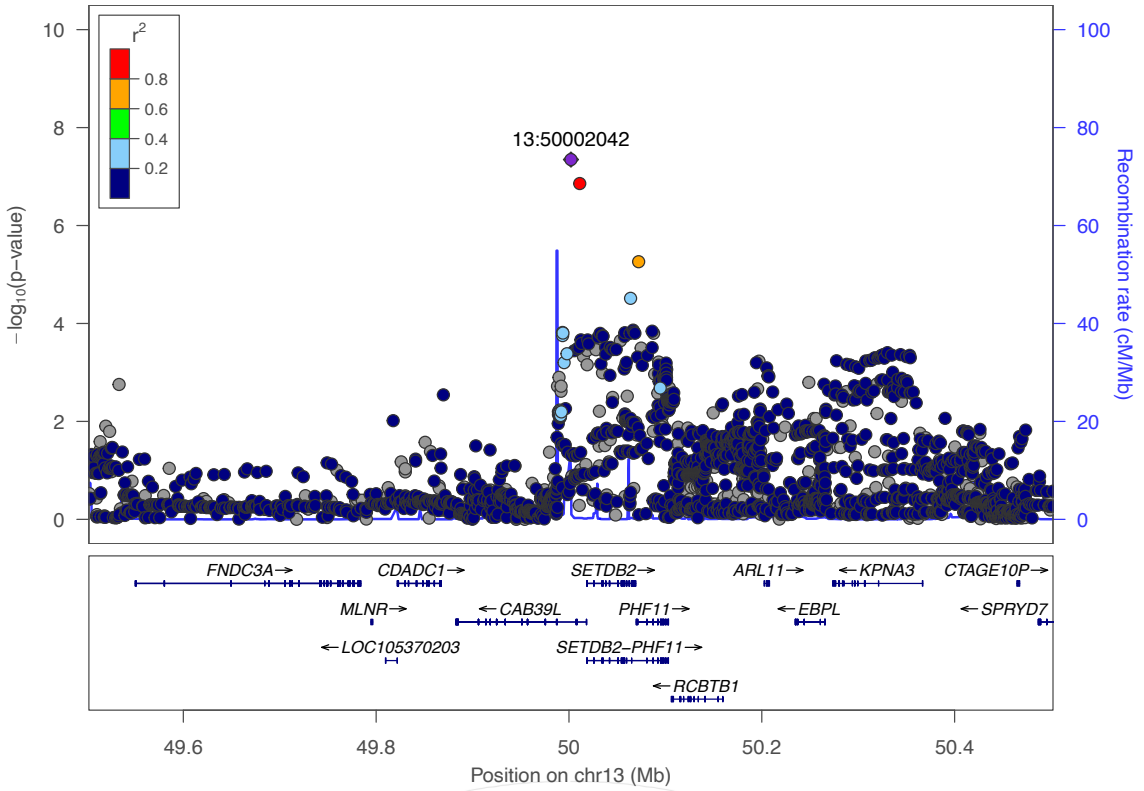

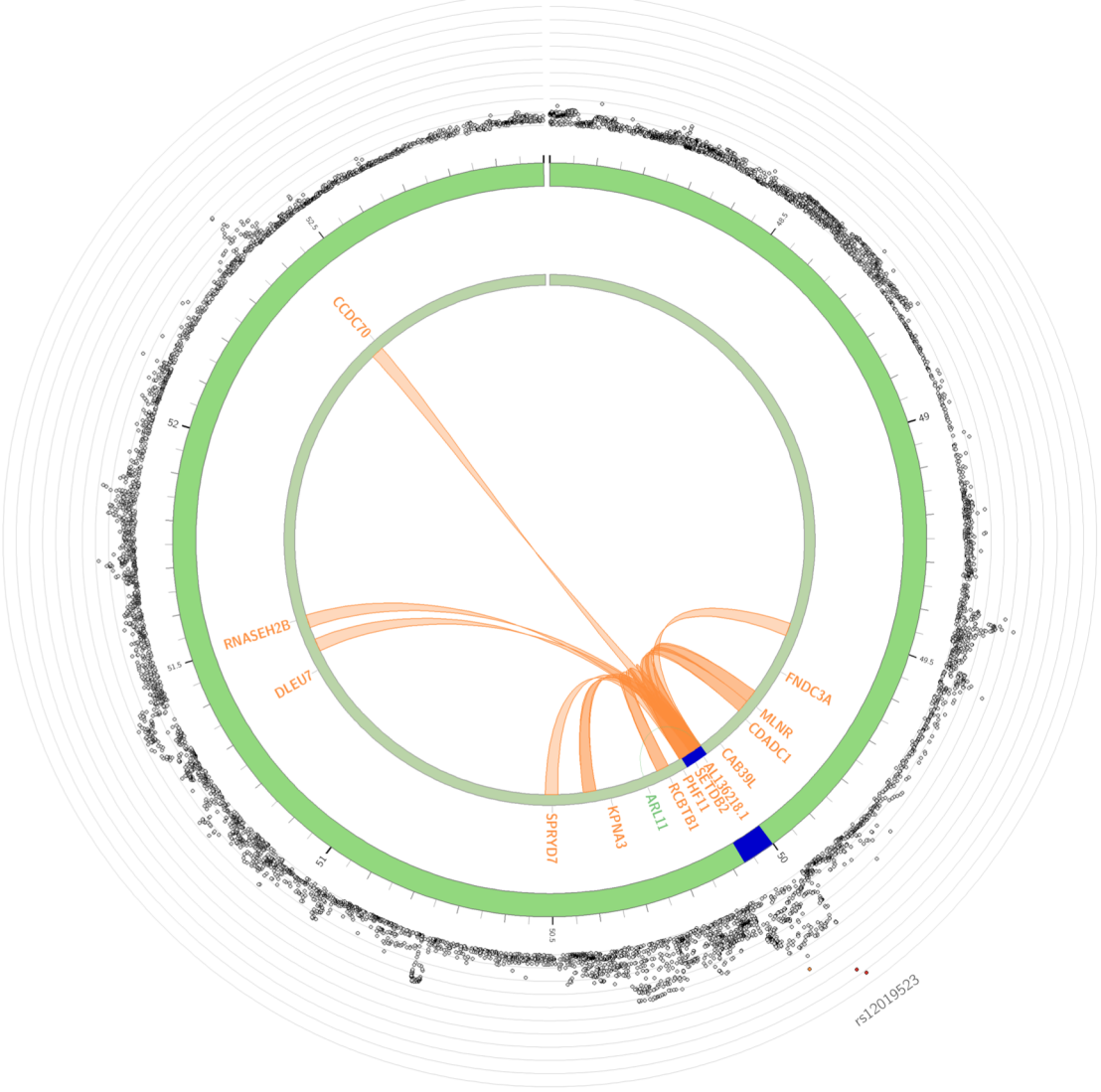

Supplementary Figure 2H: Locusplots (top), eQTL and chromatin interaction mapping (bottom) for genome-wide significant SNP rs12019523; change rate caudate; quadratic age dependency. Locus plots were created with locus zoom[98]. Circos plots were created with FUMA[66].

2I

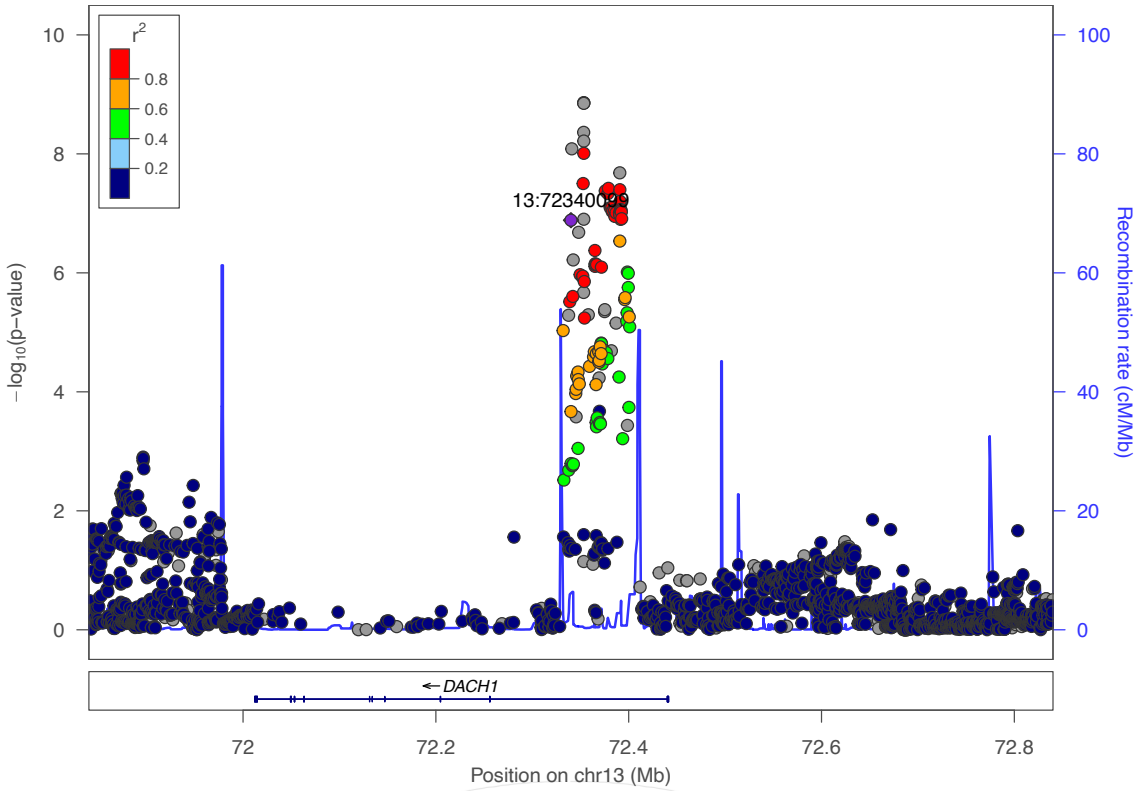

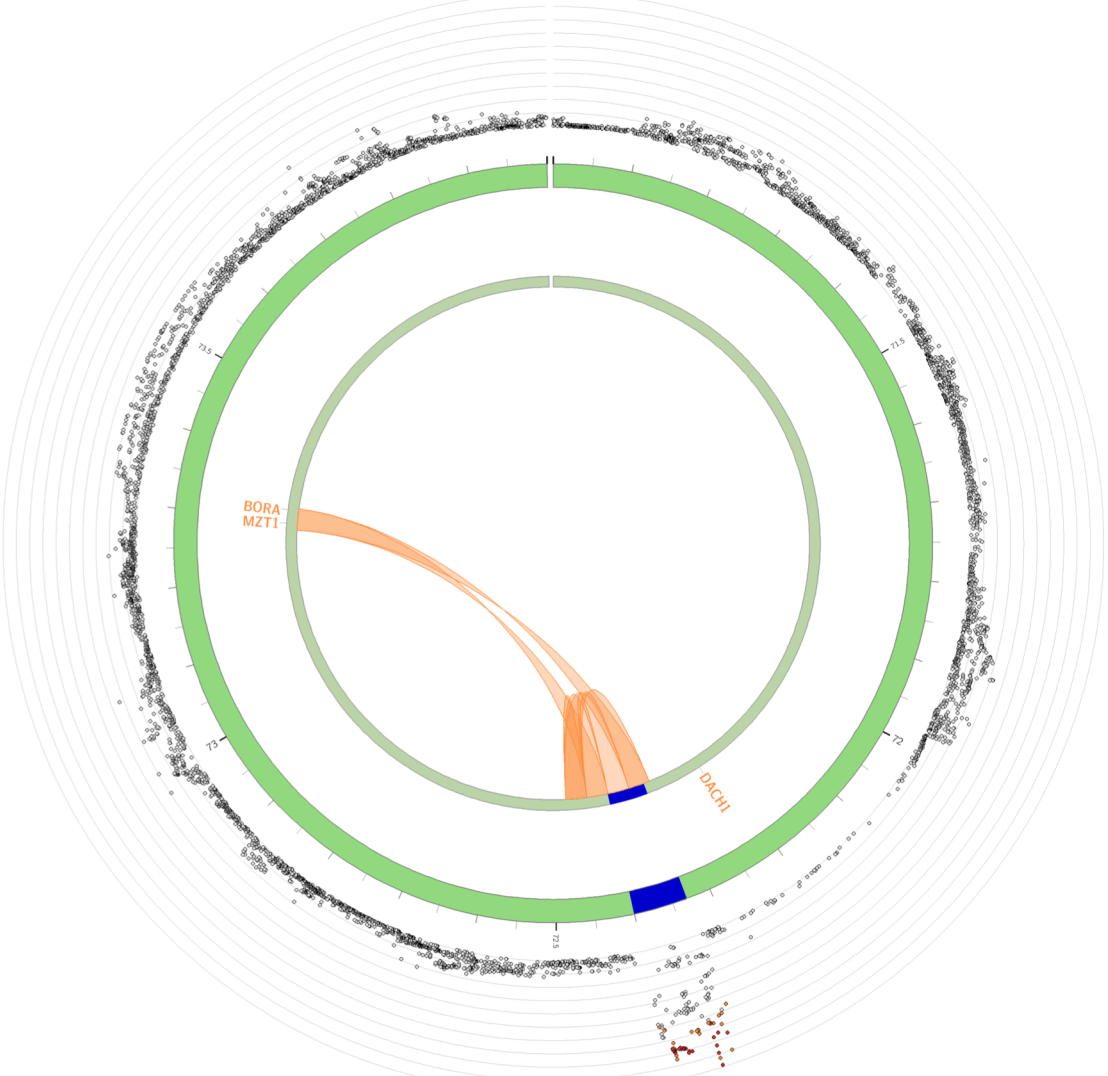

Supplementary Figure 2I: Locusplots (top), eQTL and chromatin interaction mapping (bottom) for genome-wide significant SNP 13:72353395; change rate cerebral white matter volume; quadratic age dependency; note that this SNP was not in the reference dataset containing LD structure; displayed LD structure is based on 13:7234009, R2 = 0.87 with the top-SNP. Locus plots were created with locus zoom[98]. Circos plots were created with FUMA[66].

2J

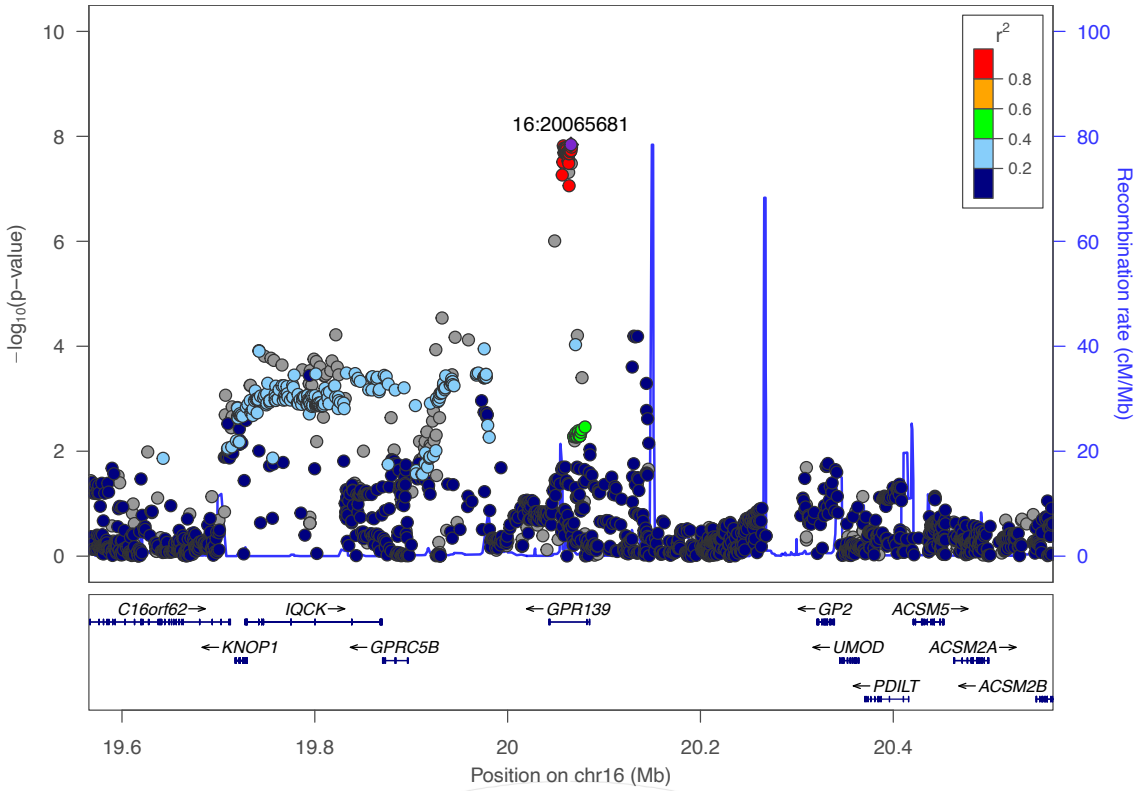

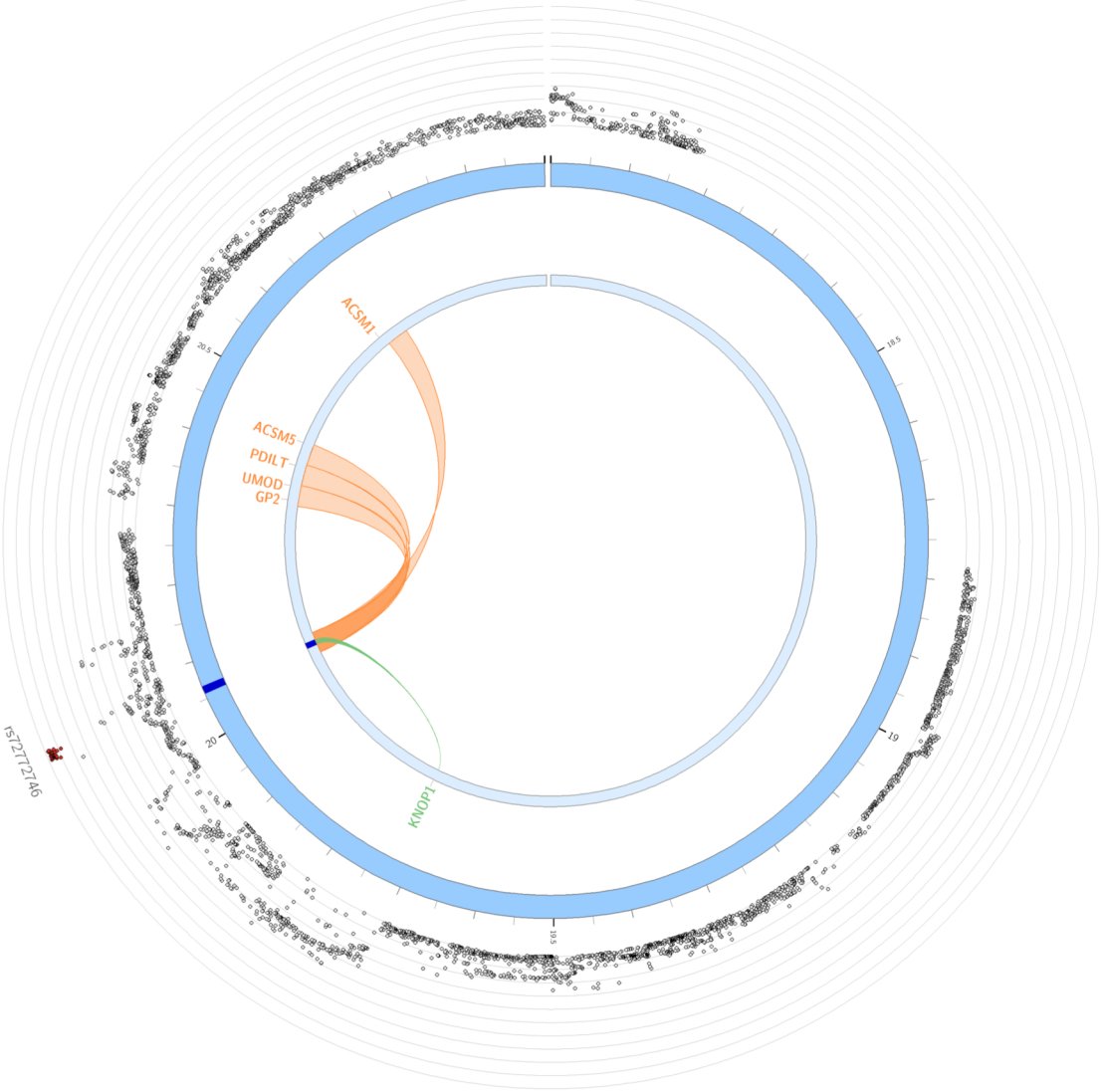

Supplementary Figure 2J: Locusplots (top), eQTL and chromatin interaction mapping (bottom) for genome-wide significant SNP rs72772746; change rate lateral ventricles; independent of age. Locus plots were created with locus zoom[98]. Circos plots were created with FUMA[66].

2K

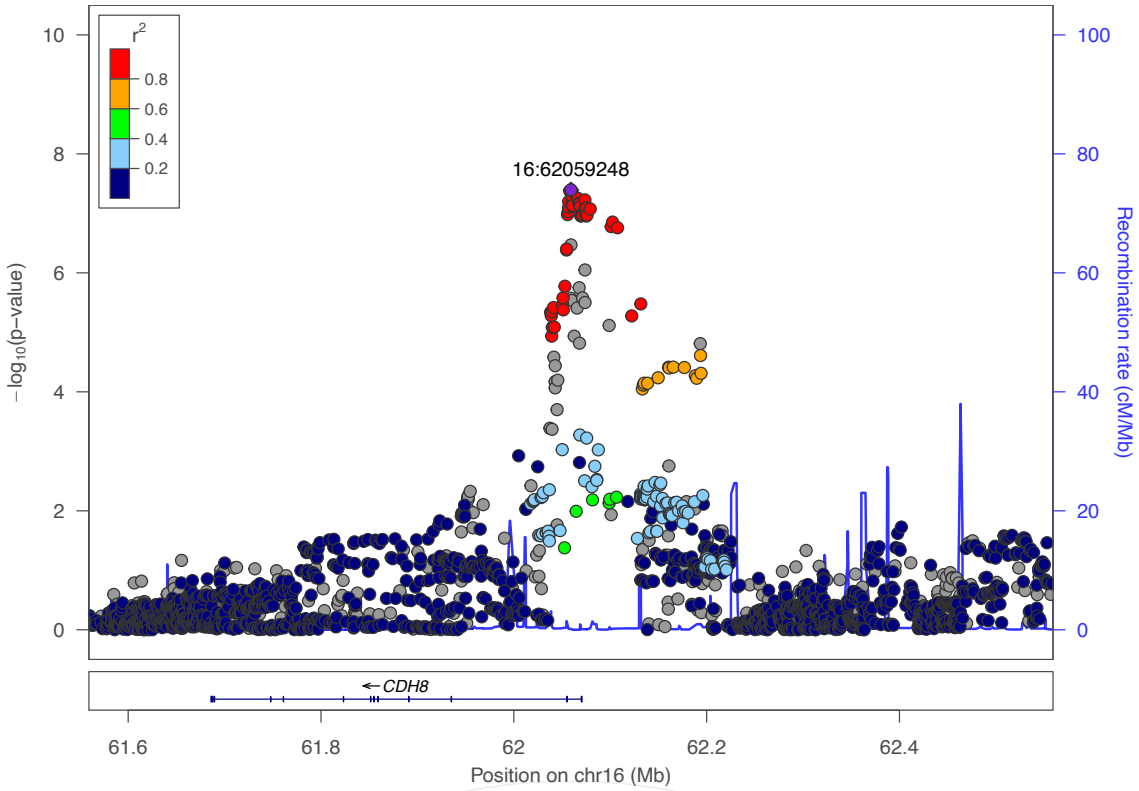

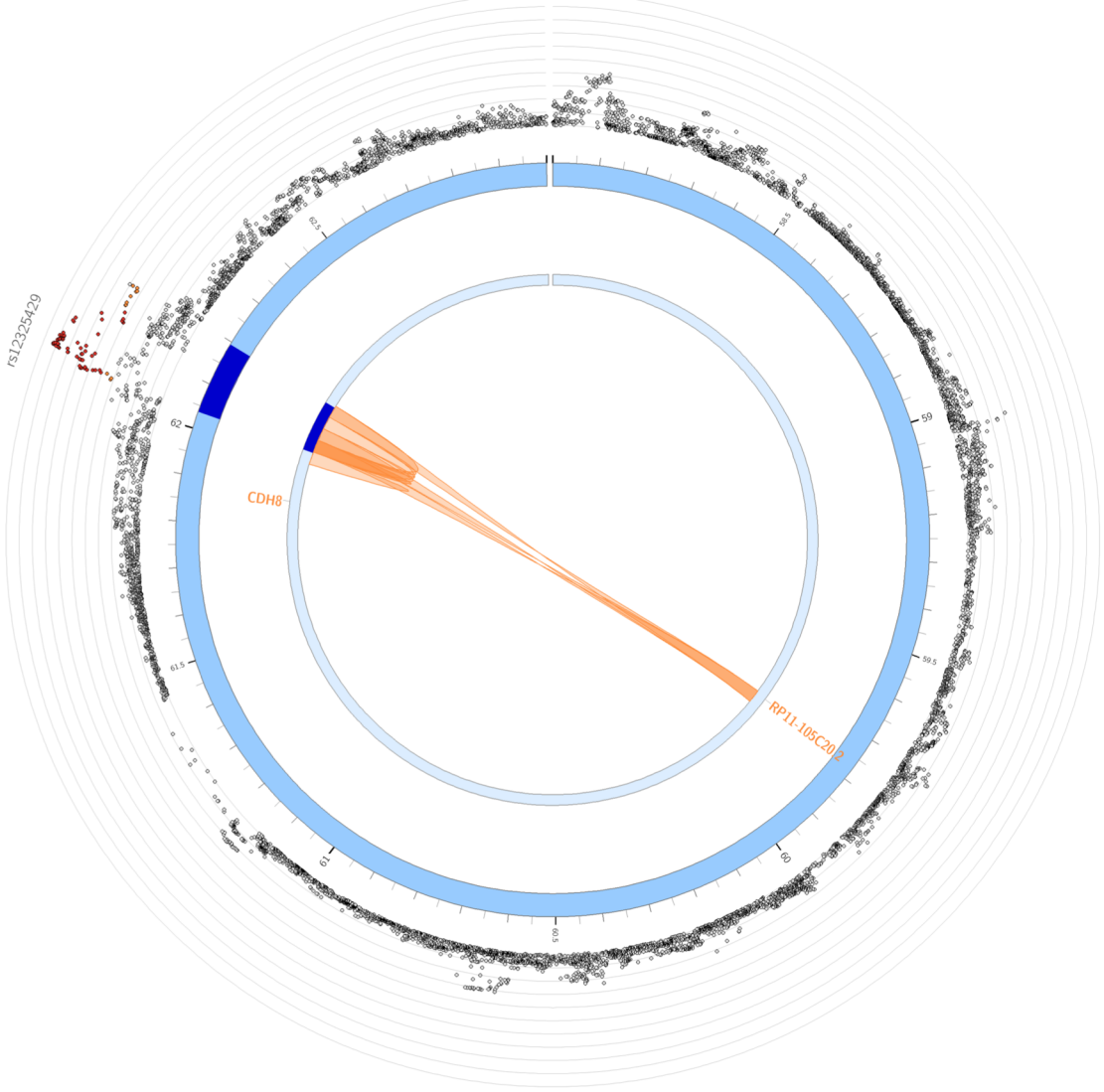

Supplementary Figure 2K: Locusplots (top), eQTL and chromatin interaction mapping (bottom) for genome-wide significant SNP rs12325429; change rate total brain volume; independent of age. Locus plots were created with locus zoom[98]. Circos plots were created with FUMA[66].

2L

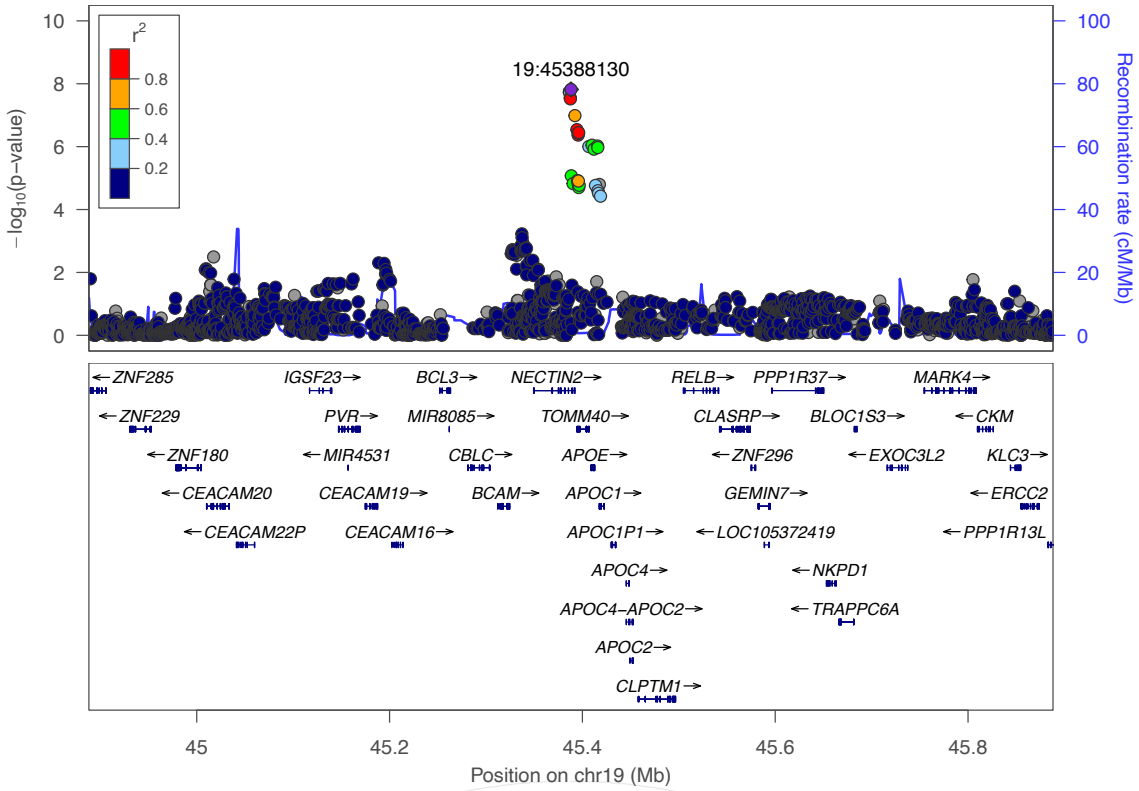

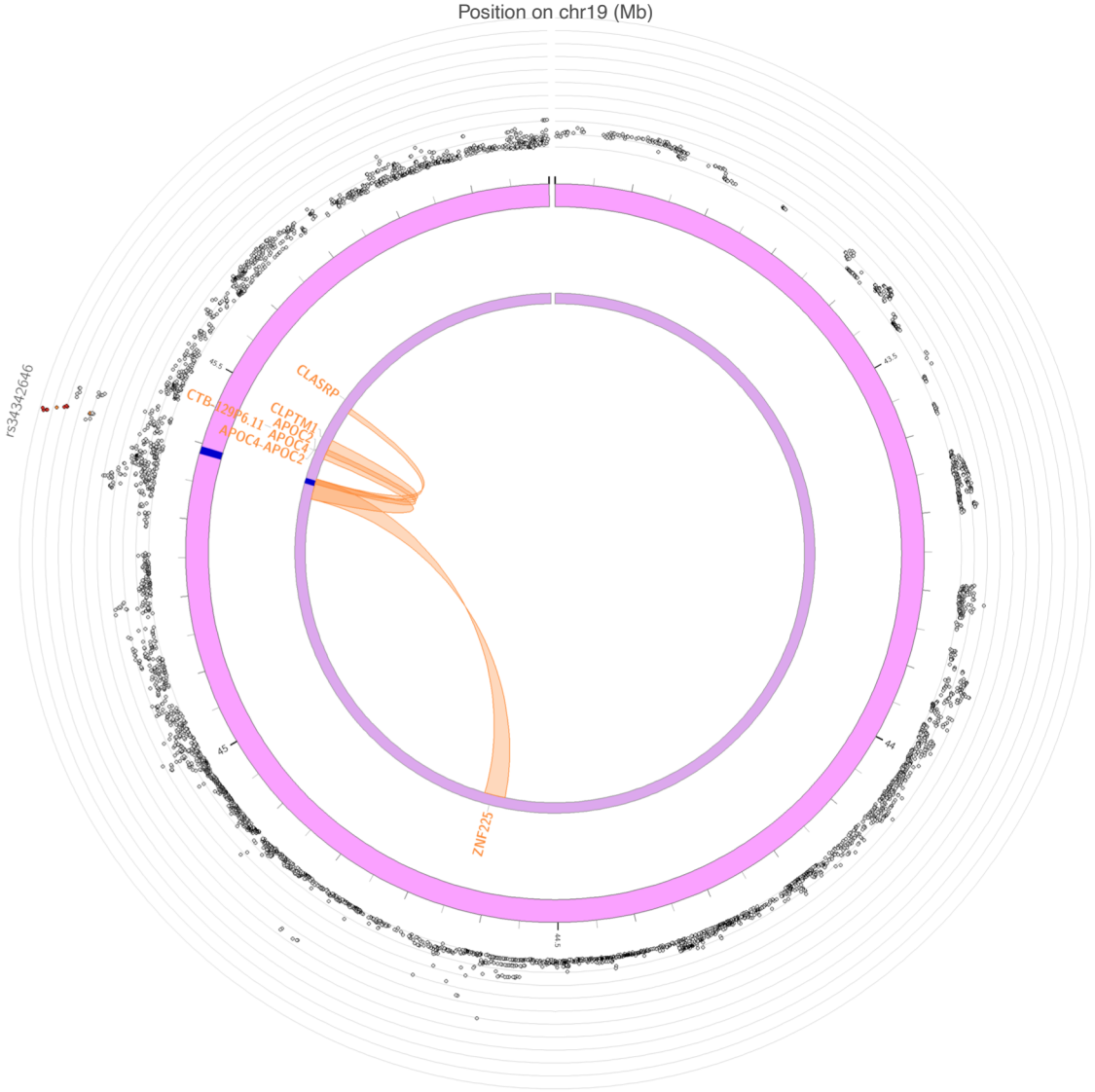

Supplementary Figure 2L: Locusplots (top), eQTL and chromatin interaction mapping (bottom) for genome-wide significant SNP rs34342646; change rate surface area; quadratic age dependency. Locus plots were created with locus zoom[98]. Circos plots were created with FUMA[66].

2M

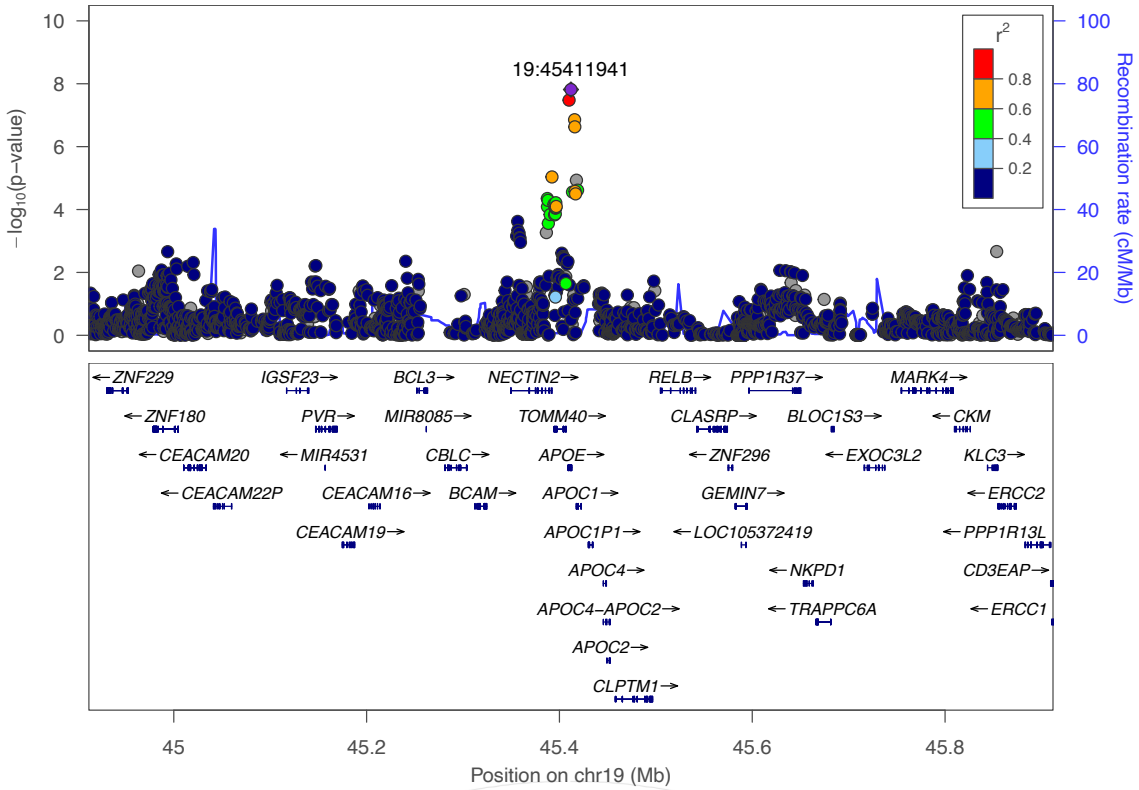

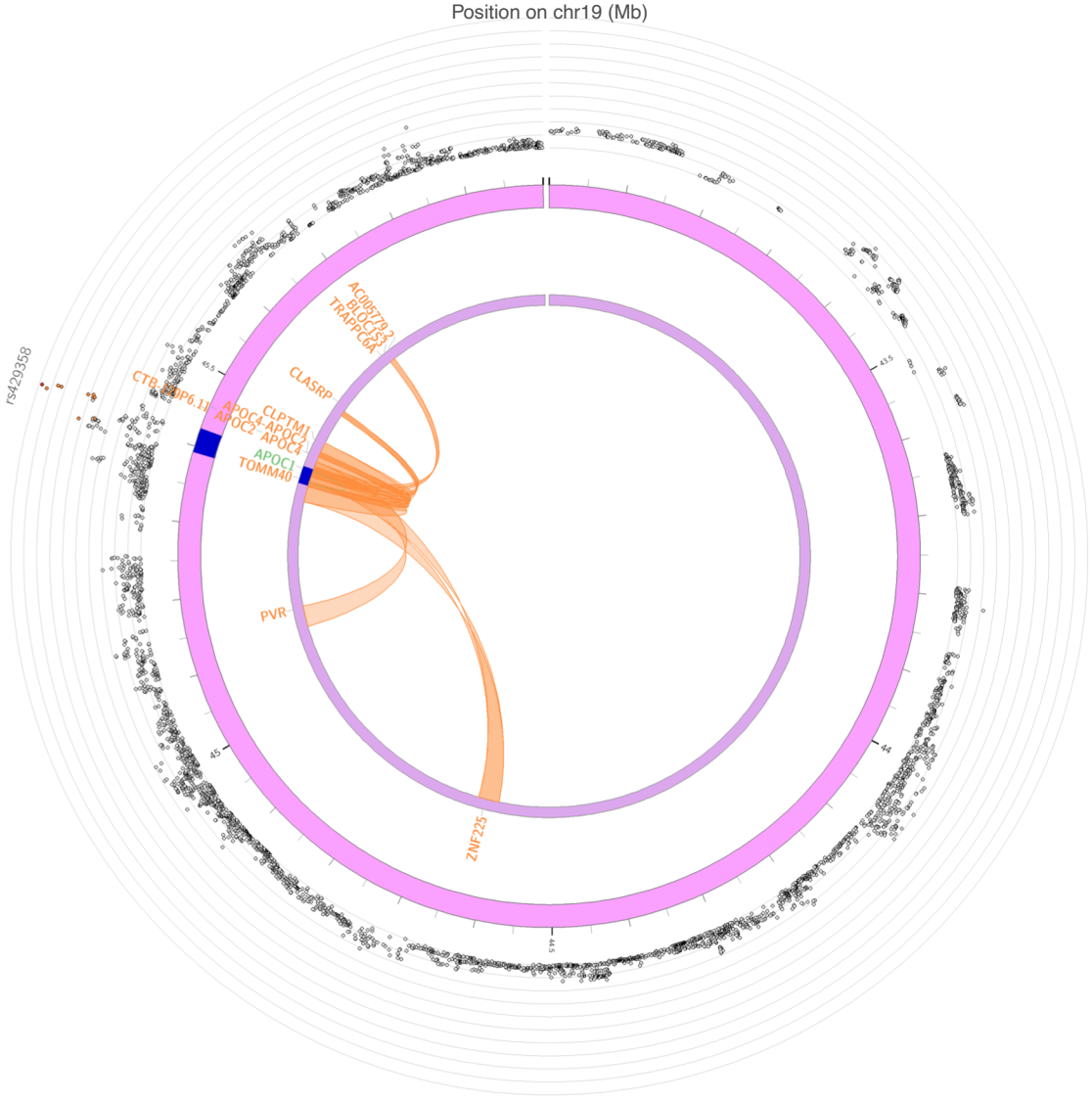

Supplementary Figure 2M: Locusplots (top), eQTL and chromatin interaction mapping (bottom) for genome-wide significant SNP rs429358; change rate hippocampus; quadratic age dependency. Locus plots were created with locus zoom[98]. Circos plots were created with FUMA[66].

3A

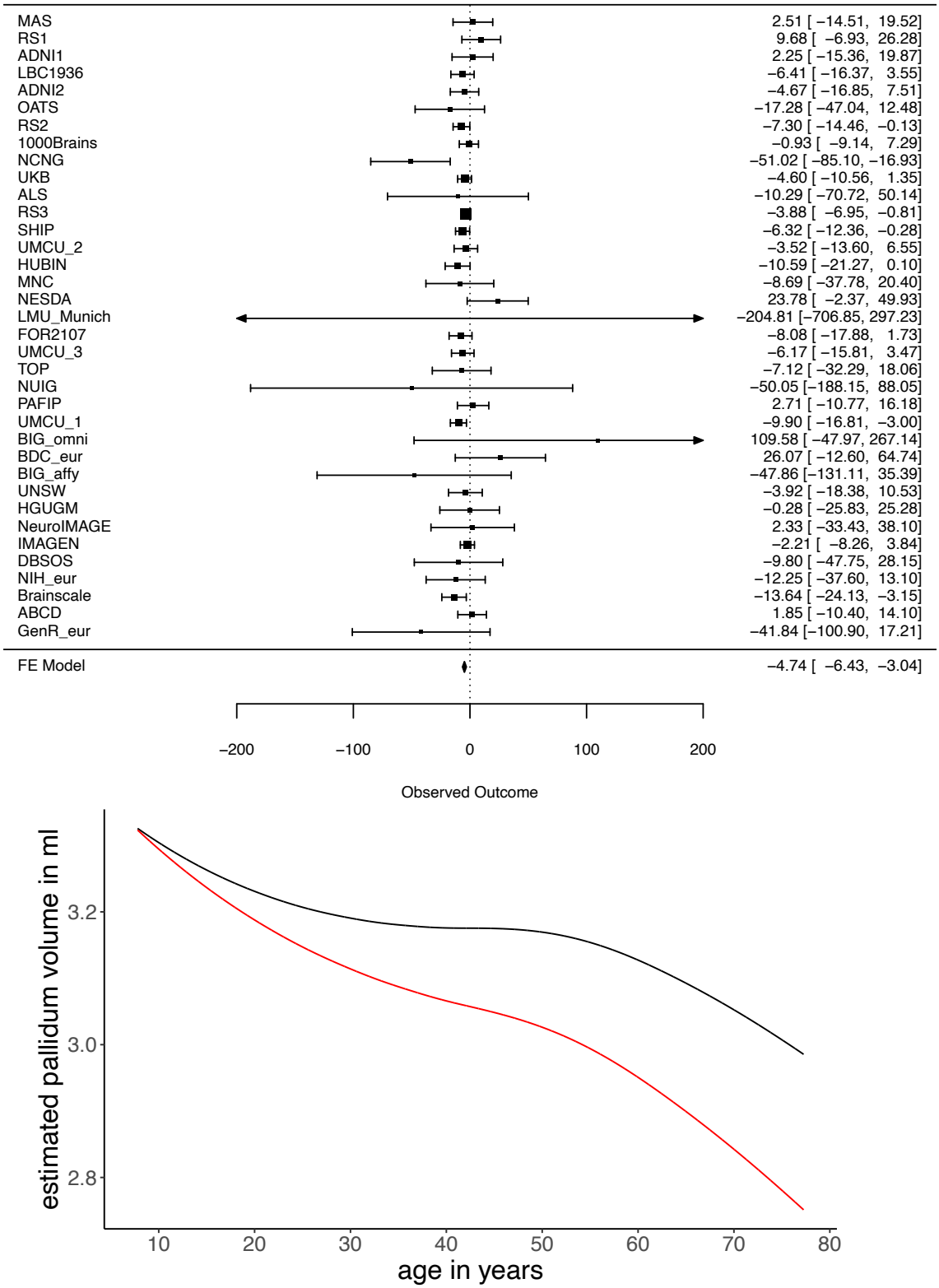

Supplementary Figure 3A: Age-independent effect of the significant SNPs/top-SNPs in significant genes. 3A) rs1425034; change rate pallidum; independent of age; total N = 14760. The top figure displays a forest-plot in which means and 95% confidence intervals are displayed for each cohort. Confidence intervals that are outside the axis of the plot are marked with an arrow. The bottom figure shows a visualization of the effect of the tested allele on the phenotype itself. The red line represents the lifespan trajectory for the carriers of the effect allele, the black line represents the lifespan trajectory of the non-carriers.

3B

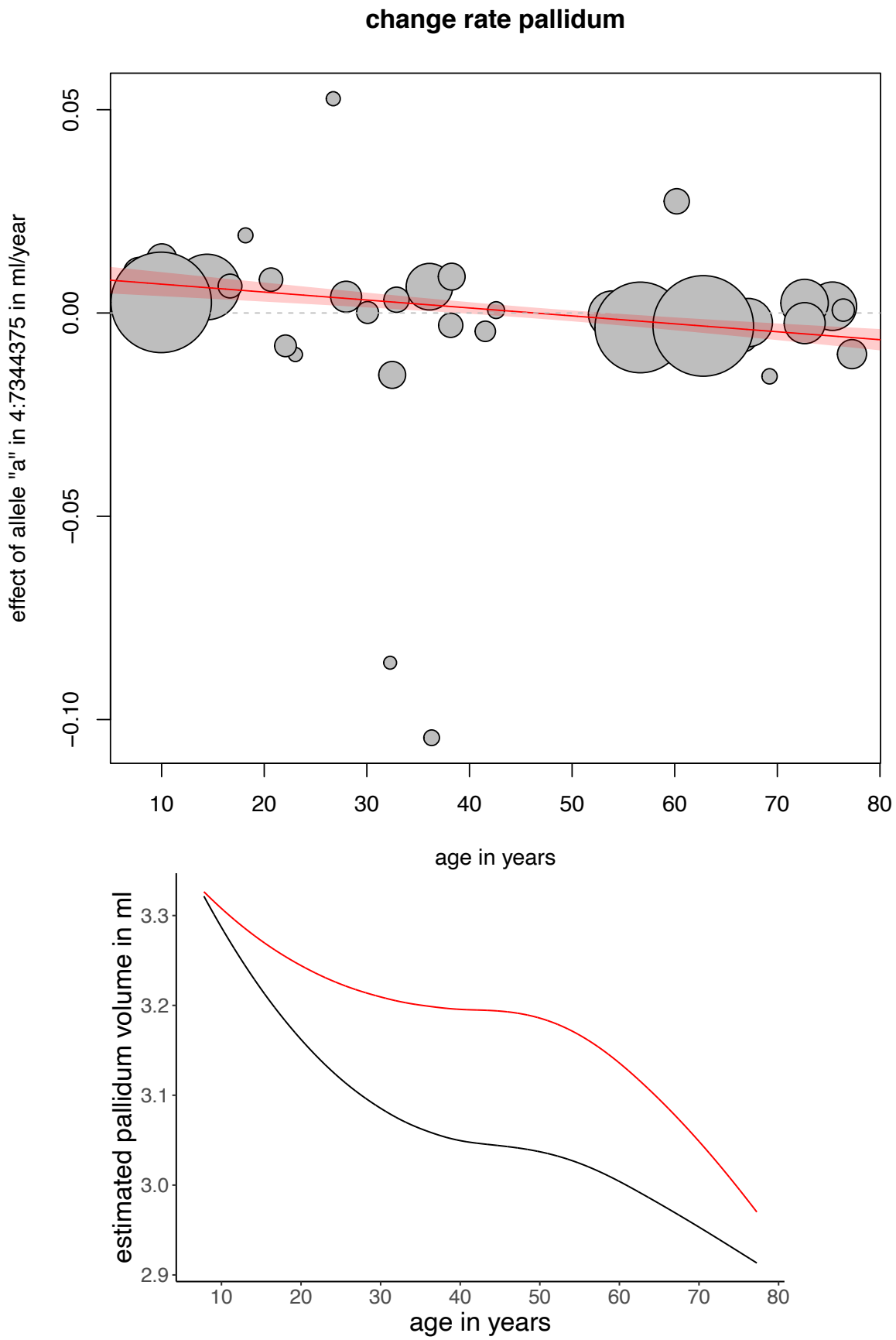

Supplementary Figure 3B: Age-dependent effect of the significant SNPs/top-SNPs in significant genes. 3B) rs73210410; change rate pallidum; linear age dependency; total N = 14760. The top figure displays the estimated effect of the tested allele on the change rate in each cohort against age. The center of the circles represent the effect size of the tested allele for each cohort, the radius of the circles are proportional to sample size. The red line displays the estimated age-effect with 95% confidence interval from the meta analysis/meta-regression. The bottom figure shows a visualization of the effect of the tested allele on the phenotype itself. The red line represents the lifespan trajectory for the carriers of the effect allele, the black line represents the lifespan trajectory of the non-carriers.

3C

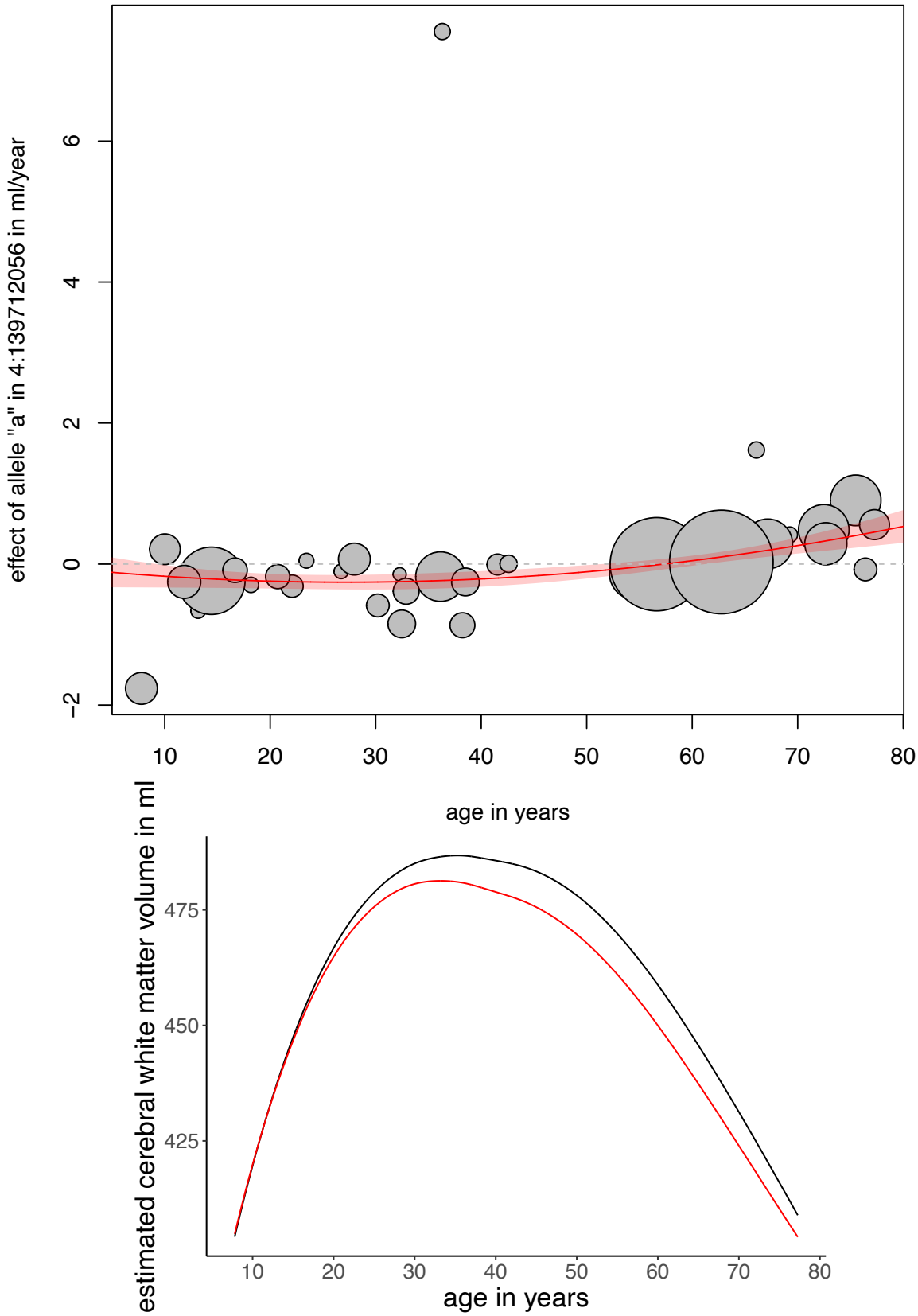

Supplementary Figure 3C: Age-dependent effect of the significant SNPs/top-SNPs in significant genes. 3C) rs11726181; change rate cerebral white matter; quadratic age dependency; total N = 12377. The top figure displays the estimated effect of the tested allele on the change rate in each cohort against age. The center of the circles represent the effect size of the tested allele for each cohort, the radius of the circles are proportional to sample size. The red line displays the estimated age-effect with 95% confidence interval from the meta analysis/meta-regression. The bottom figure shows a visualization of the effect of the tested allele on the phenotype itself. The red line represents the lifespan trajectory for the carriers of the effect allele, the black line represents the lifespan trajectory of the non-carriers.

3D

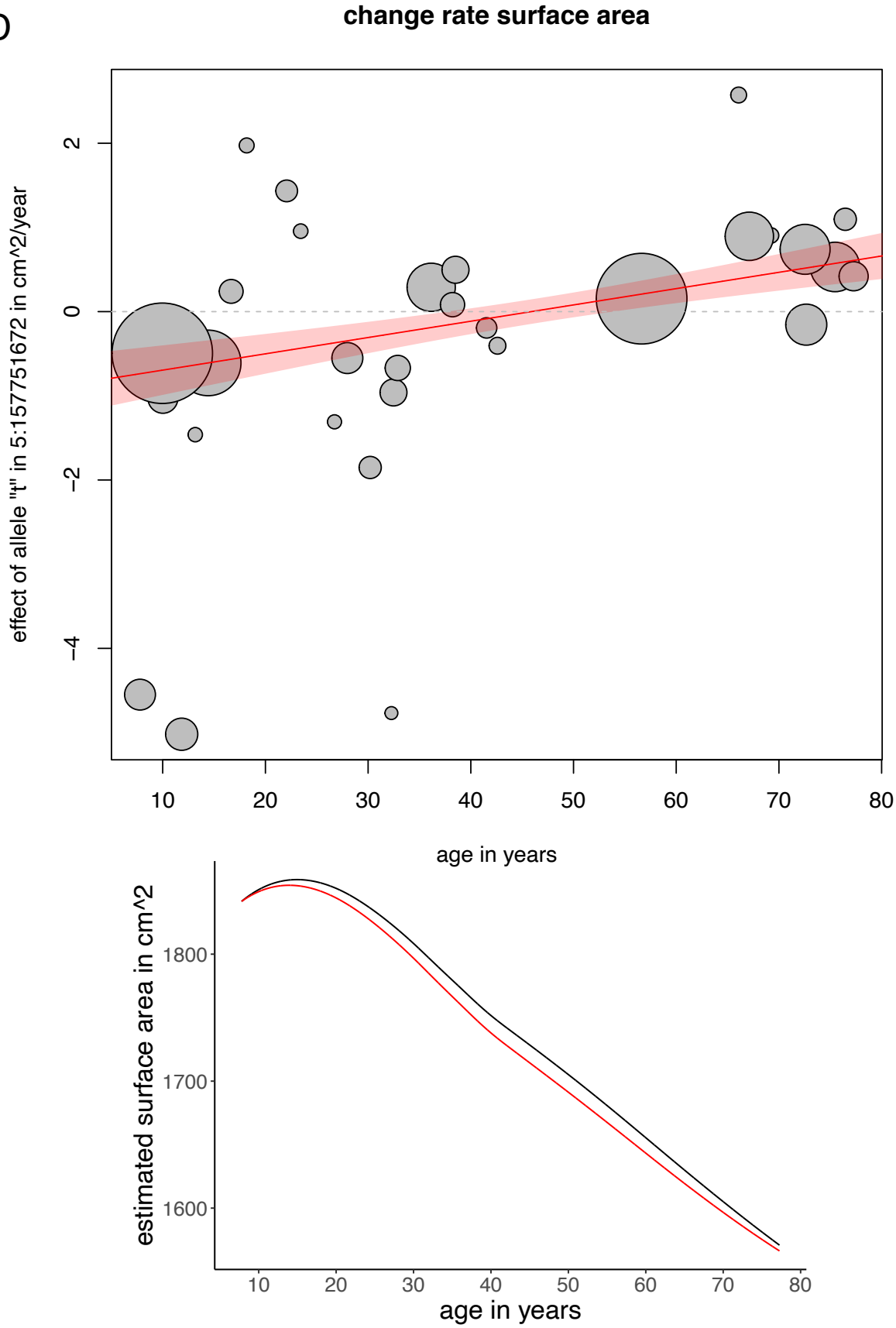

Supplementary Figure 3D: Age-dependent effect of the significant SNPs/top-SNPs in significant genes. 3D) 5:157751672; change rate surface area, linear age dependency*; total N = 11346. The top figure displays the estimated effect of the tested allele on the change rate in each cohort against age. The center of the circles represent the effect size of the tested allele for each cohort, the radius of the circles are proportional to sample size. The red line displays the estimated age-effect with 95% confidence interval from the meta analysis/meta-regression. The bottom figure shows a visualization of the effect of the tested allele on the phenotype itself. The red line represents the lifespan trajectory for the carriers of the effect allele, the black line represents the lifespan trajectory of the non-carriers. This SNP was not present in the LD database or cross-sectional GWAS, bottom figure was created assuming no effect of the variant on volume itself.

3E

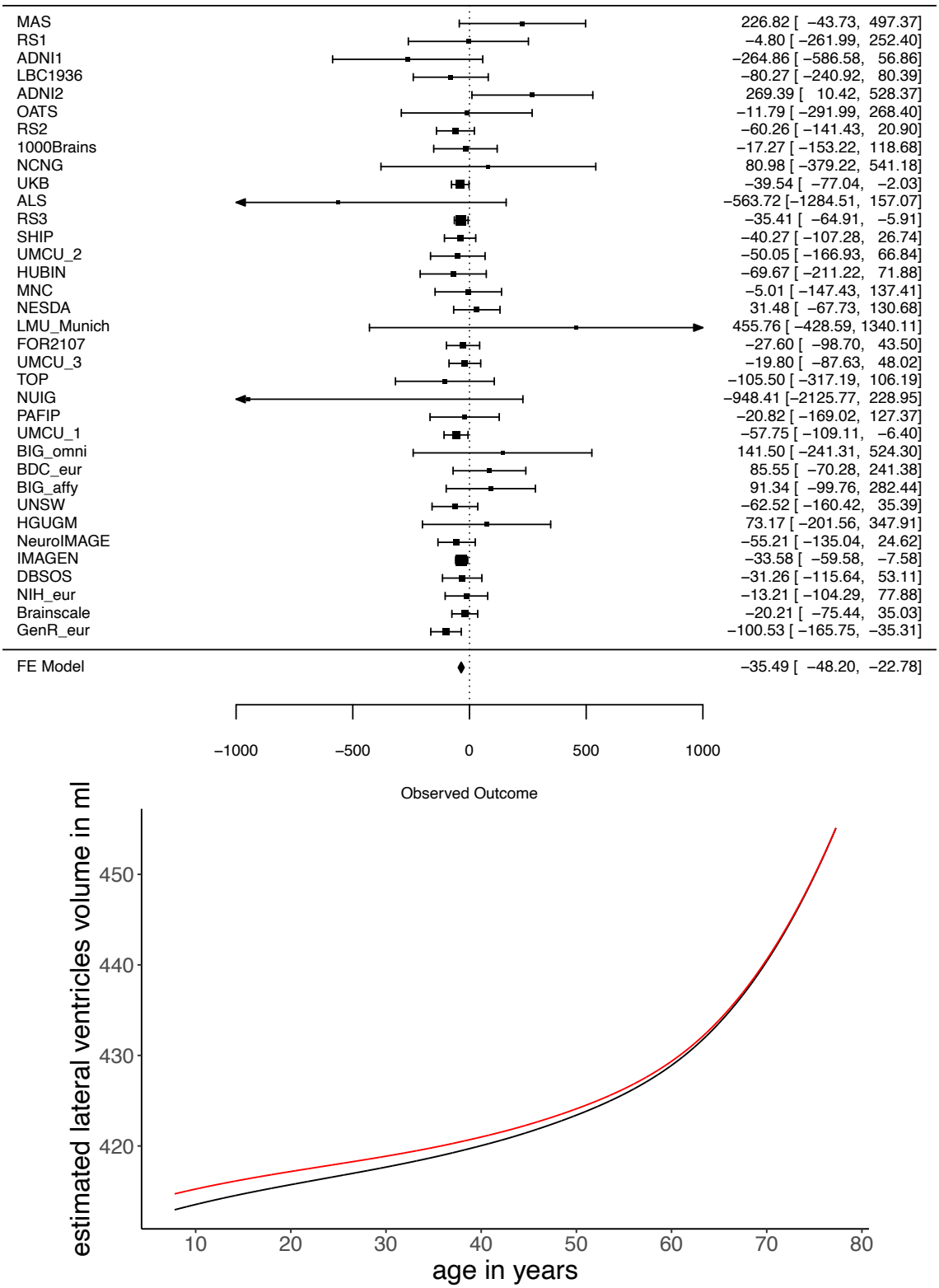

Supplementary Figure 3E: Age-independent effect of the significant SNPs/top-SNPs in significant genes. 3E) rs10990953; change rate ventricles; independent of age; total N = 12486. The top figure displays a forest-plot in which means and 95% confidence intervals are displayed for each cohort. Confidence intervals that are outside the axis of the plot are marked with an arrow. The bottom figure shows a visualization of the effect of the tested allele on the phenotype itself. The red line represents the lifespan trajectory for the carriers of the effect allele, the black line represents the lifespan trajectory of the non-carriers.

3F

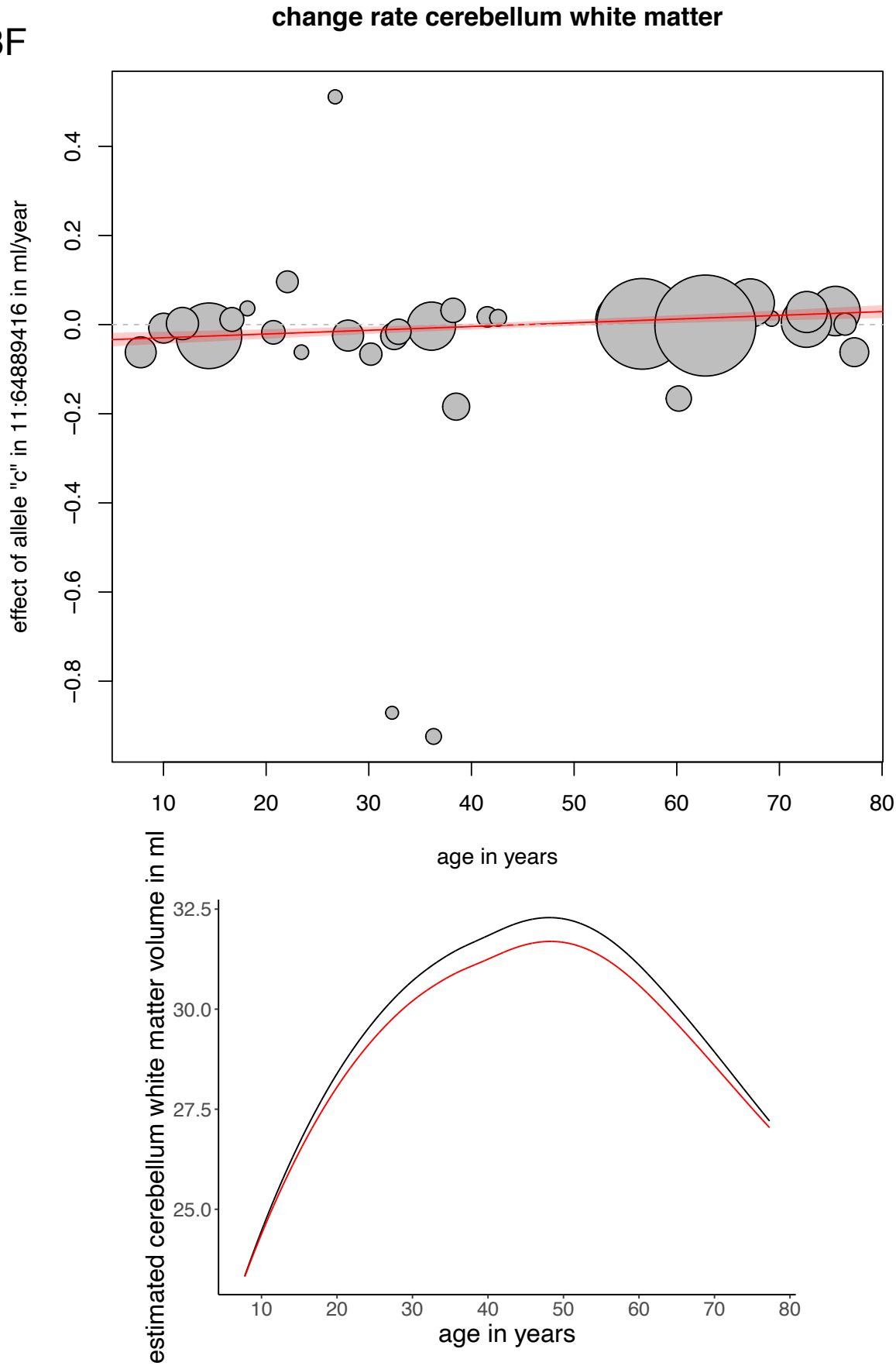

Supplementary Figure 3F: Age-dependent effect of the significant SNPs/top-SNPs in significant genes. 3F) FAU – top SNP rs769440 change rate cerebellum white matter; linear age dependency; total N = 12527. The top figure displays the estimated effect of the tested allele on the change rate in each cohort against age. The center of the circles represent the effect size of the tested allele for each cohort, the radius of the circles are proportional to sample size. The red line displays the estimated age-effect with 95% confidence interval from the meta analysis/meta-regression. The bottom figure shows a visualization of the effect of the tested allele on the phenotype itself. The red line represents the lifespan trajectory for the carriers of the effect allele, the black line represents the lifespan trajectory of the non-carriers.

3G

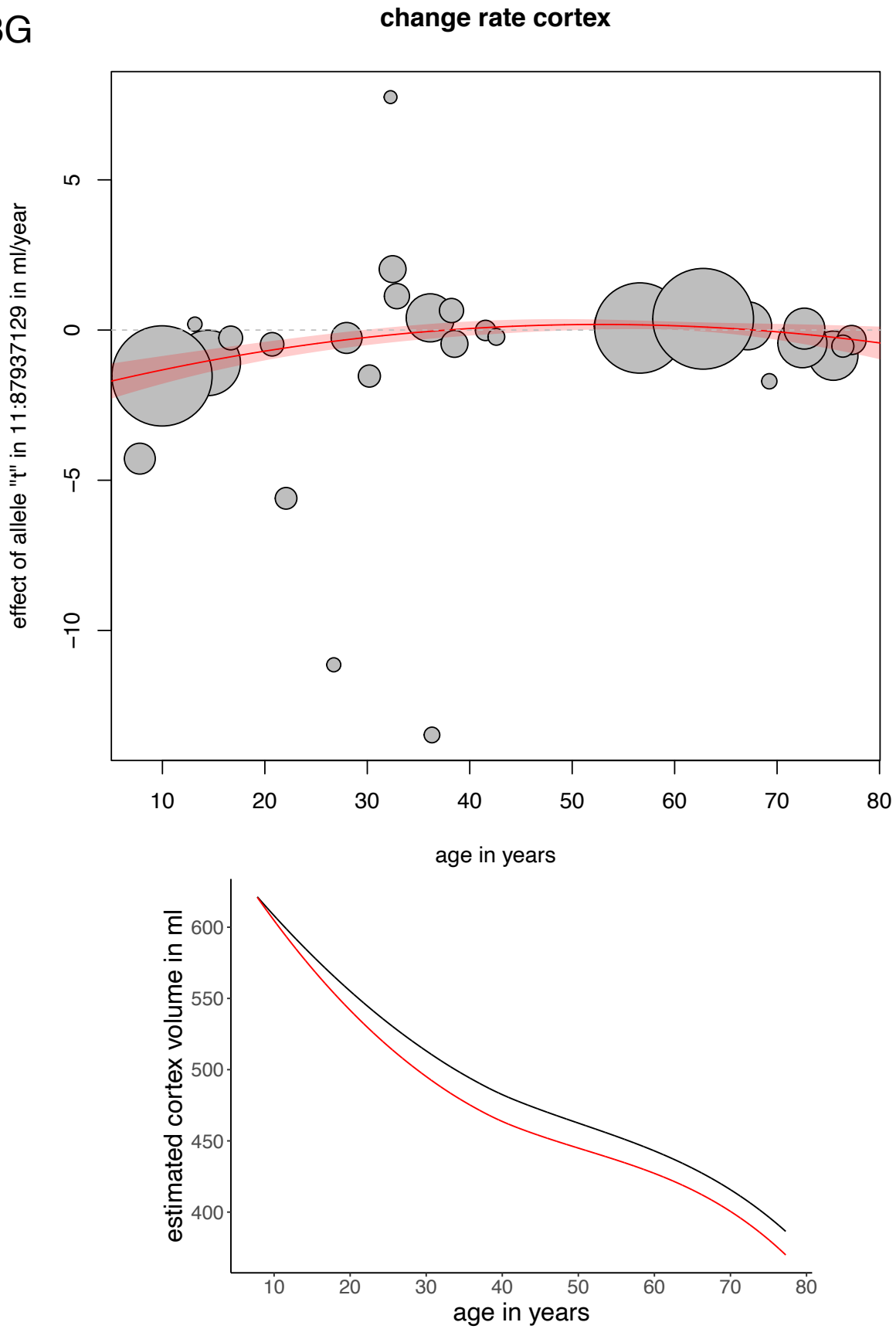

Supplementary Figure 3G: Age-dependent effect of the significant SNPs/top-SNPs in significant genes. 3G) rs17809993; change rate cortex volume quadratic age dependency; total N = 14758. The top figure displays the estimated effect of the tested allele on the change rate in each cohort against age. The center of the circles represent the effect size of the tested allele for each cohort, the radius of the circles are proportional to sample size. The red line displays the estimated age-effect with 95% confidence interval from the meta analysis/meta-regression. The bottom figure shows a visualization of the effect of the tested allele on the phenotype itself. The red line represents the lifespan trajectory for the carriers of the effect allele, the black line represents the lifespan trajectory of the non-carriers.

3H

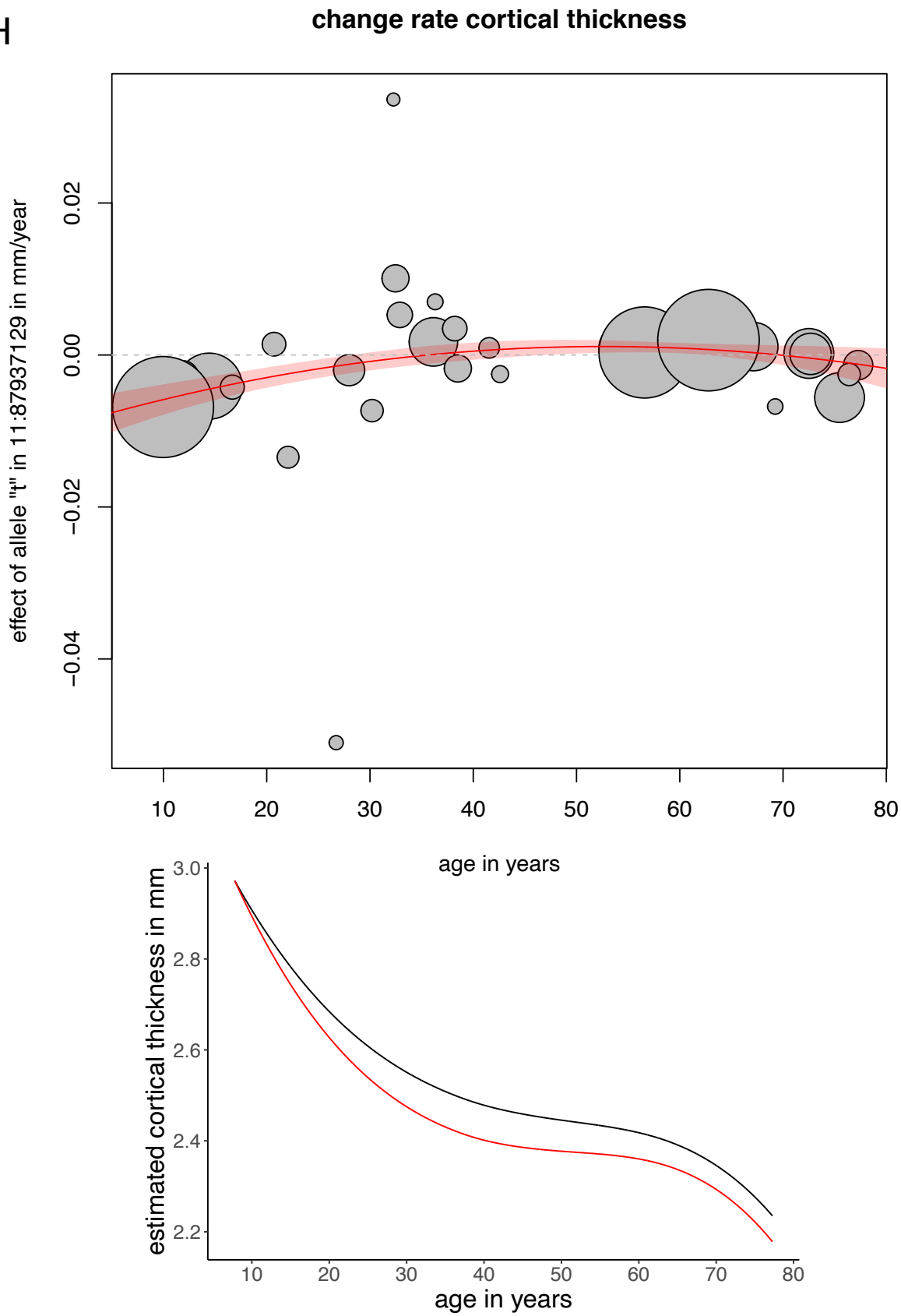

Supplementary Figure 3H: Age-dependent effect of the significant SNPs/top-SNPs in significant genes. 3H) rs17809993; change rate cortical thickness; quadratic age dependency; total N = 14769. The top figure displays the estimated effect of the tested allele on the change rate in each cohort against age. The center of the circles represent the effect size of the tested allele for each cohort, the radius of the circles are proportional to sample size. The red line displays the estimated age-effect with 95% confidence interval from the meta analysis/meta-regression. The bottom figure shows a visualization of the effect of the tested allele on the phenotype itself. The red line represents the lifespan trajectory for the carriers of the effect allele, the black line represents the lifespan trajectory of the non-carriers.

3I

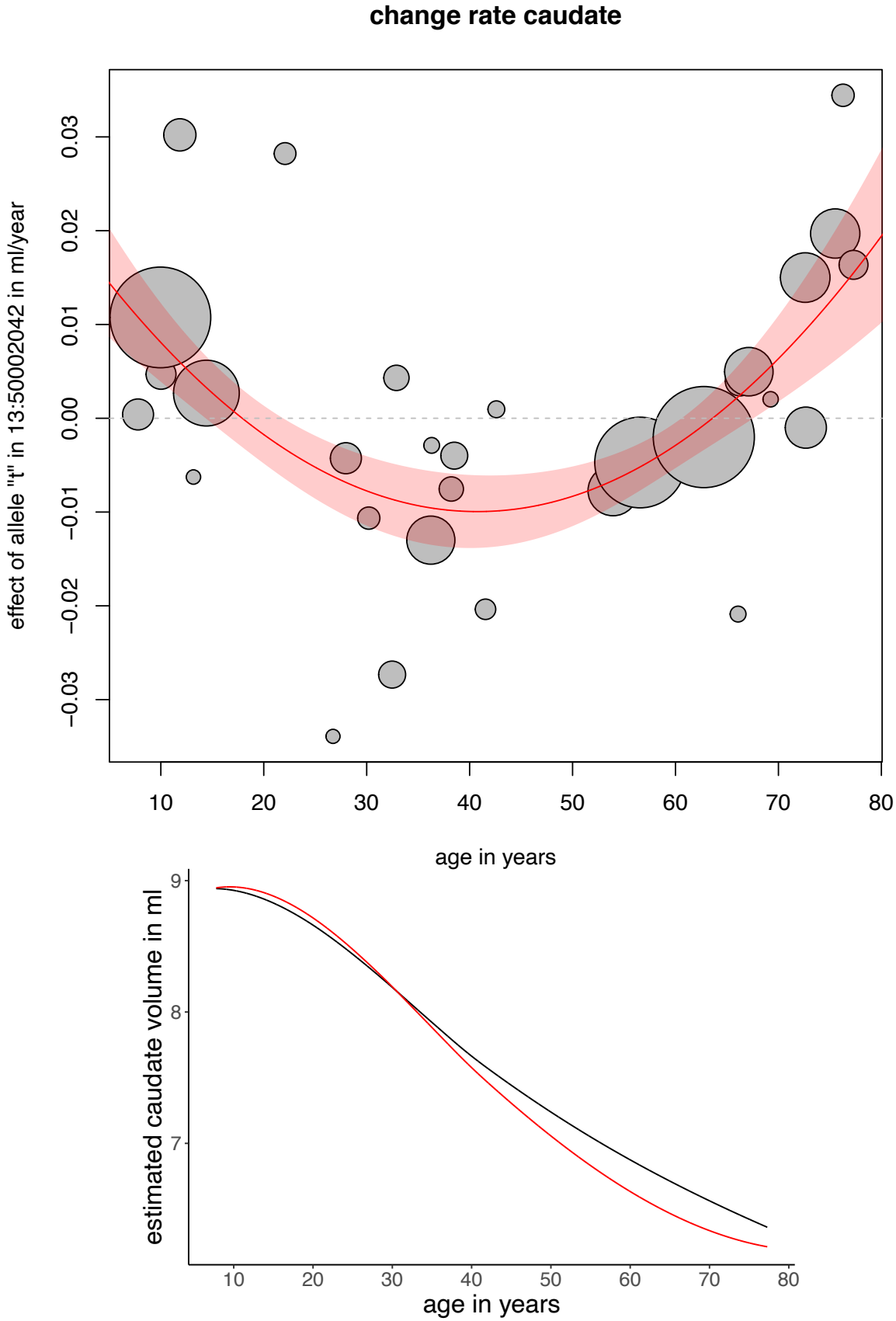

Supplementary Figure 3I: Age-dependent effect of the significant SNPs/top-SNPs in significant genes. 3I) rs12019523; change rate caudate; quadratic age dependency; total N = 14372. The top figure displays the estimated effect of the tested allele on the change rate in each cohort against age. The center of the circles represent the effect size of the tested allele for each cohort, the radius of the circles are proportional to sample size. The red line displays the estimated age-effect with 95% confidence interval from the meta analysis/meta-regression. The bottom figure shows a visualization of the effect of the tested allele on the phenotype itself. The red line represents the lifespan trajectory for the carriers of the effect allele, the black line represents the lifespan trajectory of the non-carriers.

3J

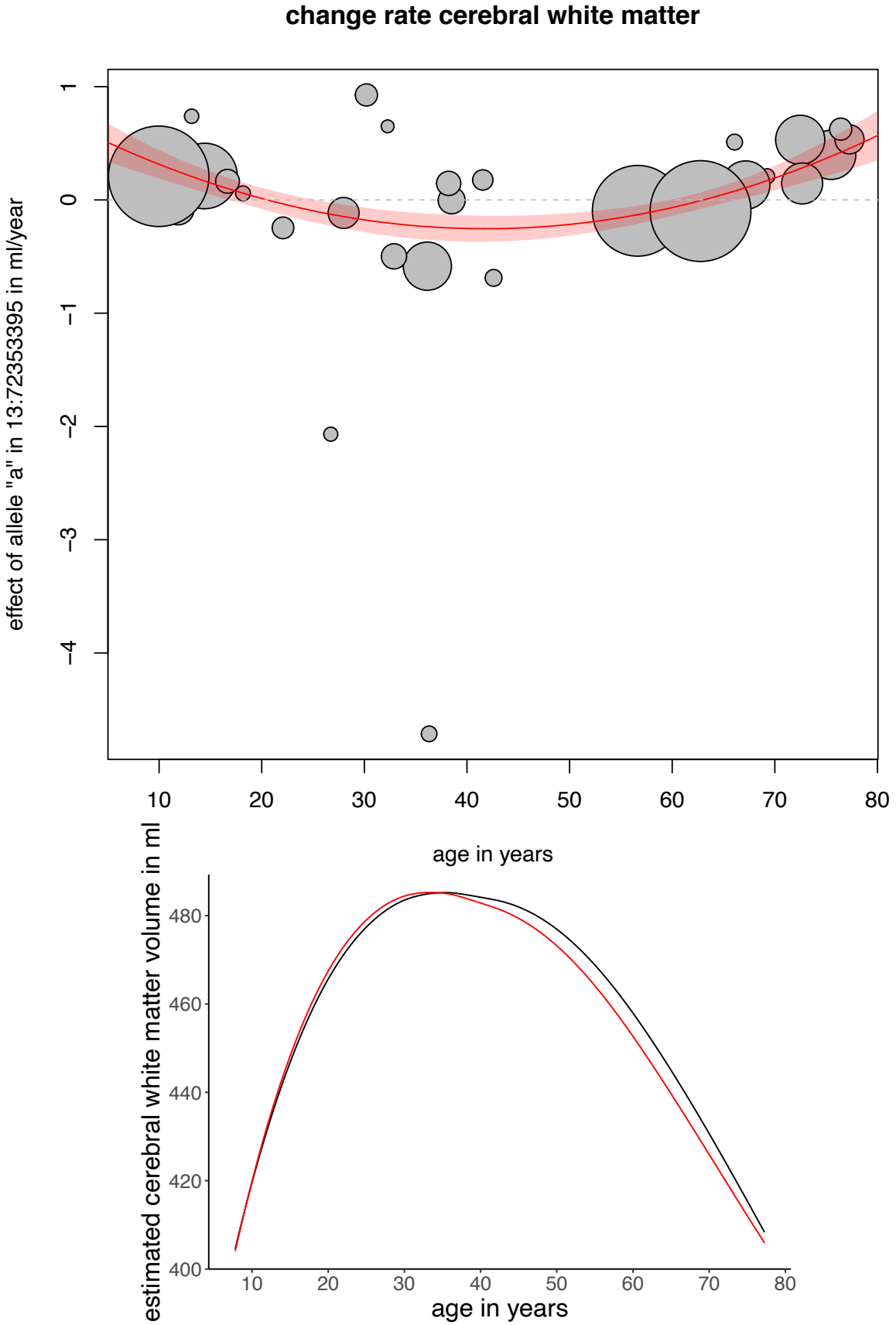

Supplementary Figure 3J: Age-dependent effect of the significant SNPs/top-SNPs in significant genes. 3J) DACH1 and 13:72353395; change rate cerebral white matter volume; quadratic age dependency; total N = 13864. The top figure displays the estimated effect of the tested allele on the change rate in each cohort against age. The center of the circles represent the effect size of the tested allele for each cohort, the radius of the circles are proportional to sample size. The red line displays the estimated age-effect with 95% confidence interval from the meta analysis/meta-regression. The bottom figure shows a visualization of the effect of the tested allele on the phenotype itself. The red line represents the lifespan trajectory for the carriers of the effect allele, the black line represents the lifespan trajectory of the non-carriers.

3K

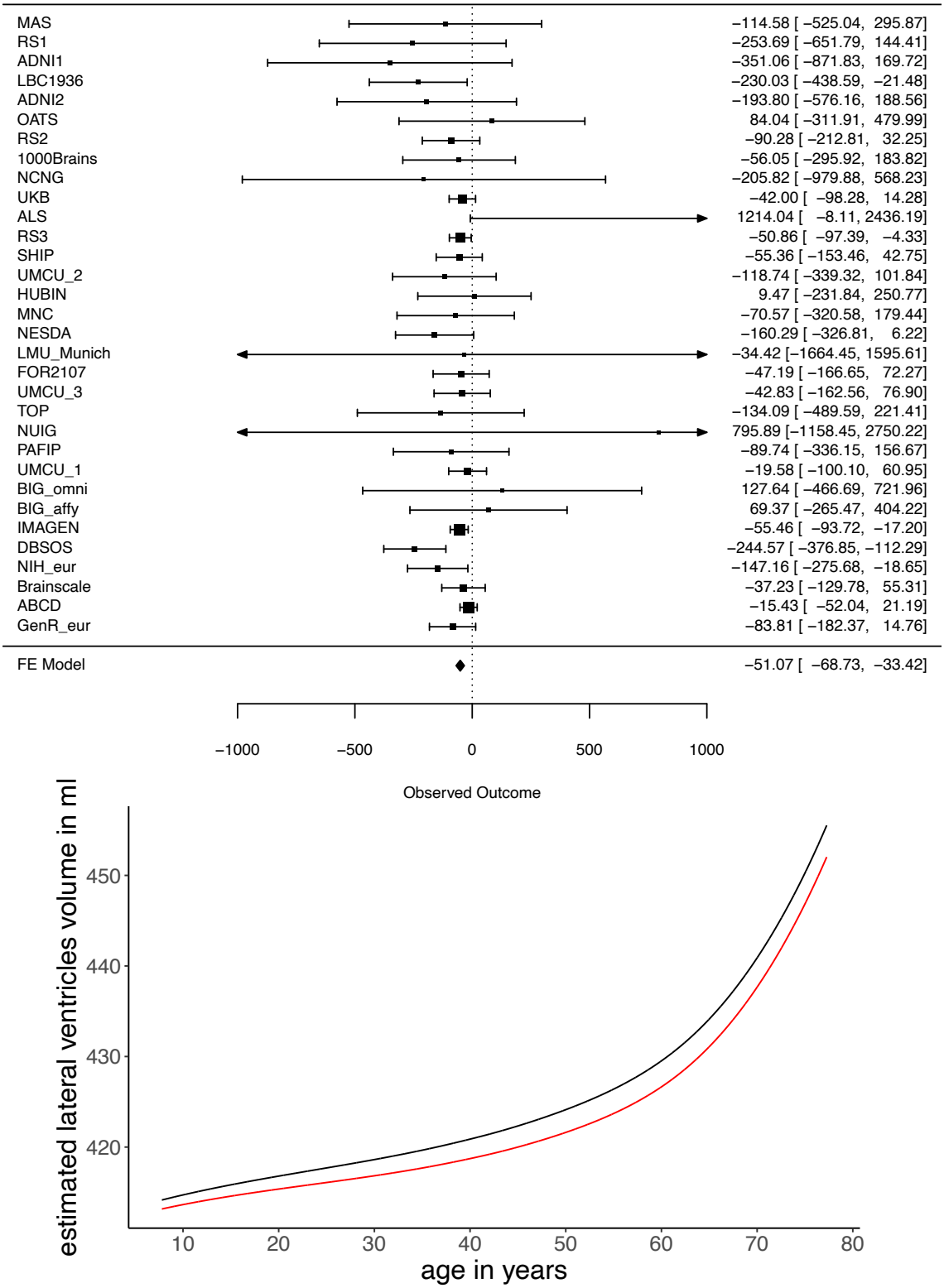

Supplementary Figure 3K: Age-independent effect of the significant SNPs/top-SNPs in significant genes. 3K) GPR139 and rs72772746; change rate lateral ventricles; independent of age; total N = 14593. The top figure displays a forest-plot in which means and 95% confidence intervals are displayed for each cohort. Confidence intervals that are outside the axis of the plot are marked with an arrow. The bottom figure shows a visualization of the effect of the tested allele on the phenotype itself. The red line represents the lifespan trajectory for the carriers of the effect allele, the black line represents the lifespan trajectory of the non-carriers.

3L

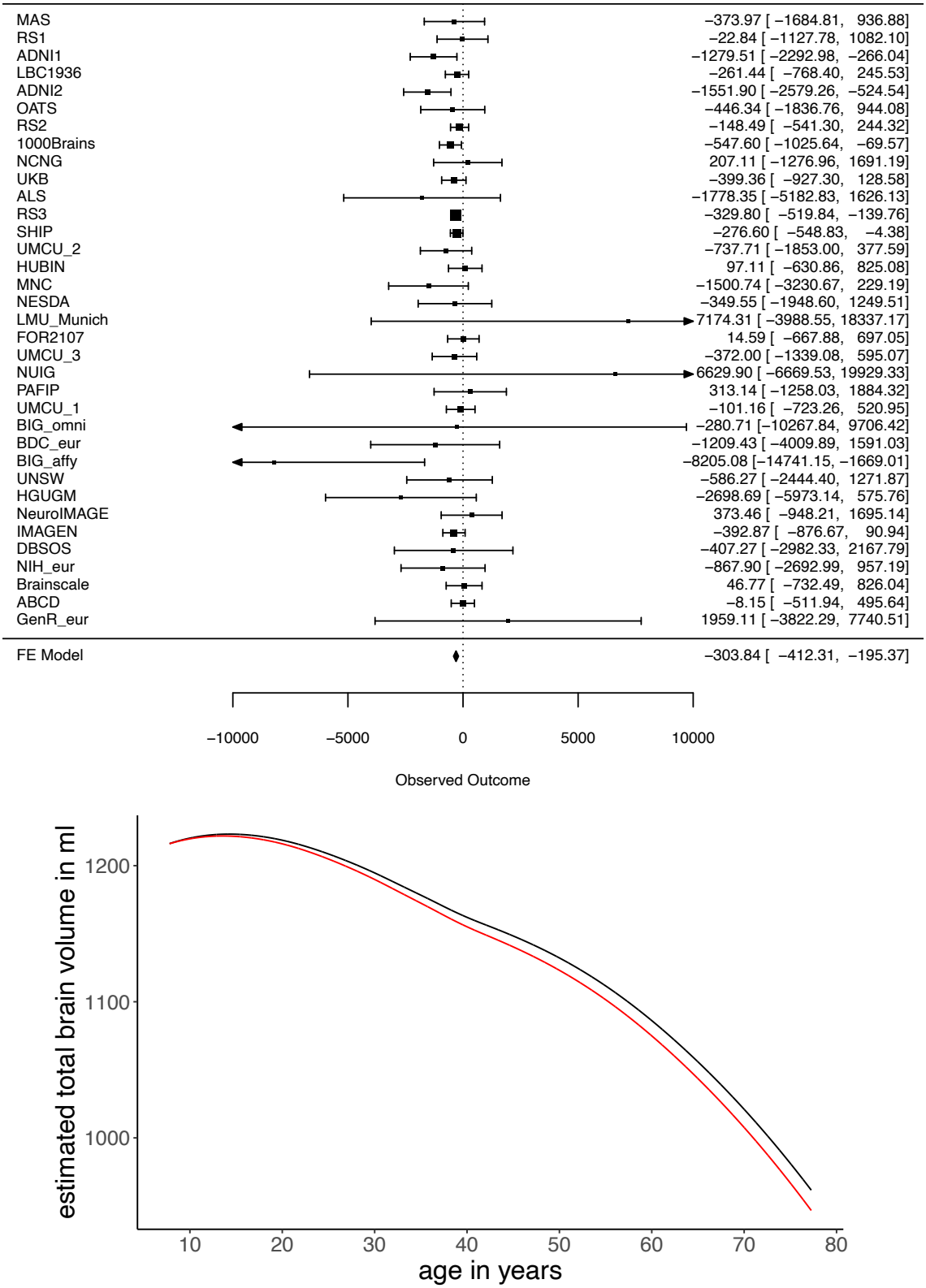

Supplementary Figure 3L: Age-independent effect of the significant SNPs/top-SNPs in significant genes. 3L) rs12325429; change rate total brain volume; independent of age; total N = 14773. The top figure displays a forest-plot in which means and 95% confidence intervals are displayed for each cohort. Confidence intervals that are outside the axis of the plot are marked with an arrow. The bottom figure shows a visualization of the effect of the tested allele on the phenotype itself. The red line represents the lifespan trajectory for the carriers of the effect allele, the black line represents the lifespan trajectory of the non-carriers.

3M

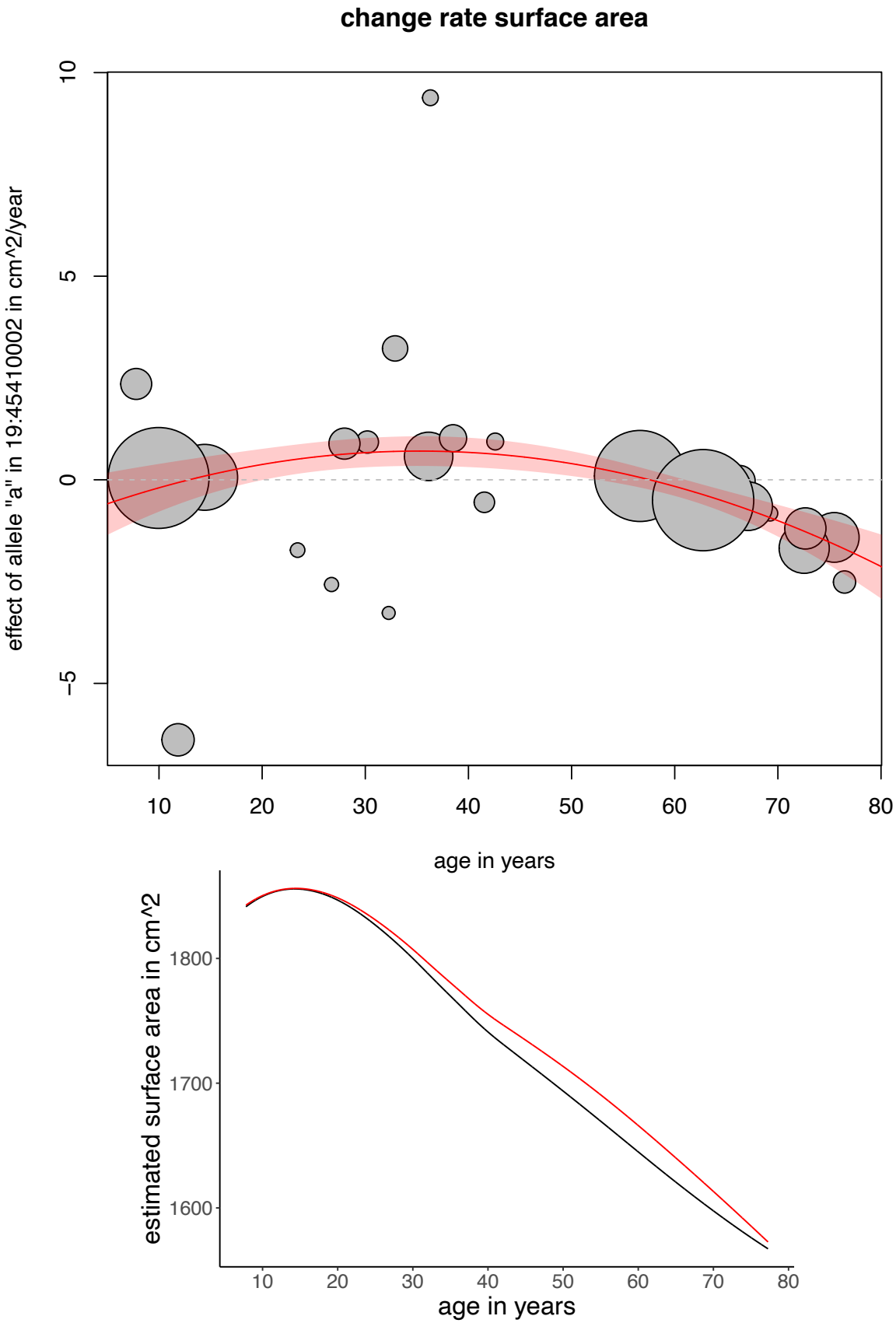

Supplementary Figure 3M: Age-dependent effect of the significant SNPs/top-SNPs in significant genes. 3M) APOE – top SNP rs769449; change rate surface area; quadratic age dependency; total N = 13030. The top figure displays the estimated effect of the tested allele on the change rate in each cohort against age. The center of the circles represent the effect size of the tested allele for each cohort, the radius of the circles are proportional to sample size. The red line displays the estimated age-effect with 95% confidence interval from the meta analysis/meta-regression. The bottom figure shows a visualization of the effect of the tested allele on the phenotype itself. The red line represents the lifespan trajectory for the carriers of the effect allele, the black line represents the lifespan trajectory of the non-carriers.

3N

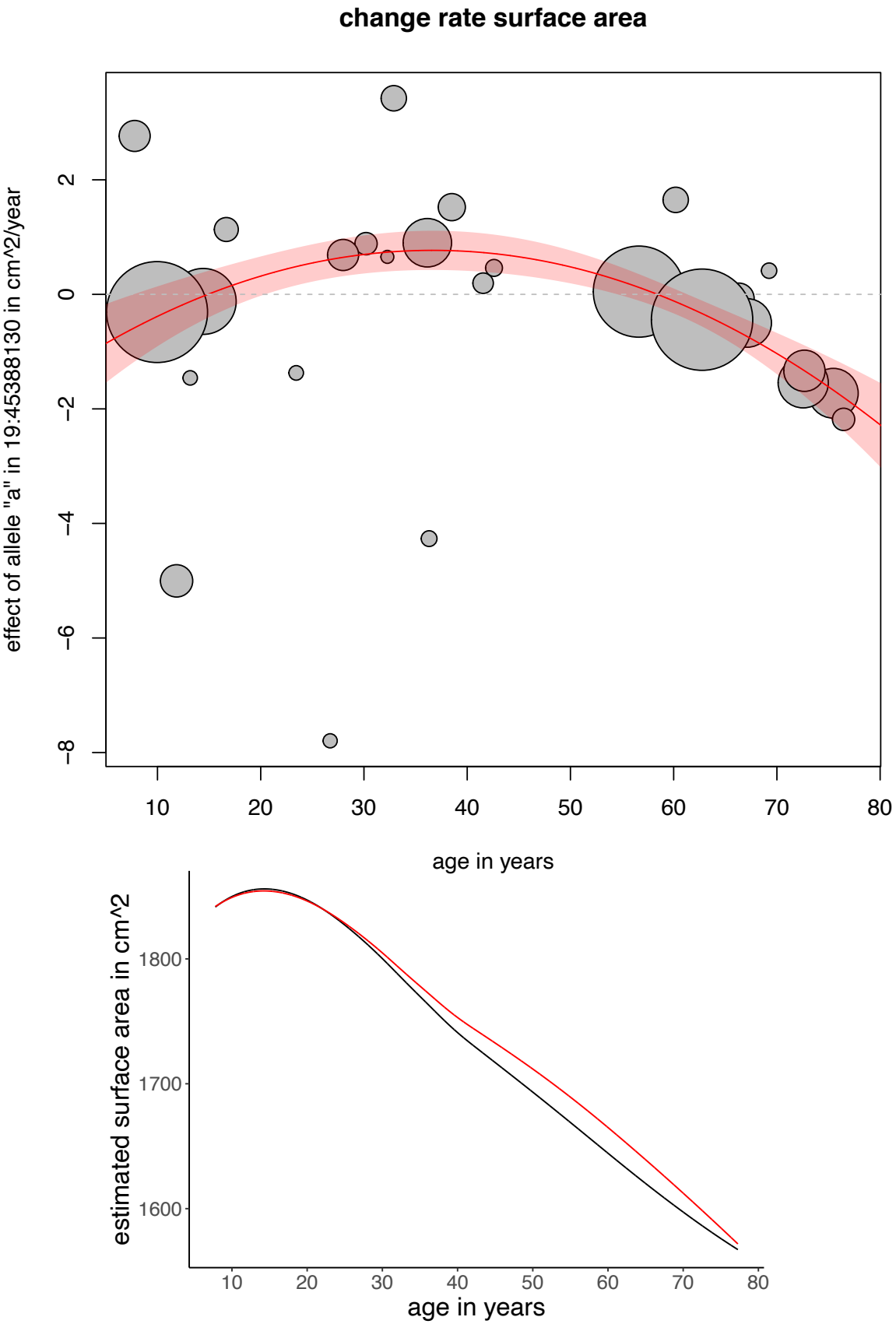

Supplementary Figure 3N: Age-dependent effect of the significant SNPs/top-SNPs in significant genes. 3N) rs34342646; change rate surface area, quadratic age dependency; total N – 13329. The top figure displays the estimated effect of the tested allele on the change rate in each cohort against age. The center of the circles represent the effect size of the tested allele for each cohort, the radius of the circles are proportional to sample size. The red line displays the estimated age-effect with 95% confidence interval from the meta analysis/meta-regression. The bottom figure shows a visualization of the effect of the tested allele on the phenotype itself. The red line represents the lifespan trajectory for the carriers of the effect allele, the black line represents the lifespan trajectory of the non-carriers.

3O

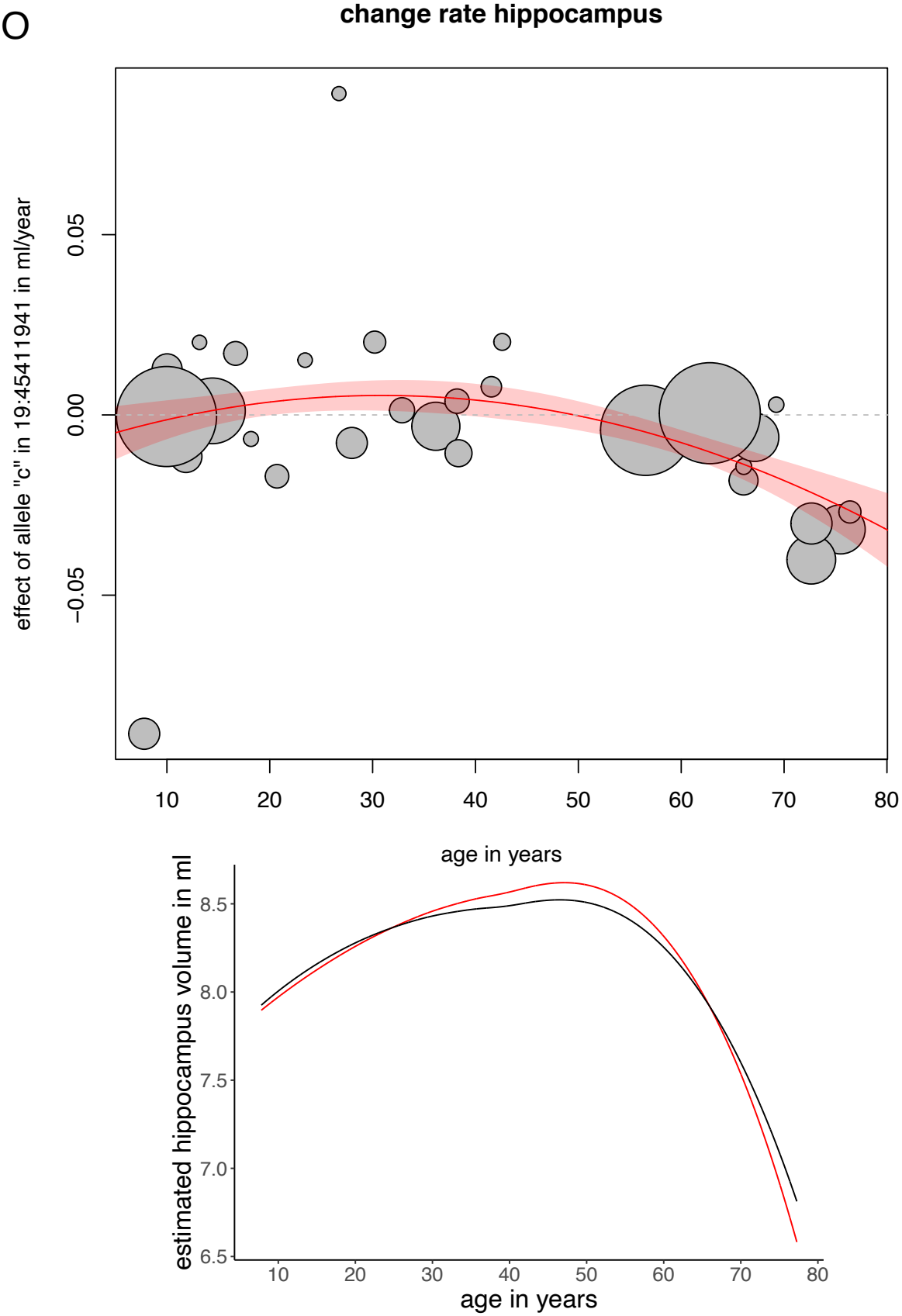

Supplementary Figure 3O: Age-dependent effect of the significant SNPs/top-SNPs in significant genes. 3O) APOE and rs429358; change rate hippocampus; quadratic age dependency total N = 13329. The top figure displays the estimated effect of the tested allele on the change rate in each cohort against age. The center of the circles represent the effect size of the tested allele for each cohort, the radius of the circles are proportional to sample size. The red line displays the estimated age-effect with 95% confidence interval from the meta analysis/meta-regression. The bottom figure shows a visualization of the effect of the tested allele on the phenotype itself. The red line represents the lifespan trajectory for the carriers of the effect allele, the black line represents the lifespan trajectory of the non-carriers.

3P

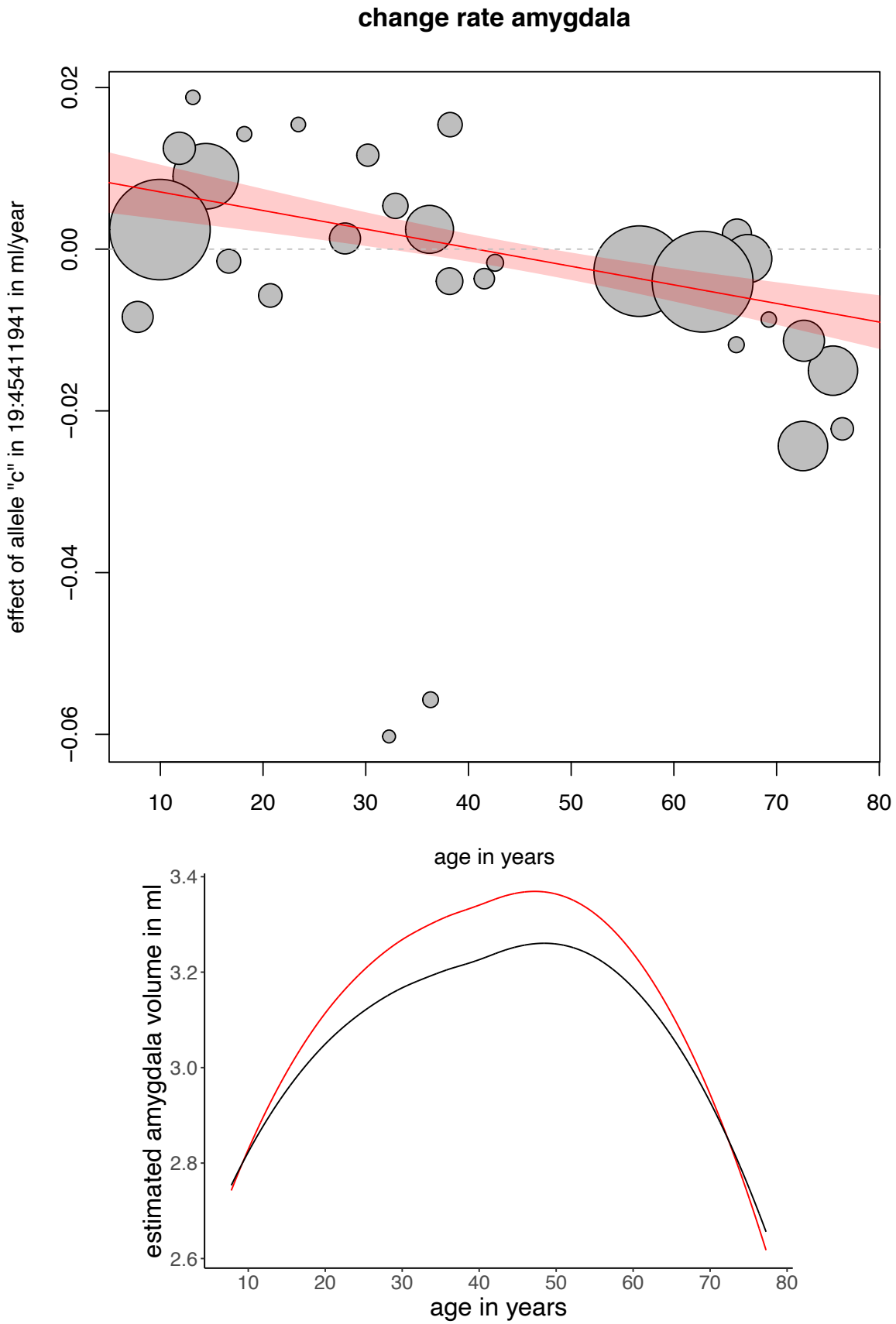

Supplementary Figure 3P: Age-dependent effect of the significant SNPs/top-SNPs in significant genes. 3P) APOE – top SNP rs429358; change rate amygdala; linear age dependency*; total N = 13685. The top figure displays the estimated effect of the tested allele on the change rate in each cohort against age. The center of the circles represent the effect size of the tested allele for each cohort, the radius of the circles are proportional to sample size. The red line displays the estimated age-effect with 95% confidence interval from the meta analysis/meta-regression. The bottom figure shows a visualization of the effect of the tested allele on the phenotype itself. The red line represents the lifespan trajectory for the carriers of the effect allele, the black line represents the lifespan trajectory of the non-carriers. *APOE also showed a significant quadratic age dependency for change rate of amygdala; the most parsimonious model is shown.

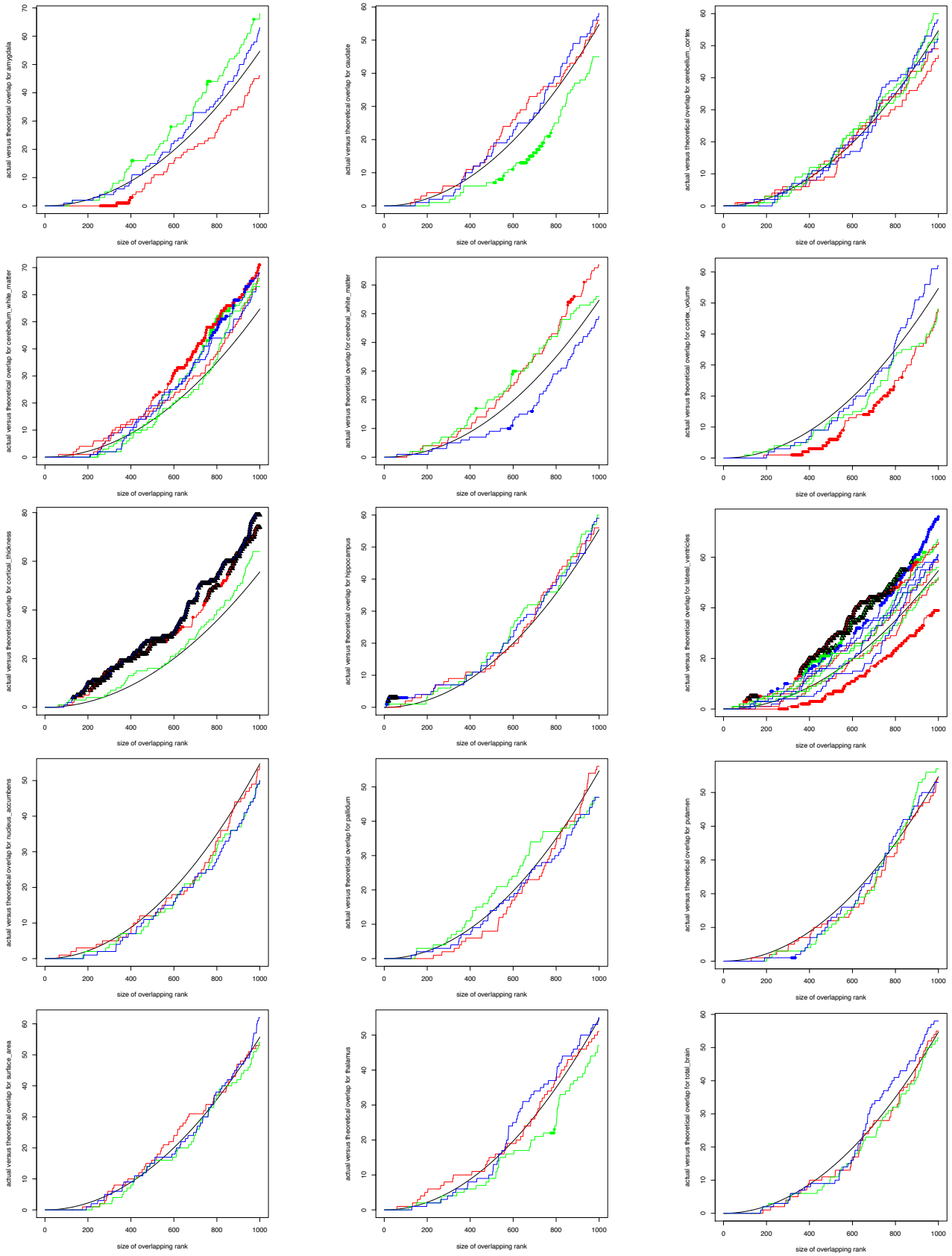

Supplementary Figure 4: Expected versus actual overlap for the first top-1000 ranked genes for the phase 2 analysis. Results from age-independent analysis(red), linear age -dependent analysis (green) and quadratic age-dependent analysis (blue) are shown in one figure. Top-N ranks are marked for nominally (dots) or FDR-corrected (within the top-1000 genes for this phenotype; triangles) significance for over- or under-representation of genes associated with brain structural rates of change amongst the top-N ranked genes for cross-sectional brain measures. For lateral ventricles and cerebellum grey and white matter, summary statistics for the cross-sectional phenotype were only available for left and right lateral and inferior lateral ventricle, and left and right cerebellum grey and white matter, separately. Therefore, for those measures we show curves for overlap with the separate cross-sectional phenotypes.

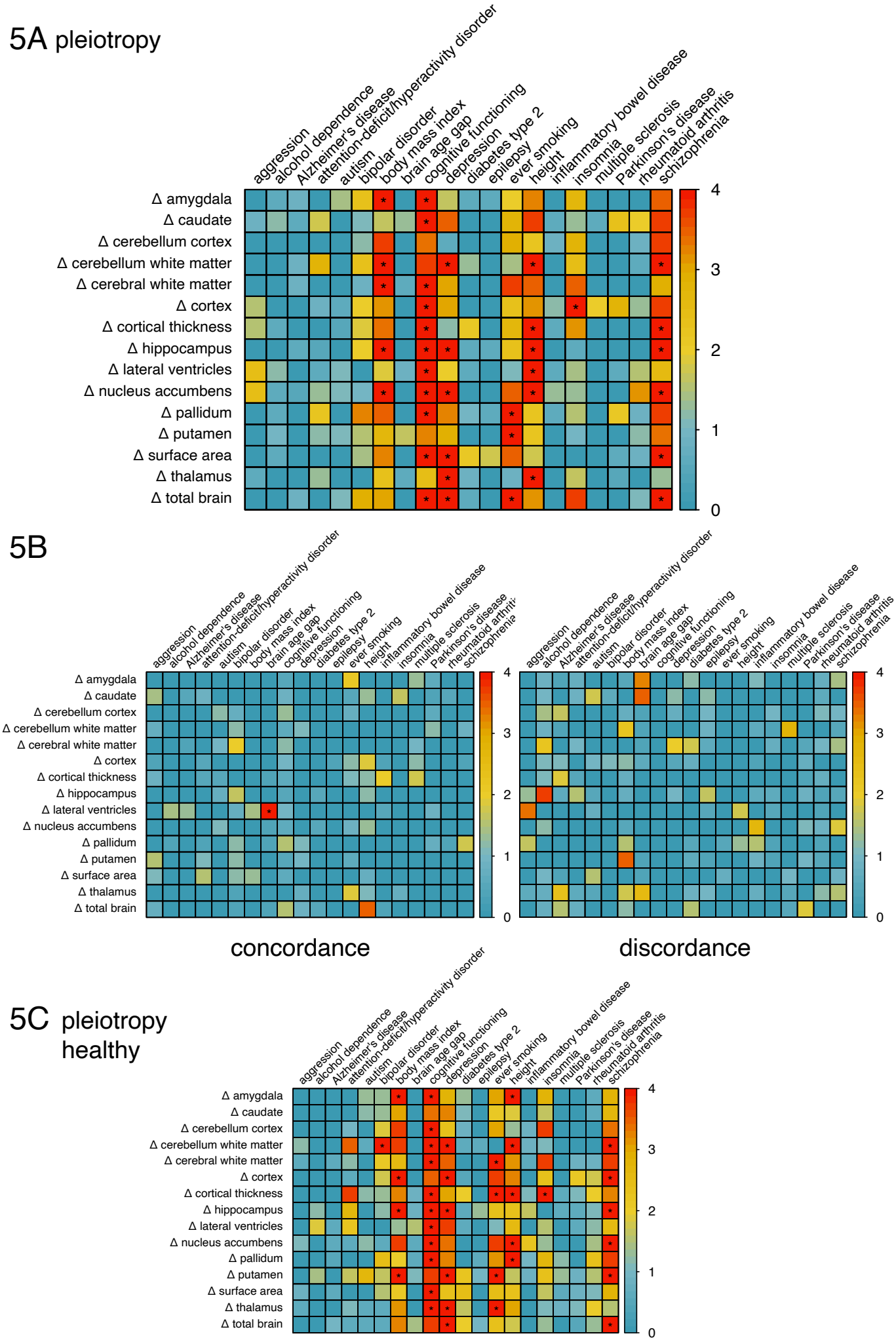
5A pleiotropy
aggression
alcohol dependence
Alzheimer's disease
attention-deficit/hyperactivity disorder
autism
bipolar disorder
body mass index
brain age gap
cognitive functioning
depression
diabetes type 2
epilepsy
ever smoking
height
inflammatory bowel disease
insomnia
multiple sclerosis
Parkinson's disease
rheumatoid arthritis
schizophrenia
Δ amygdala
Δ caudate
Δ cerebellum cortex
Δ cerebellum white matter
Δ cerebral white matter
Δ cortex
Δ cortical thickness
Δ hippocampus
Δ lateral ventricles
Δ nucleus accumbens
Δ pallidum
Δ putamen
Δ surface area
Δ thalamus
Δ total brain
0
1
2
3
4
5B
concordance
discordance
5C pleiotropy healthy

5D pleiotropy

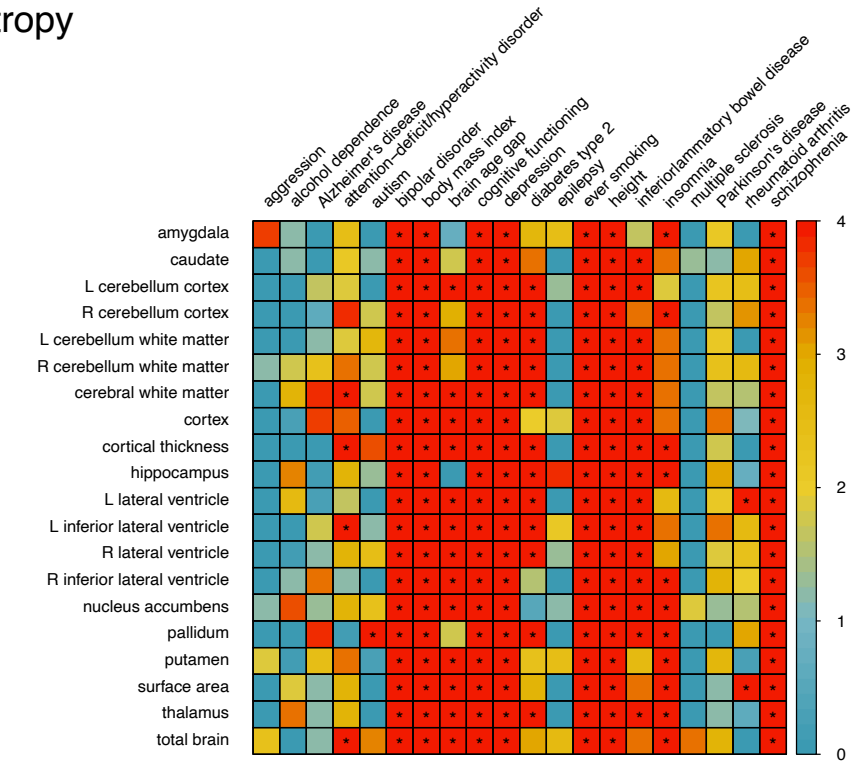

5E

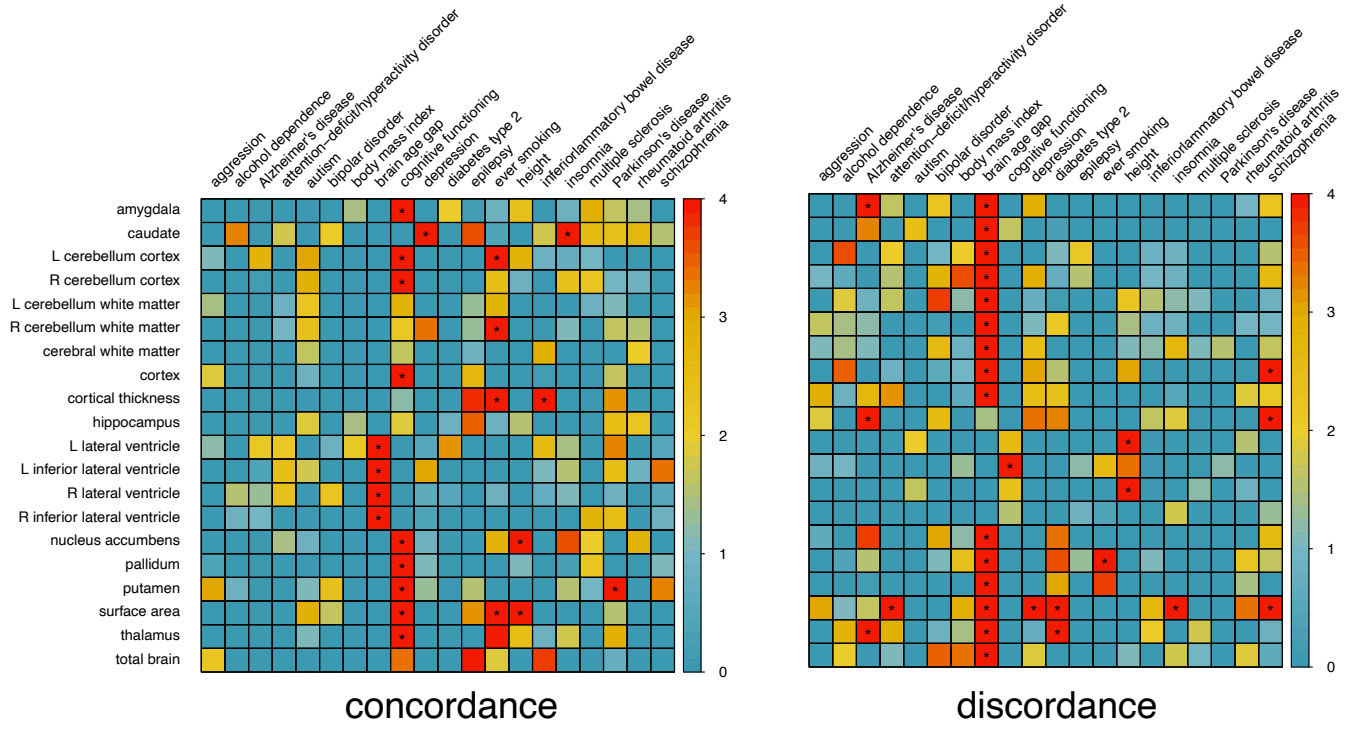

Supplementary Figure 5: iSECA results for overlap between GWAS summary statistics of structural brain change with GWAS summary statistics of other phenotypes testing for pleiotropy (A), concordance and discordance of effects (B) and pleiotropy in the subgroup excluding subjects with a diagnosis (C). For comparison, we also present the same analysis for cross-sectional volumes, again showing pleiotropy results (D), concordance and discordance (E). Colors display the significance level on a log-10 scale. Associations that are significant based are marked with *. For a fair comparison, the cross-sectional analyses (D-E) used the same significance threshold as the change analyses (A-C); even though the latter contained more brain structures.

6A

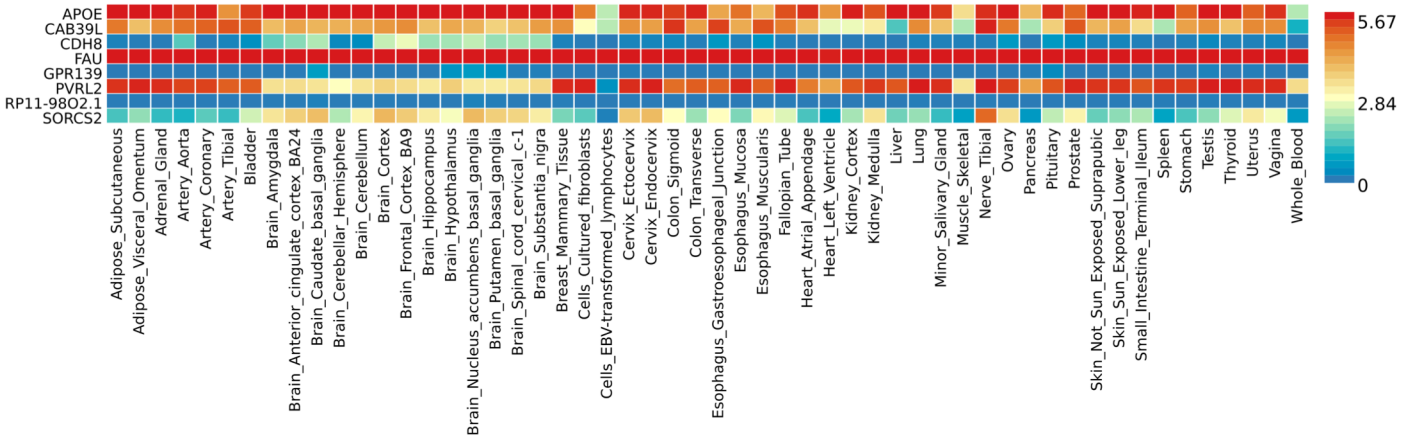

6B

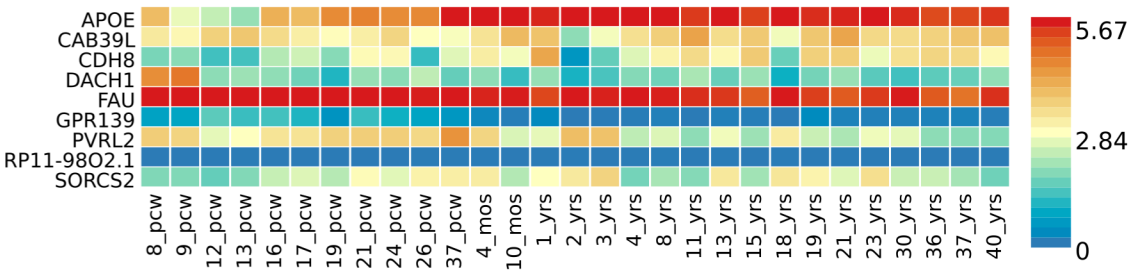

Supplementary Figure 6: Heatmaps display normalized expression value (zero mean normalization of log2 transformed expression) for prioritized genes, for GTEx v8 RNAseq data (A) and BrainSpan data (B). Darker red means higher expression of that gene in each label, compared to a darker blue color in the same label. Note that *PVRL2* is an alias for *NECTIN2*.

7A

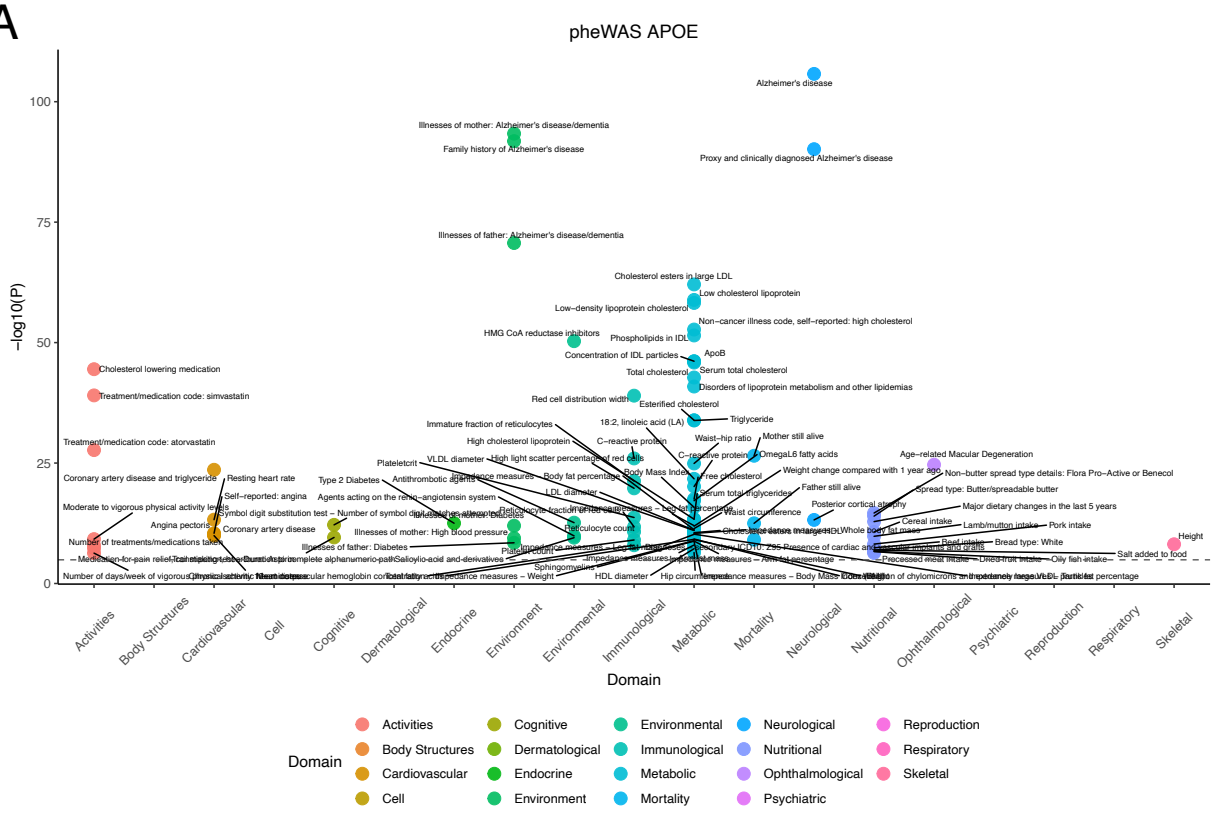

7B

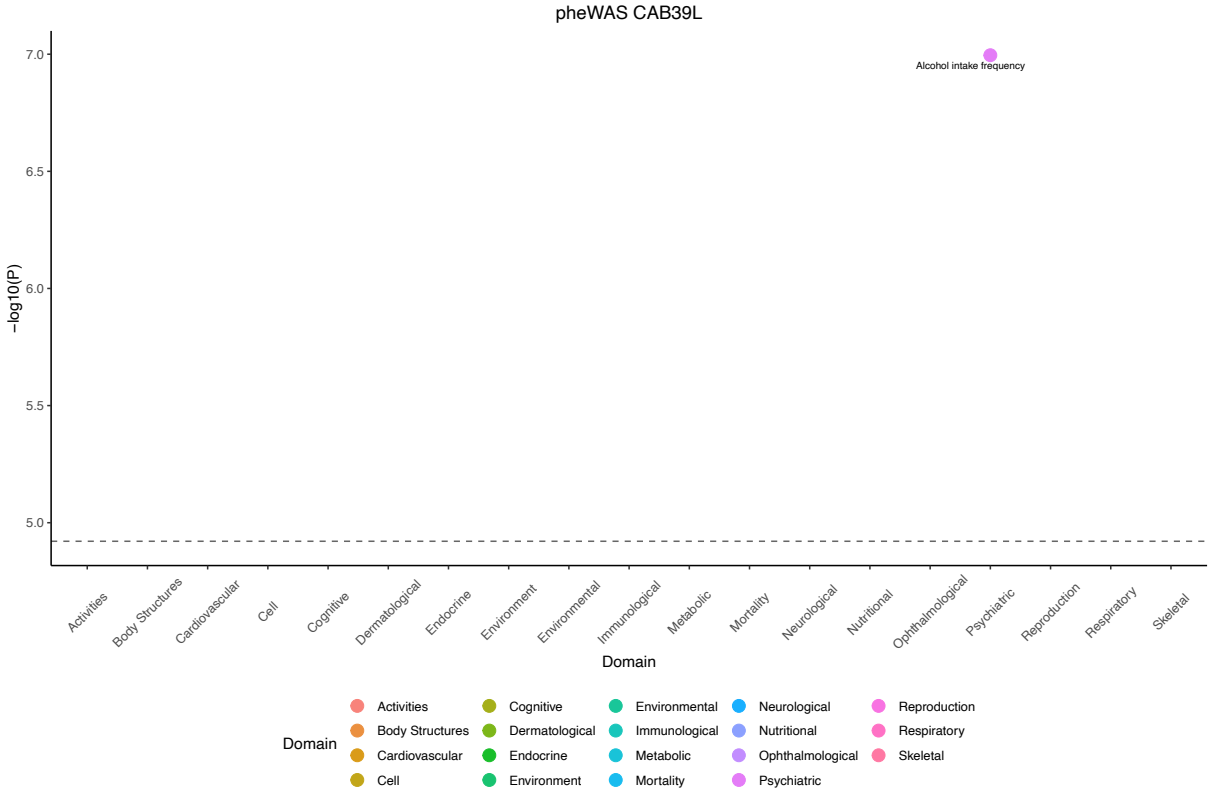

Supplementary Figure 7: PheWAS plots for *APOE* (A), *CAB39L* (B), *CDH8* (C), *DACH1* (D), *FAU* (E), *GPR139* (F), *NECTIN2* (G) and *SORCS2* (H). PheWAS plots show the significance of a gene on a range of traits based on MAGMA gene-based tests (Bonferroni corrected P-value threshold: 7.51e-07), as obtained from GWASAtlas[32] (https://atlas.ctglab.nl). Redundant traits were removed for visualization and trait names were shortened. Full list of significant gene-based associations is in Supplementary Table 17.

7C

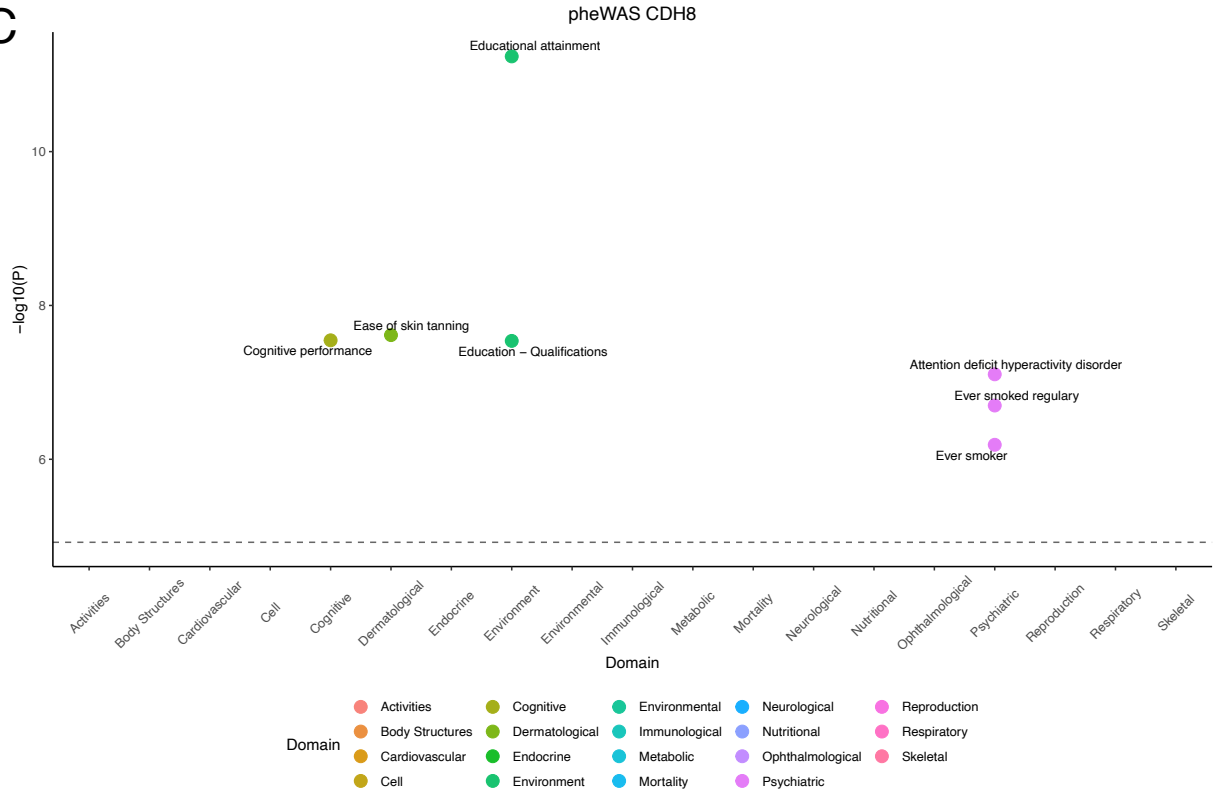

7D

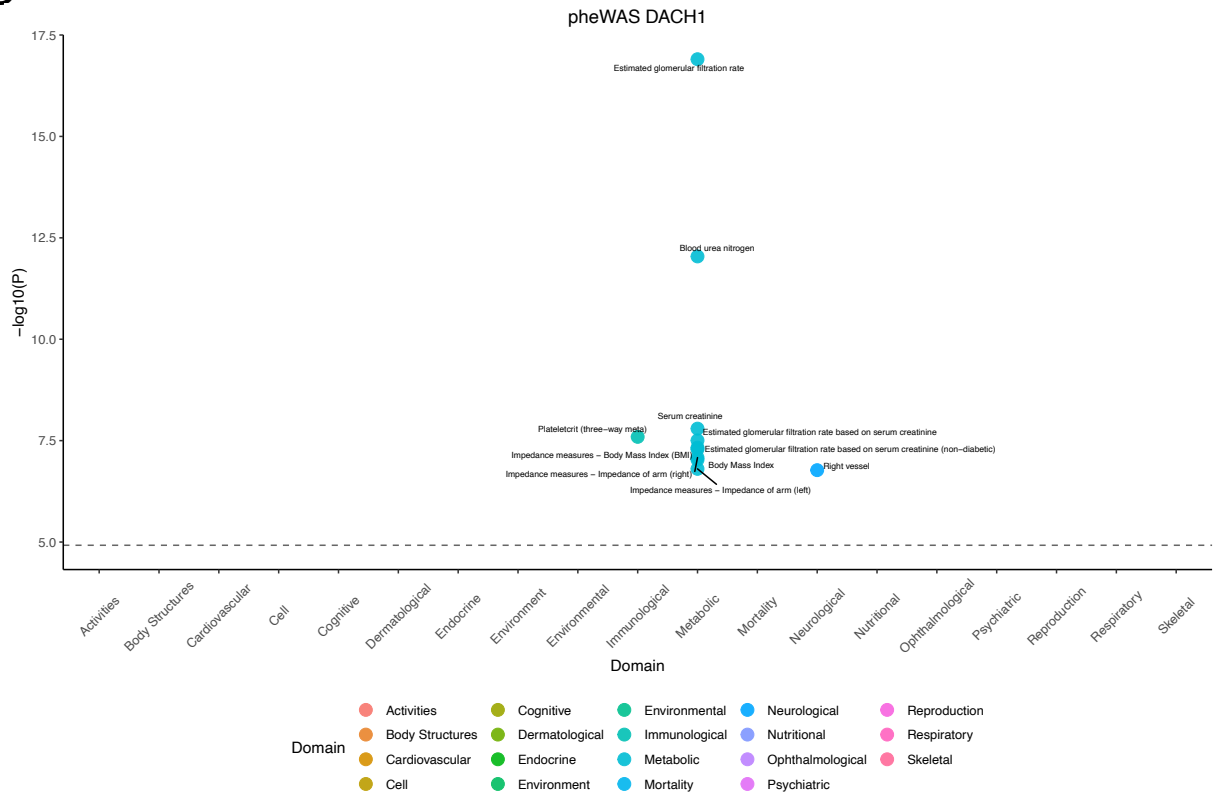

Supplementary Figure 7: PheWAS plots for *APOE* (A), *CAB39L* (B), *CDH8* (C), *DACH1* (D), *FAU* (E), *GPR139* (F), *NECTIN2* (G) and *SORCS2* (H). PheWAS plots show the significance of a gene on a range of traits based on MAGMA gene-based tests (Bonferroni corrected P-value threshold: 7.51e-07), as obtained from GWASAtlas[32] (https://atlas.ctglab.nl). Redundant traits were removed for visualization and trait names were shortened. Full list of significant gene-based associations is in Supplementary Table 17.

7E

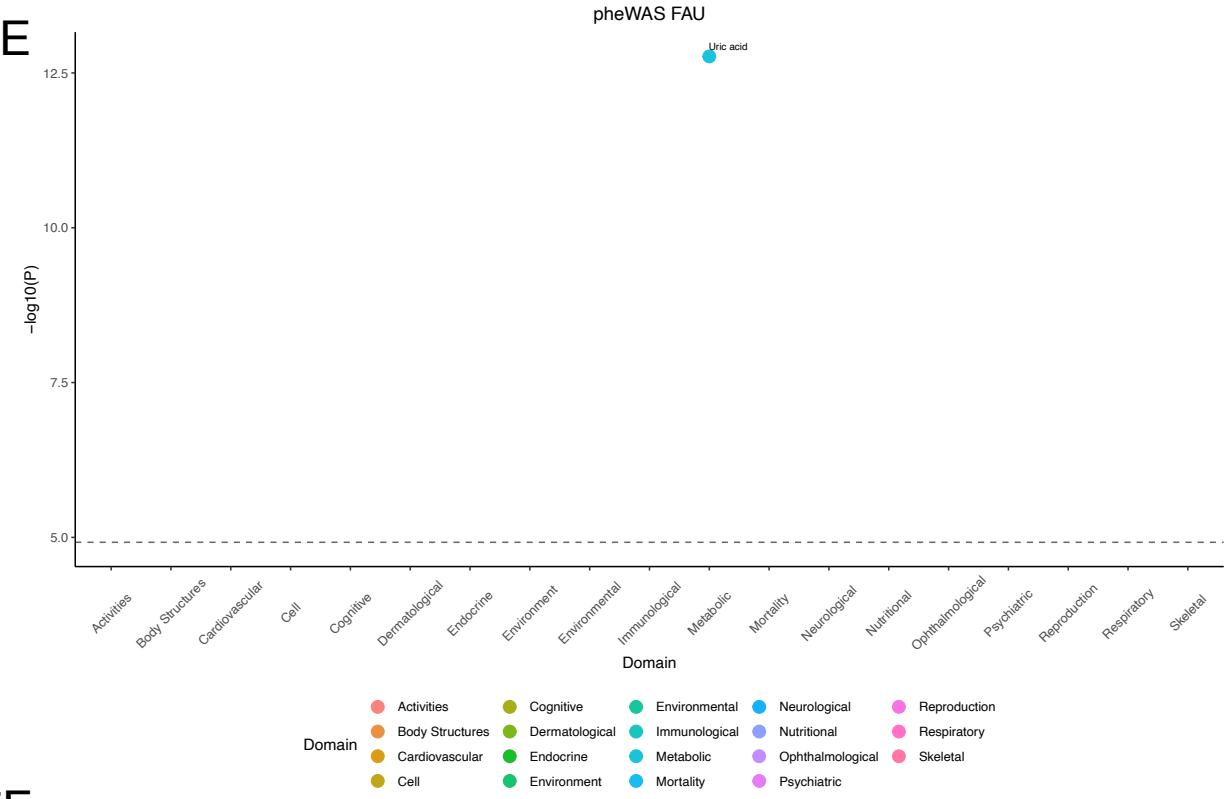

7F

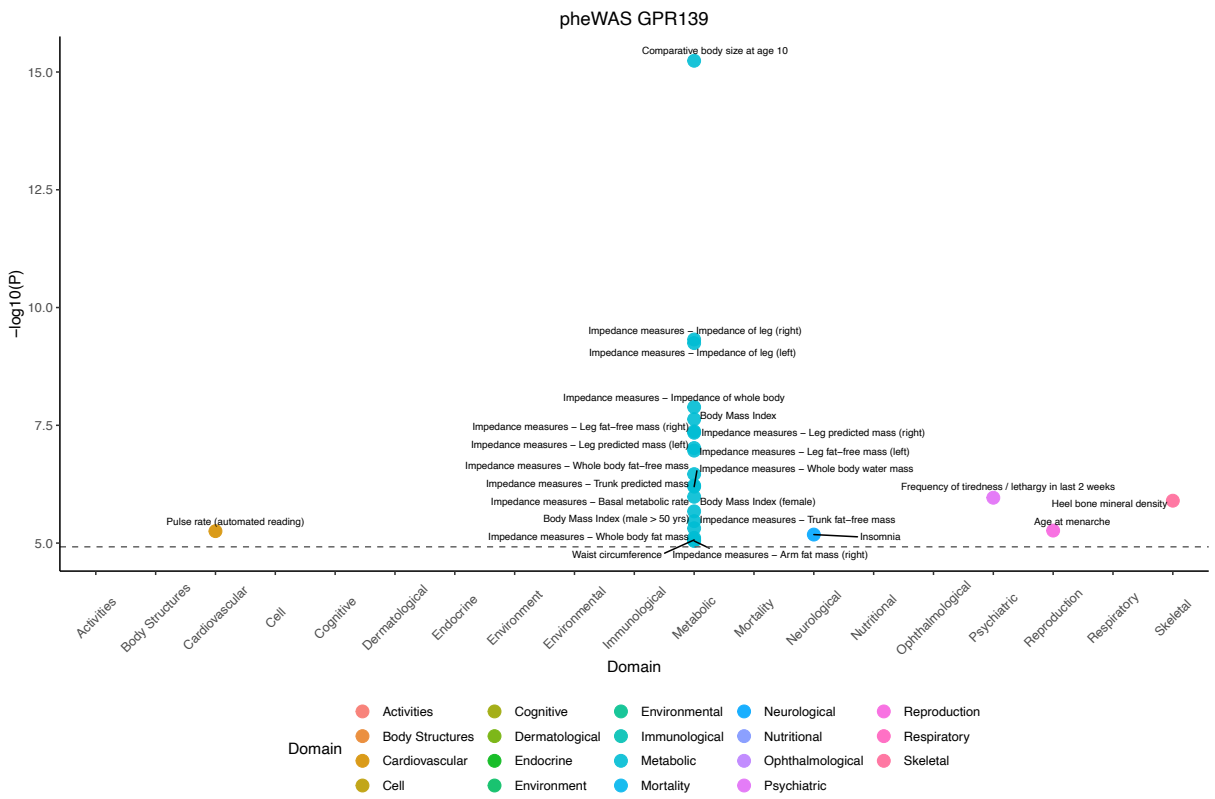

Supplementary Figure 7: PheWAS plots for *APOE* (A), *CAB39L* (B), *CDH8* (C), *DACH1* (D), *FAU* (E), *GPR139* (F), *NECTIN2* (G) and *SORCS2* (H). PheWAS plots show the significance of a gene on a range of traits based on MAGMA gene-based tests (Bonferroni corrected P-value threshold: 7.51e-07), as obtained from GWASAtlas[32] (https://atlas.ctglab.nl). Redundant traits were removed for visualization and trait names were shortened. Full list of significant gene-based associations is in Supplementary Table 17.

7G

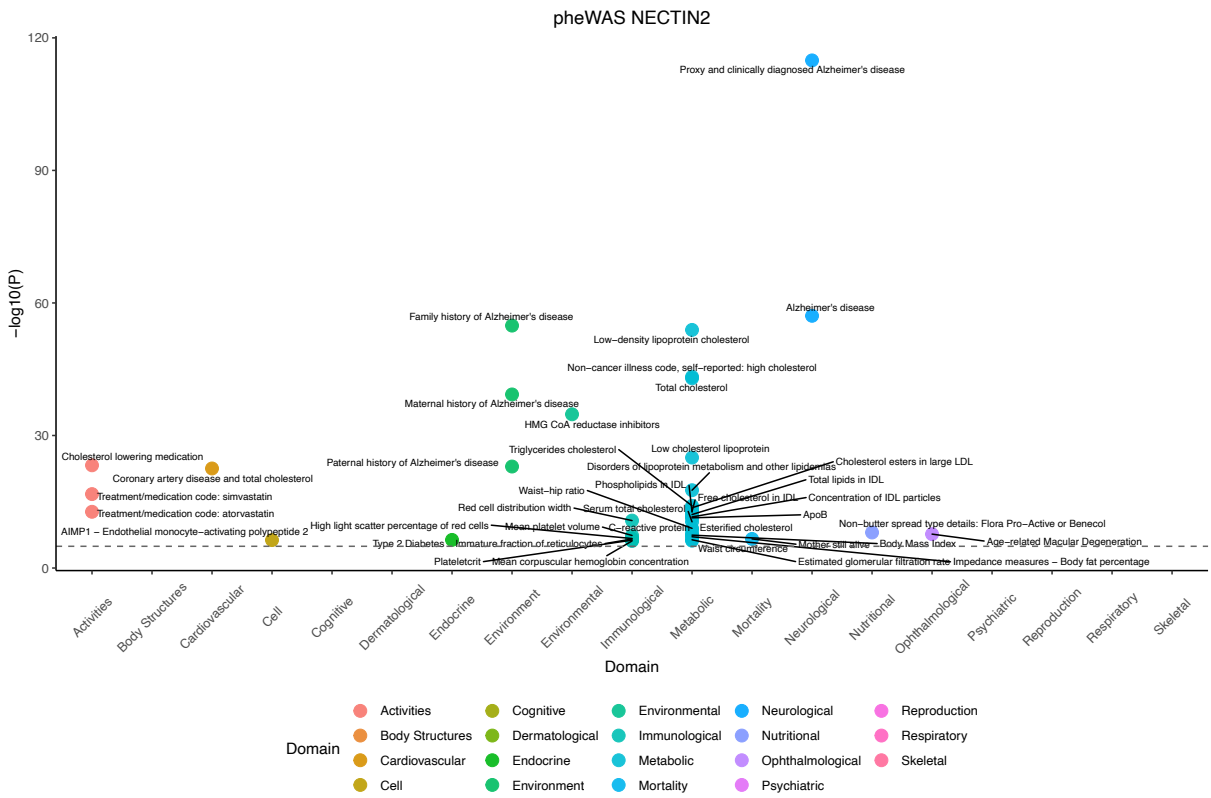

7H

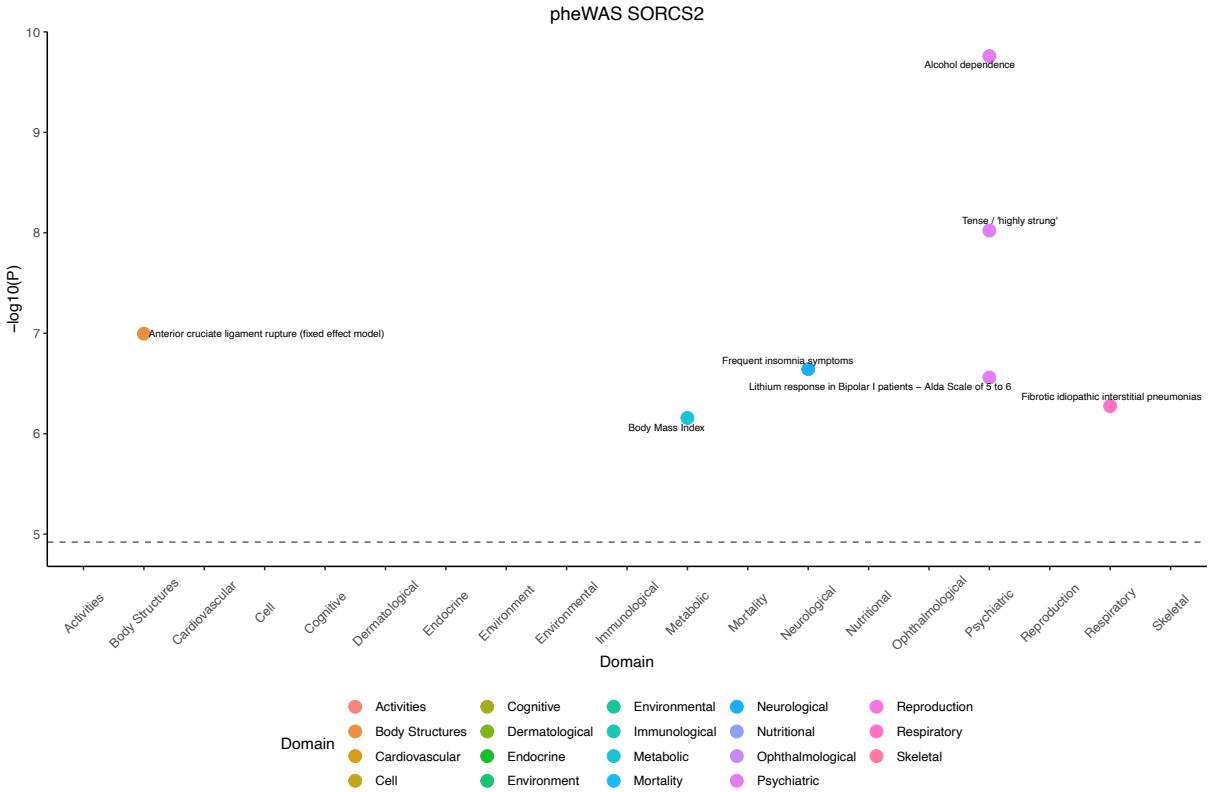

Supplementary Figure 7: PheWAS plots for *APOE* (A), *CAB39L* (B), *CDH8* (C), *DACH1* (D), *FAU* (E), *GPR139* (F), *NECTIN2* (G) and *SORCS2* (H). PheWAS plots show the significance of a gene on a range of traits based on MAGMA gene-based tests (Bonferroni corrected P-value threshold: 7.51e-07), as obtained from GWASAtlas[32] (https://atlas.ctglab.nl). Redundant traits were removed for visualization and trait names were shortened. Full list of significant gene-based associations is in Supplementary Table 17.

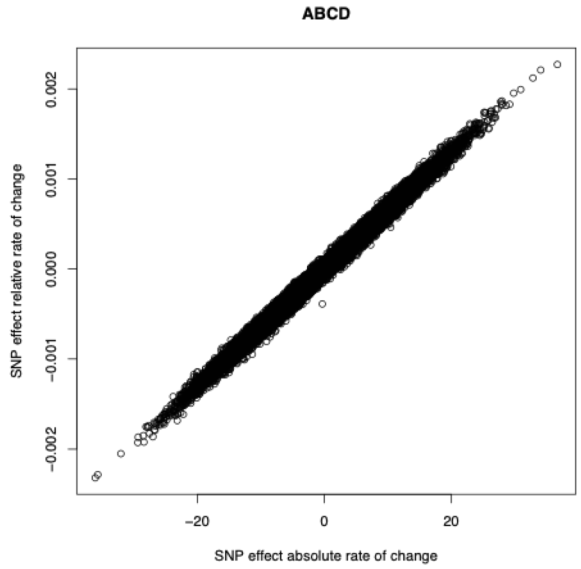

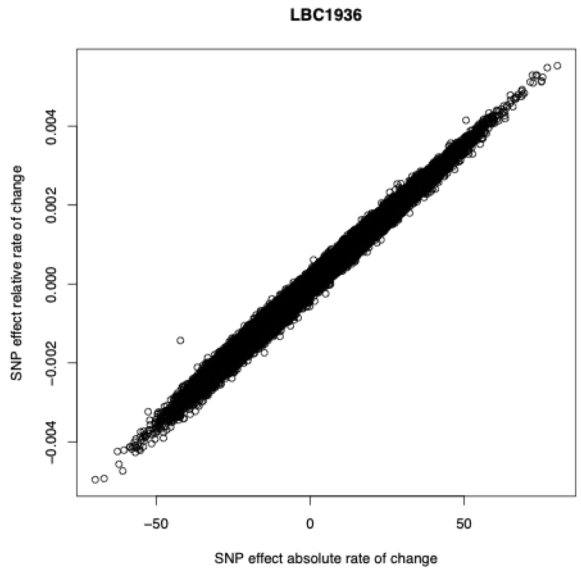

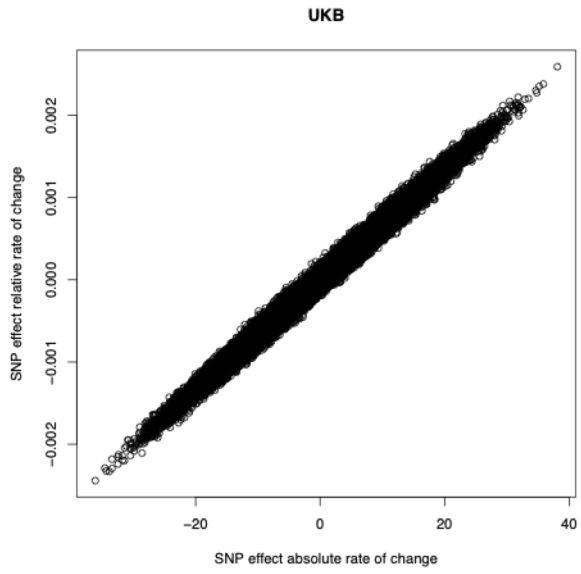

Supplementary Figure 8: Scatter plots showing the SNP effects for rate of change of hippocampus volume (absolute, x-axes) and rate of change of hippocampus volume divided by intracranial volume (relative; y-axes) for the three cohorts added in phase 2. SNPs were clumped at r2 < 0.1 for visualization purposes.

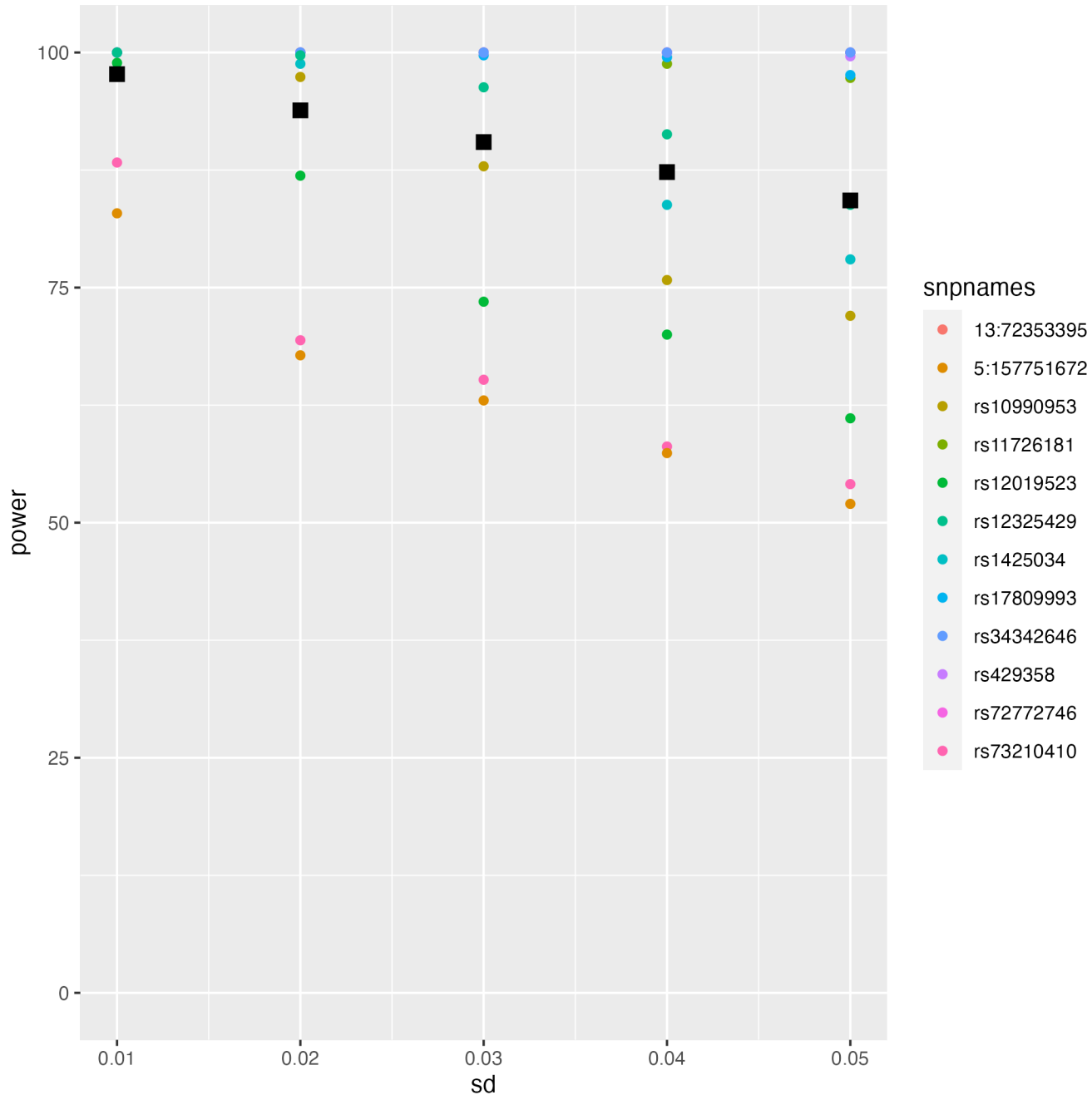

Supplementary Figure 9: For each of the genome-wide significant SNPs in phase 2, we simulated multiplicative scanner effects (independently drawn from N(1,s) per cohort; repeated 1000 times) and applied these to the original effect sizes and standard errors per cohort, after which we recalculated the meta-analysis or meta-regression. The x-axis shows the variation of the simulated effects, the y-axis shows the percentage of cases where the top-findings were still significant. Colors represent the different SNPs. The black squares are the average power over all SNPs tested.

Supplementary Figure 10: QQ plots separately for each participating cohort

QQ plots of summary statistics uploaded per phenotype and per participating cohort, showing expected (x-axis; under the null hypothesis of no genetic signal) versus observed (y-axis) minus $\log_{10}$-transformed p-values.

QQ plots Amygdala

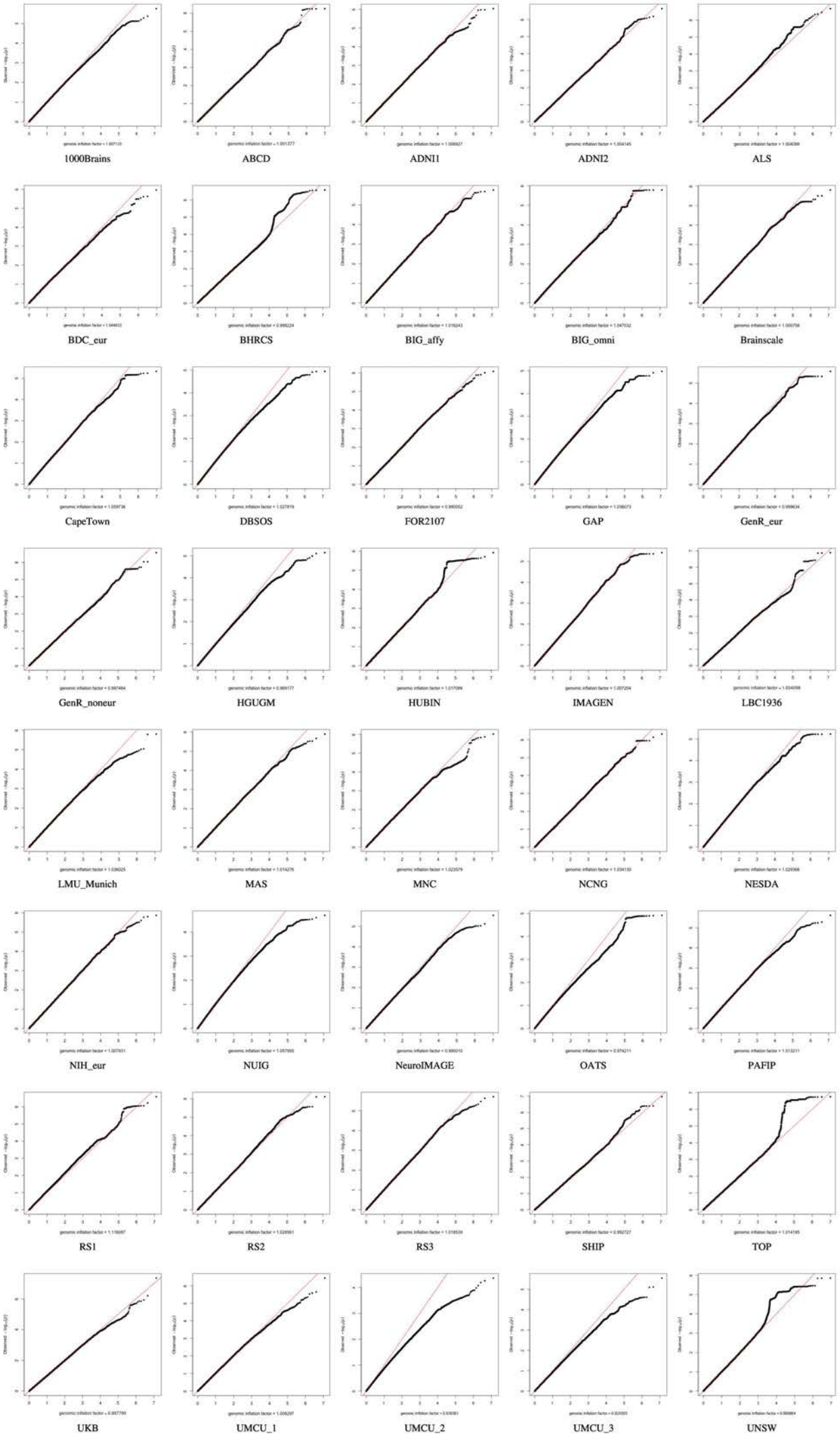

QQ plots Caudate

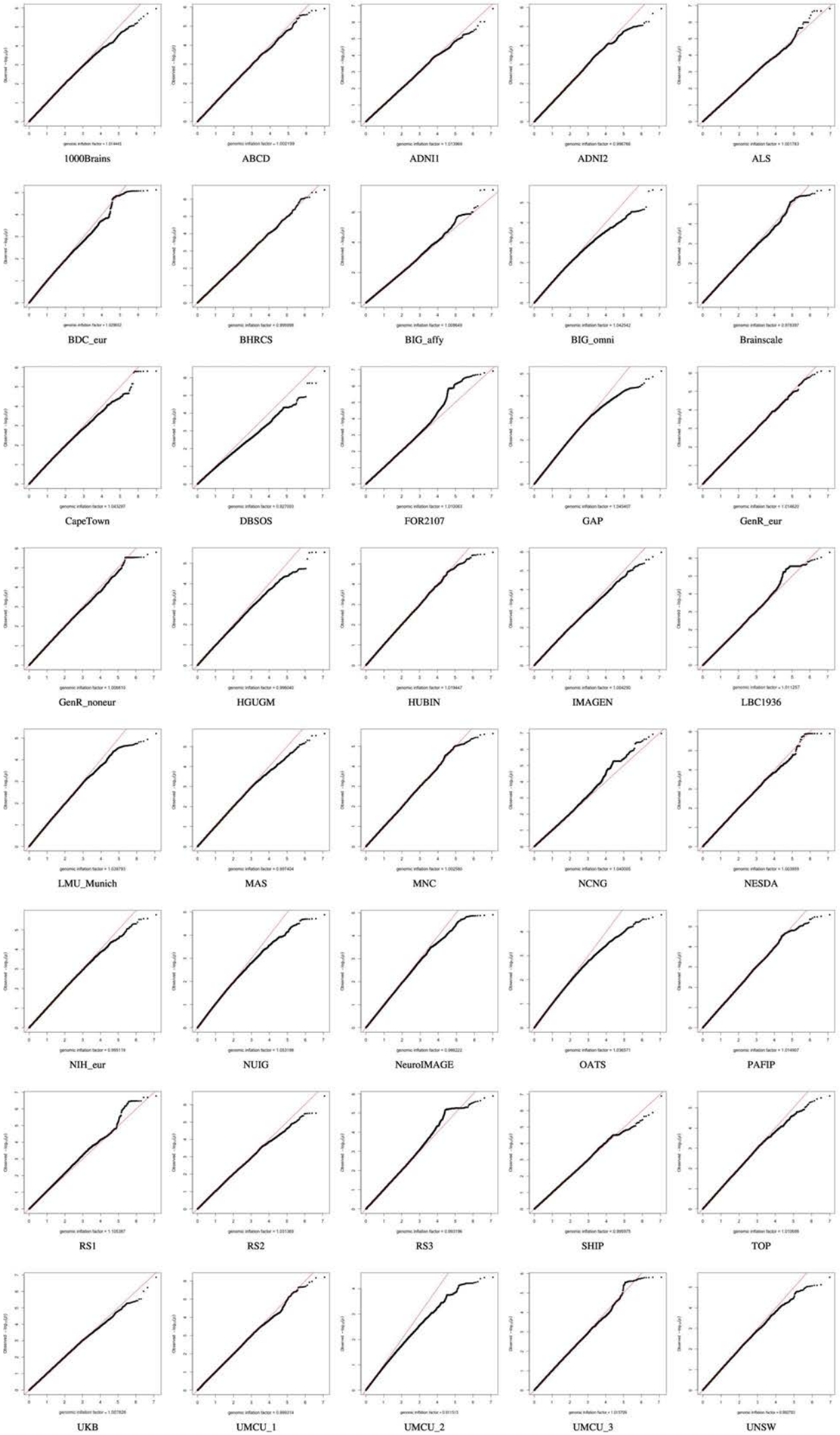

QQ plots Cerebellum Cortex

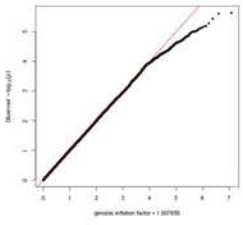
1000Brains

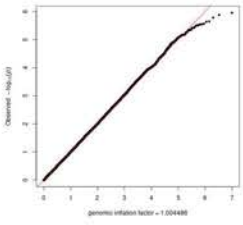
ABCD

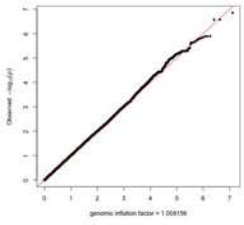
ADNI1

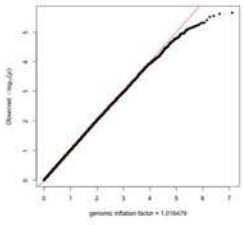
ADNI2

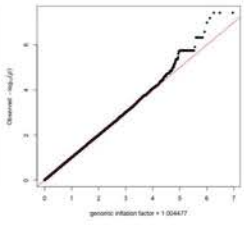
ALS

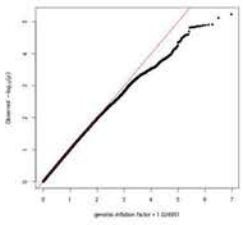
BDC_eur

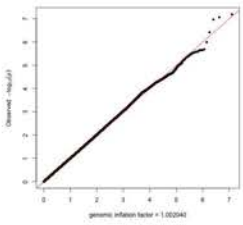
BHRCS

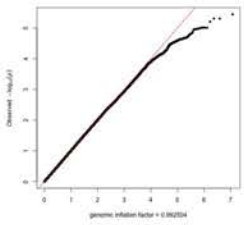
BIG_affy

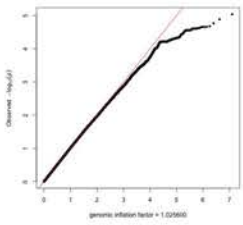
BIG_omni

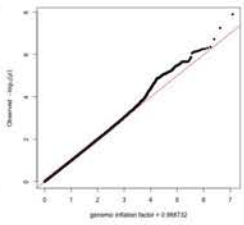
Brainscale

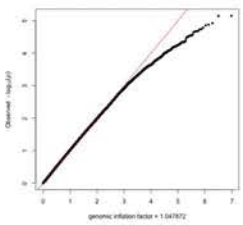
CapeTown

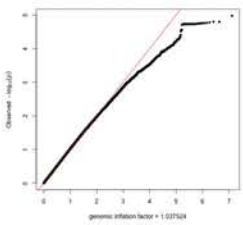
DBSOS

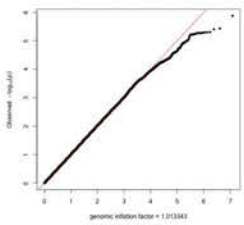
FOR2107

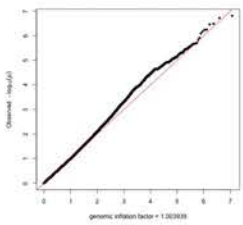
GAP

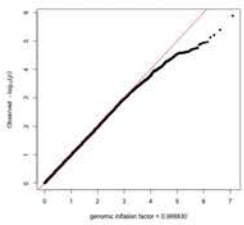
GenR_eur

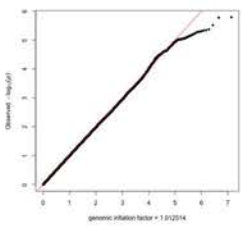
GenR_noneur

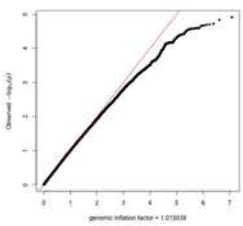
HGUGM

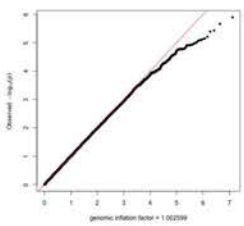
HUBIN

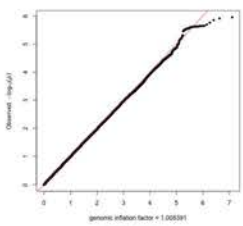
IMAGEN

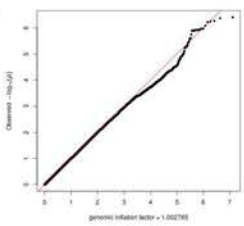
LBC1936

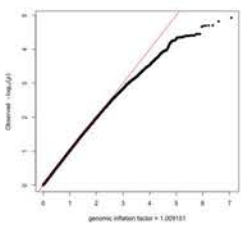
LMU_Munich

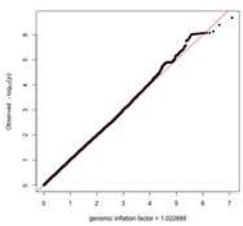
MAS

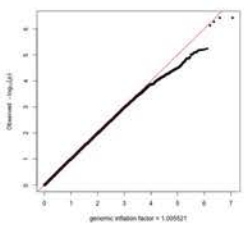
MNC

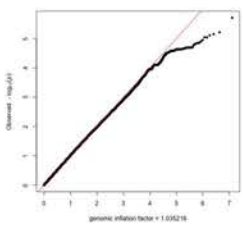
NCNG

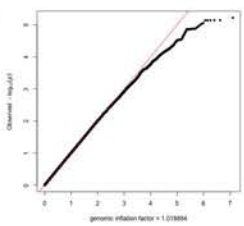
NESDA

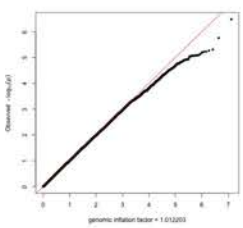
NIH_eur

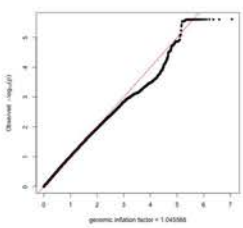
NUIG

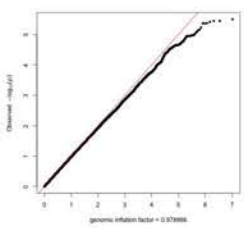
NeuroIMAGE

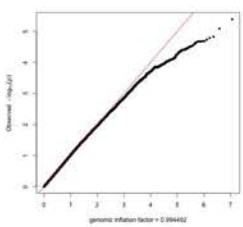
OATS

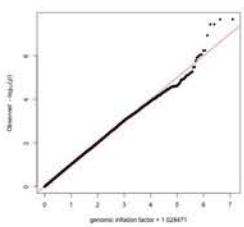
PAFIP

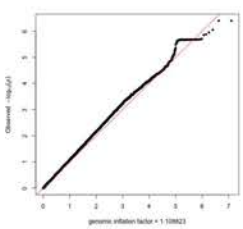
RS1

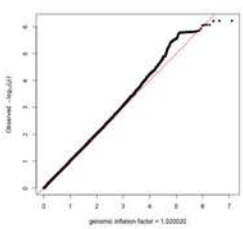
RS2

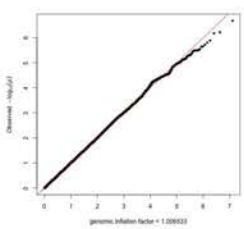
RS3

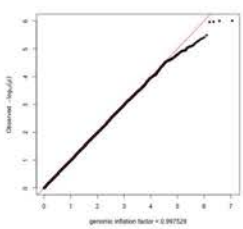
SHIP

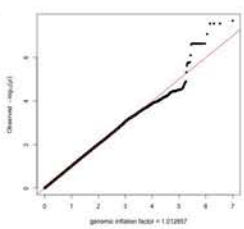
TOP

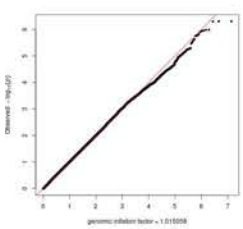
UKB

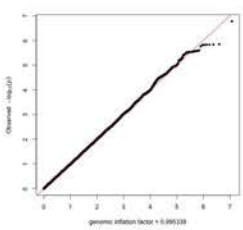
UMCU_1

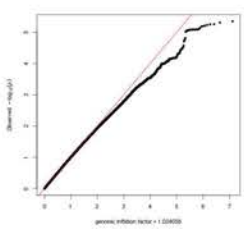
UMCU_2

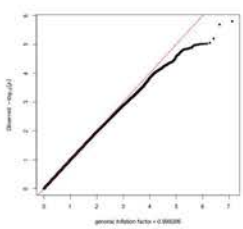
UMCU_3

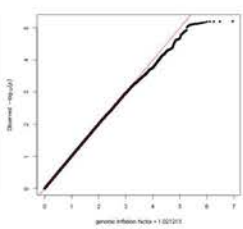
UNSW

QQ plots Cerebellum White Matter

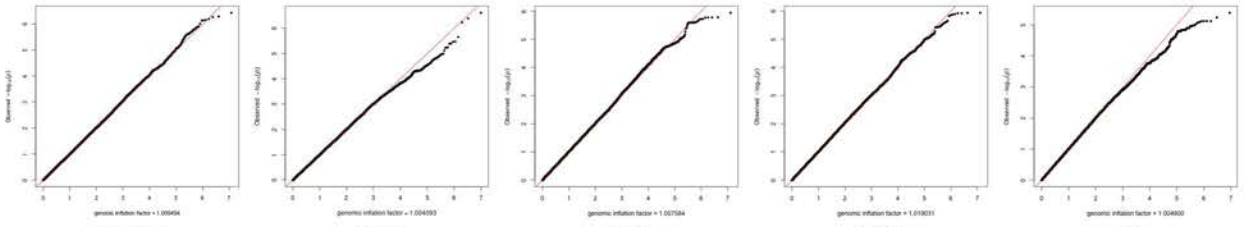

1000Brains ABCD ADNI1 ADNI2 ALS

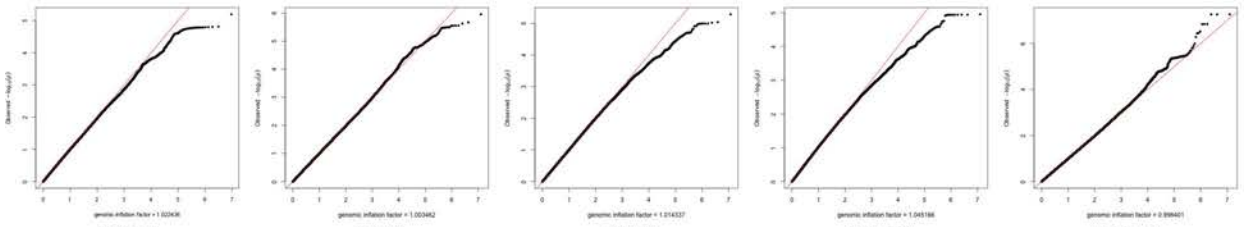

BDC_eur BHRCS BIG_affy BIG_omni Brainscale

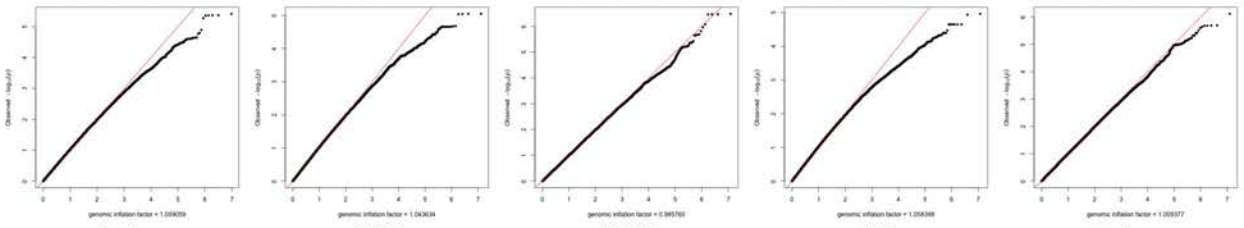

CapeTown DBSOS FOR2107 GAP GenR_eur

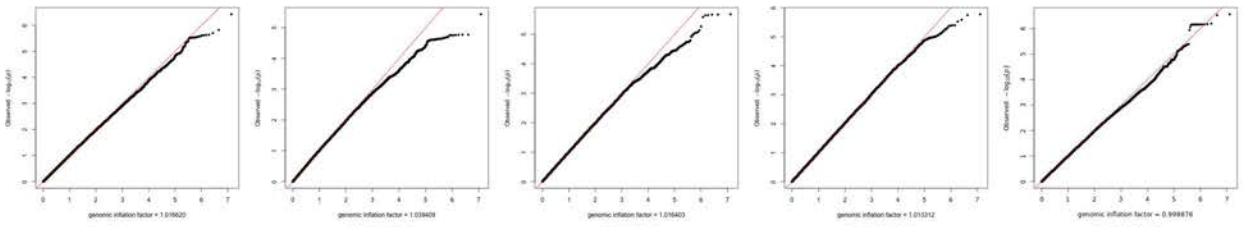

GenR_noneur HGUGM HUBIN IMAGEN LBC1936

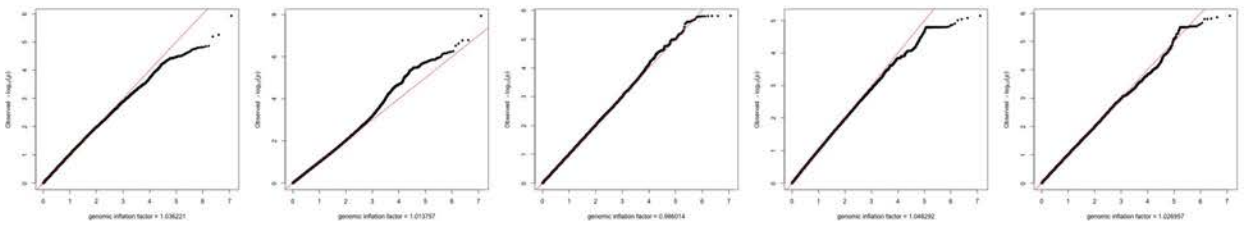

LMU_Munich MAS MNC NCNG NESDA

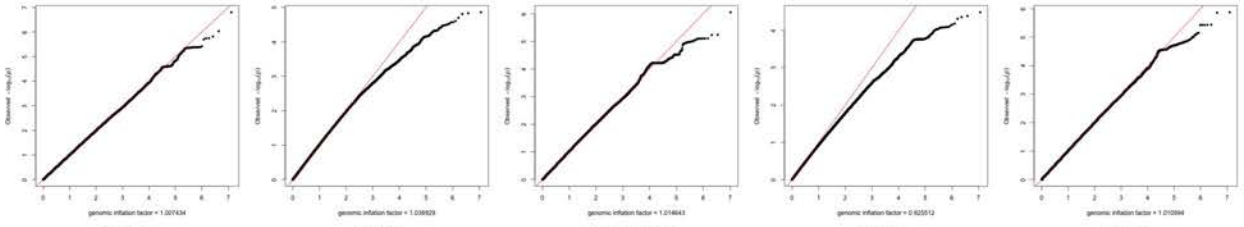

NIH_eur NUIG NeuroIMAGE OATS PAFIP

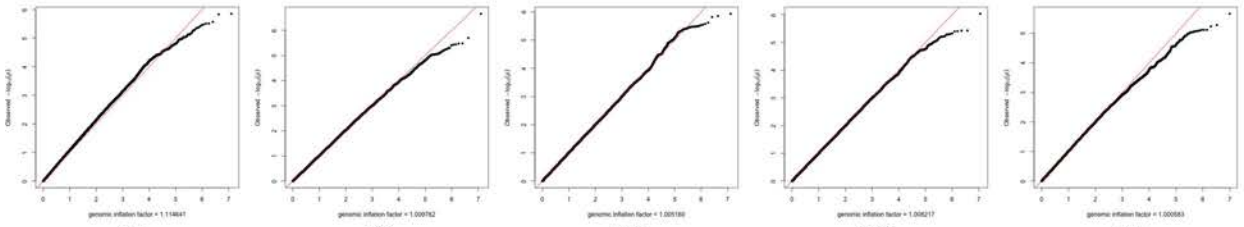

RS1 RS2 RS3 SHIP TOP

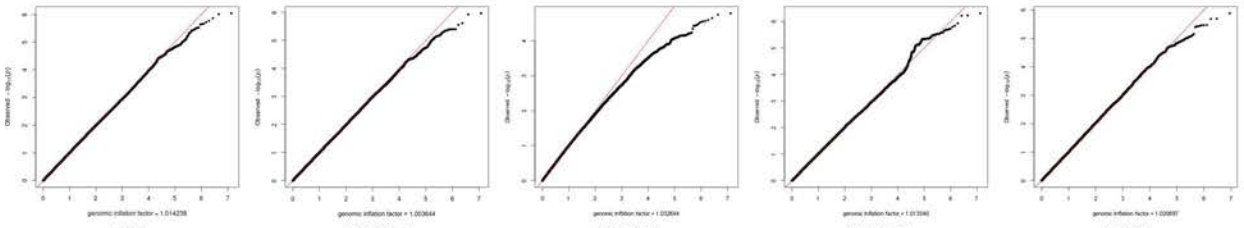

UKB UMCU_1 UMCU_2 UMCU_3 UNSW

QQ plots Cerebral White Matter

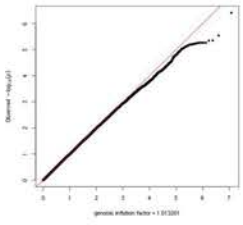
1000Brains

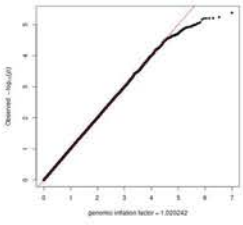
ABCD

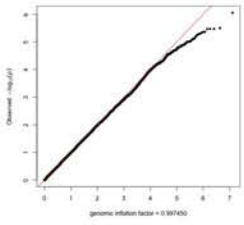
ADNI1

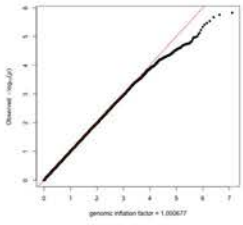
ADNI2

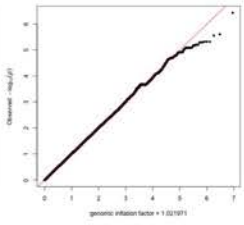
ALS

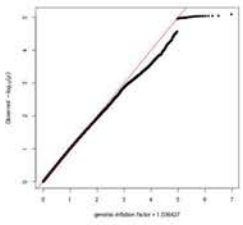
BDC_eur

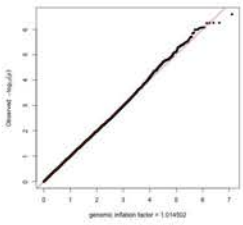
BHRCS

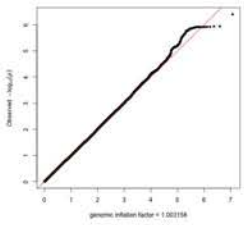
BIG_affy

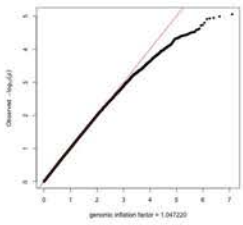
BIG_omni

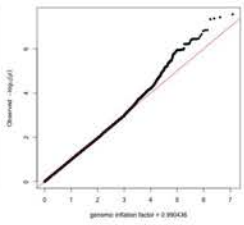
Brainscale

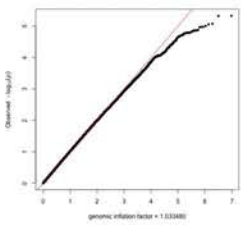
CapeTown

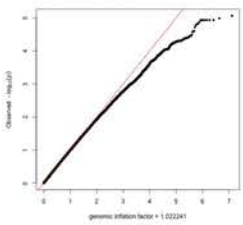
DBSOS

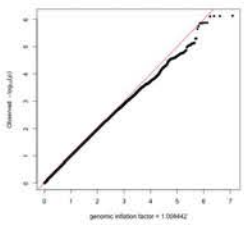
FOR2107

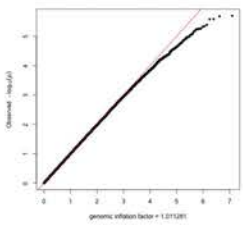
GenR_eur

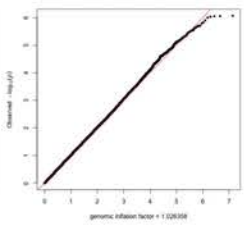
GenR_noneur

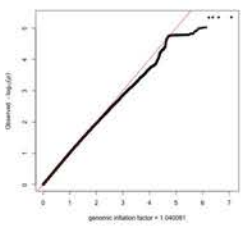
HGUGM

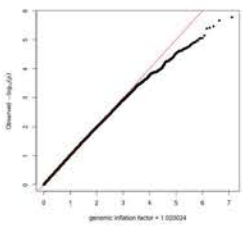
HUBIN

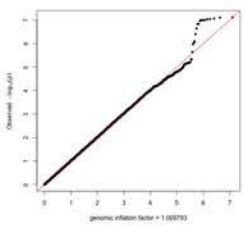
IMAGEN

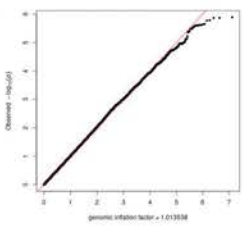
LBC1936

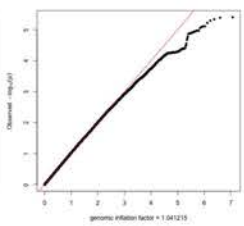
LMU_Munich

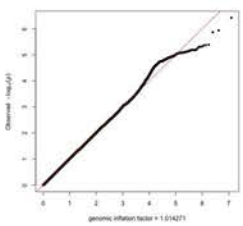
MAS

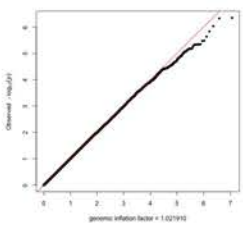
MNC

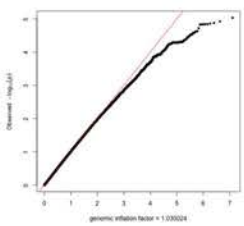
NCNG

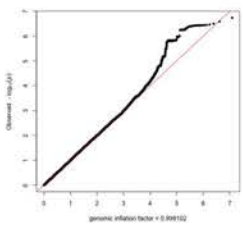
NESDA

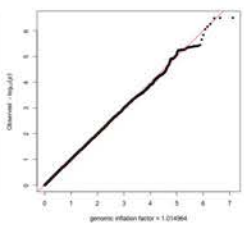
NIH_eur

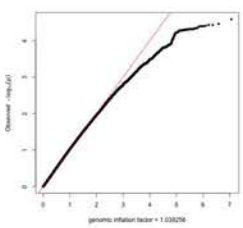
NUIG

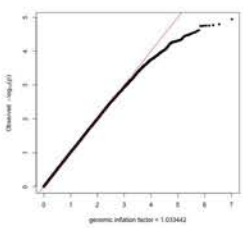
NeuroIMAGE

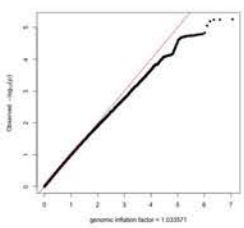
OATS

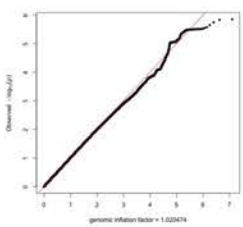
PAFIP

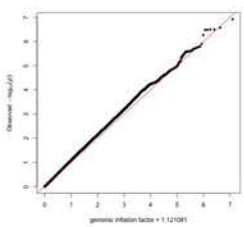
RS1

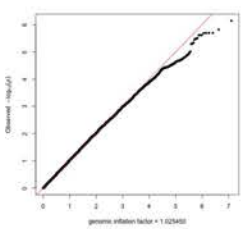
RS2

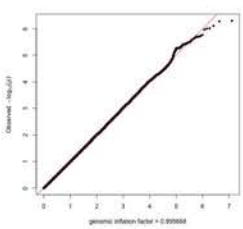
RS3

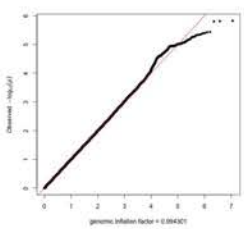
SHIP

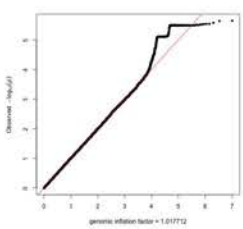
TOP

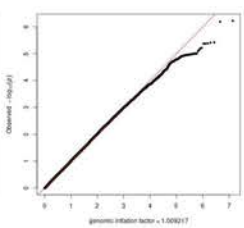
UKB

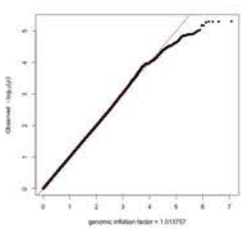
UMCU_1

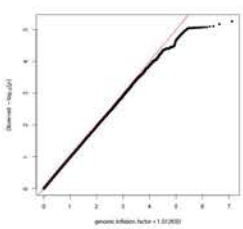
UMCU_2

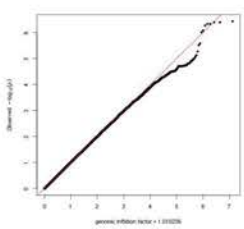
UMCU_3

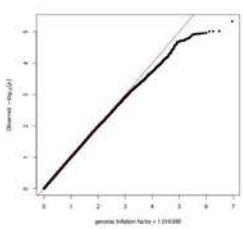
UNSW

QQ plots Cortex

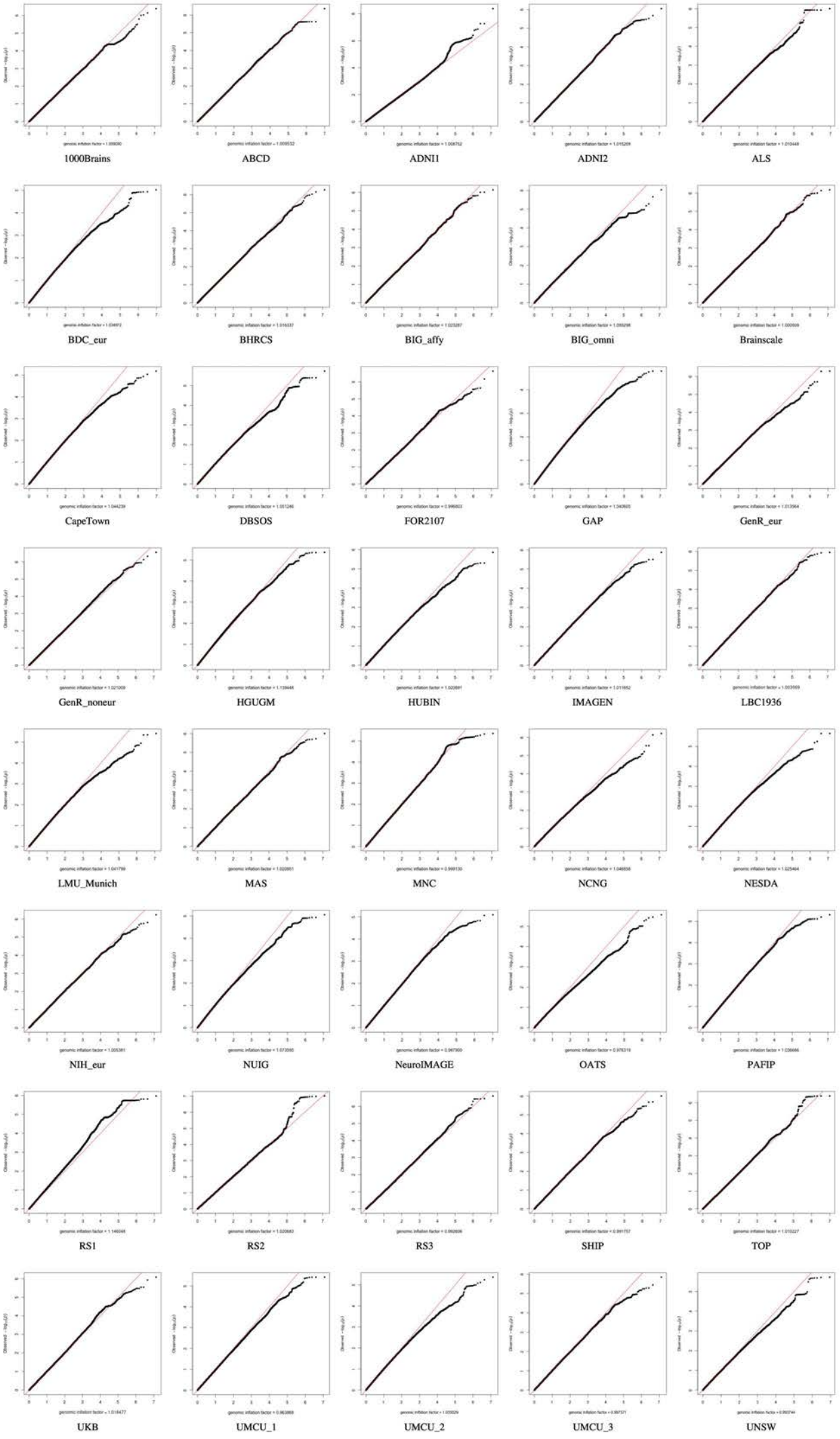

QQ plots Cortical Thickness

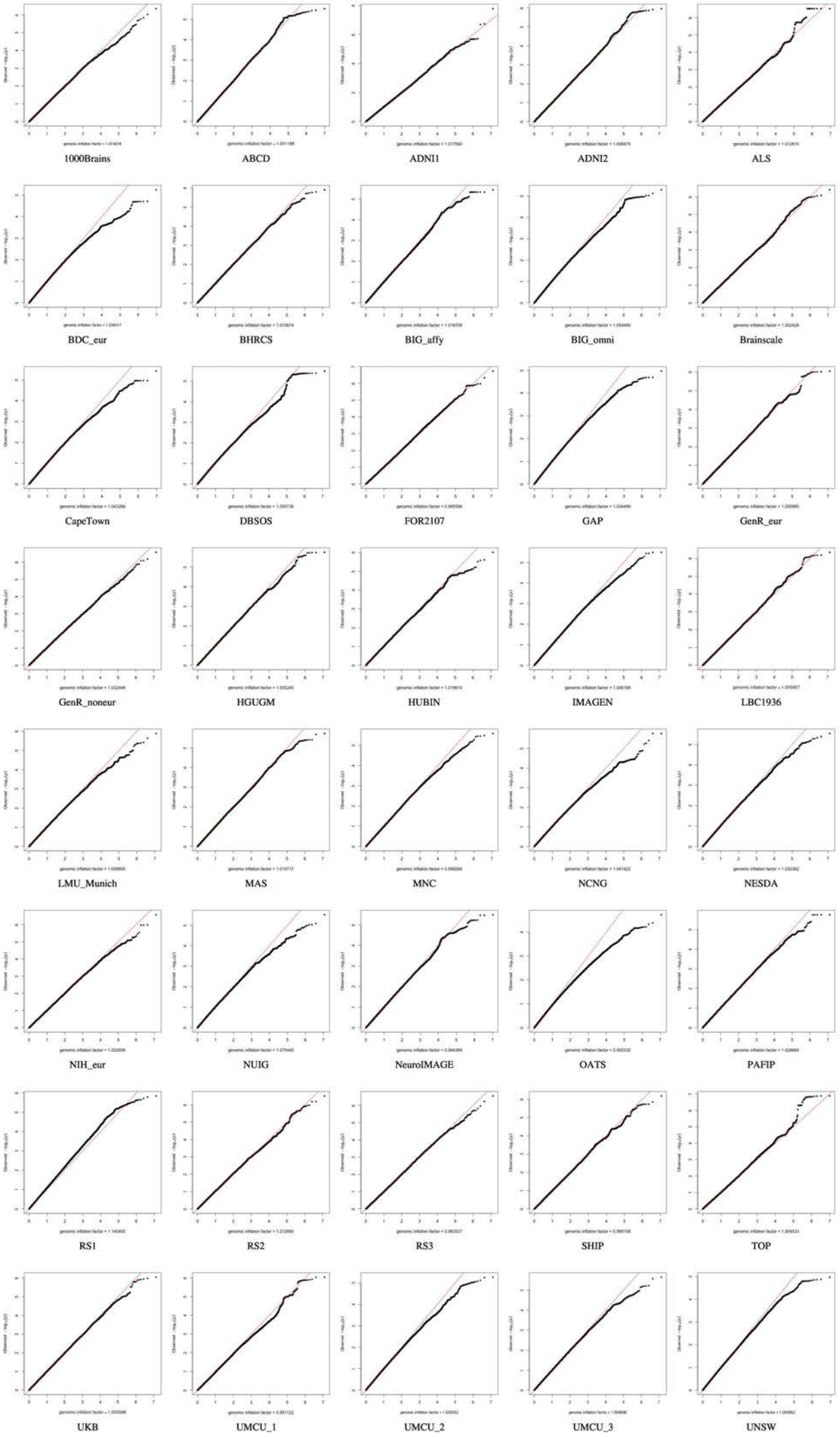

QQ plots Hippocampus

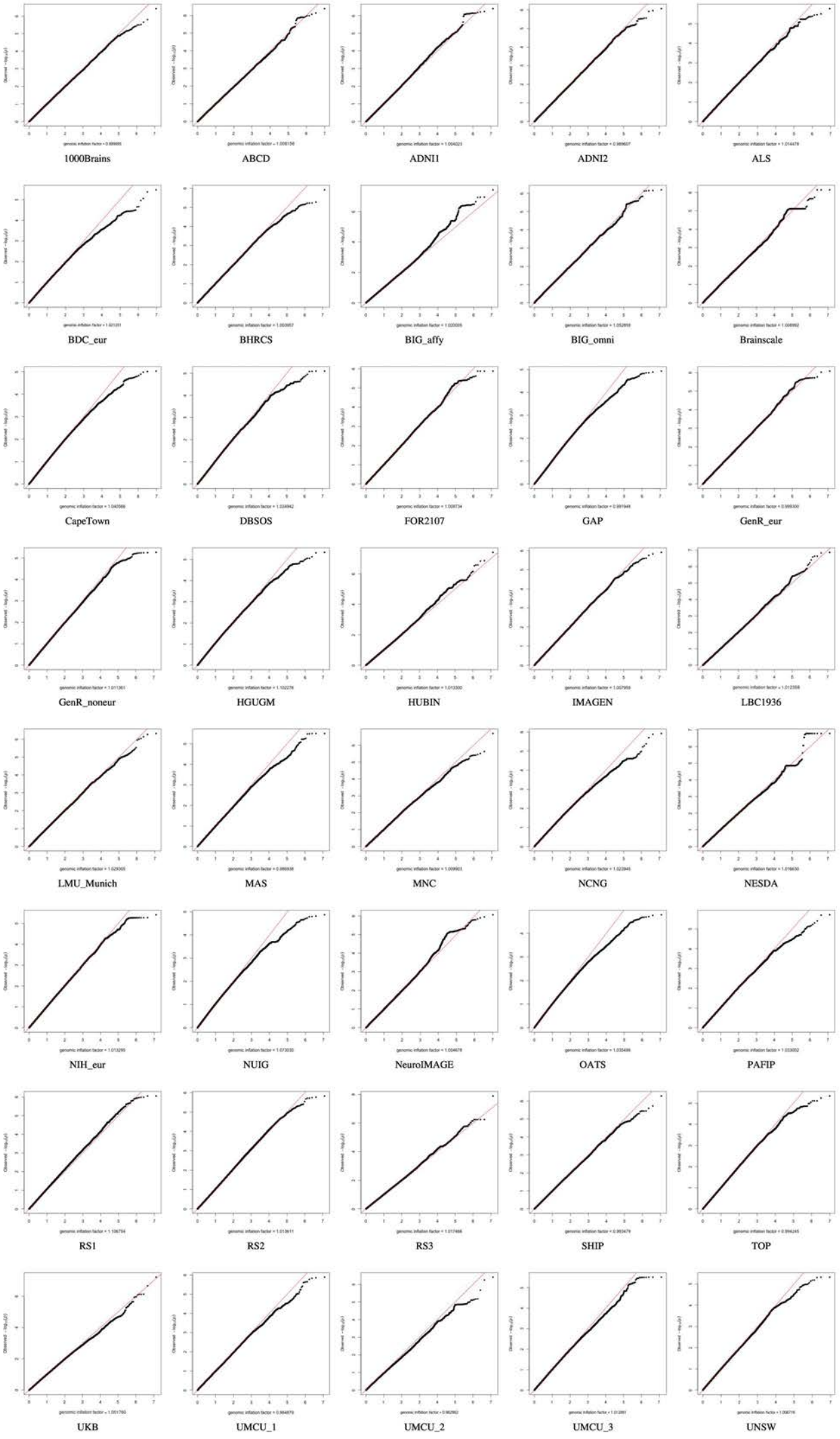

QQ plots Lateral Ventricles

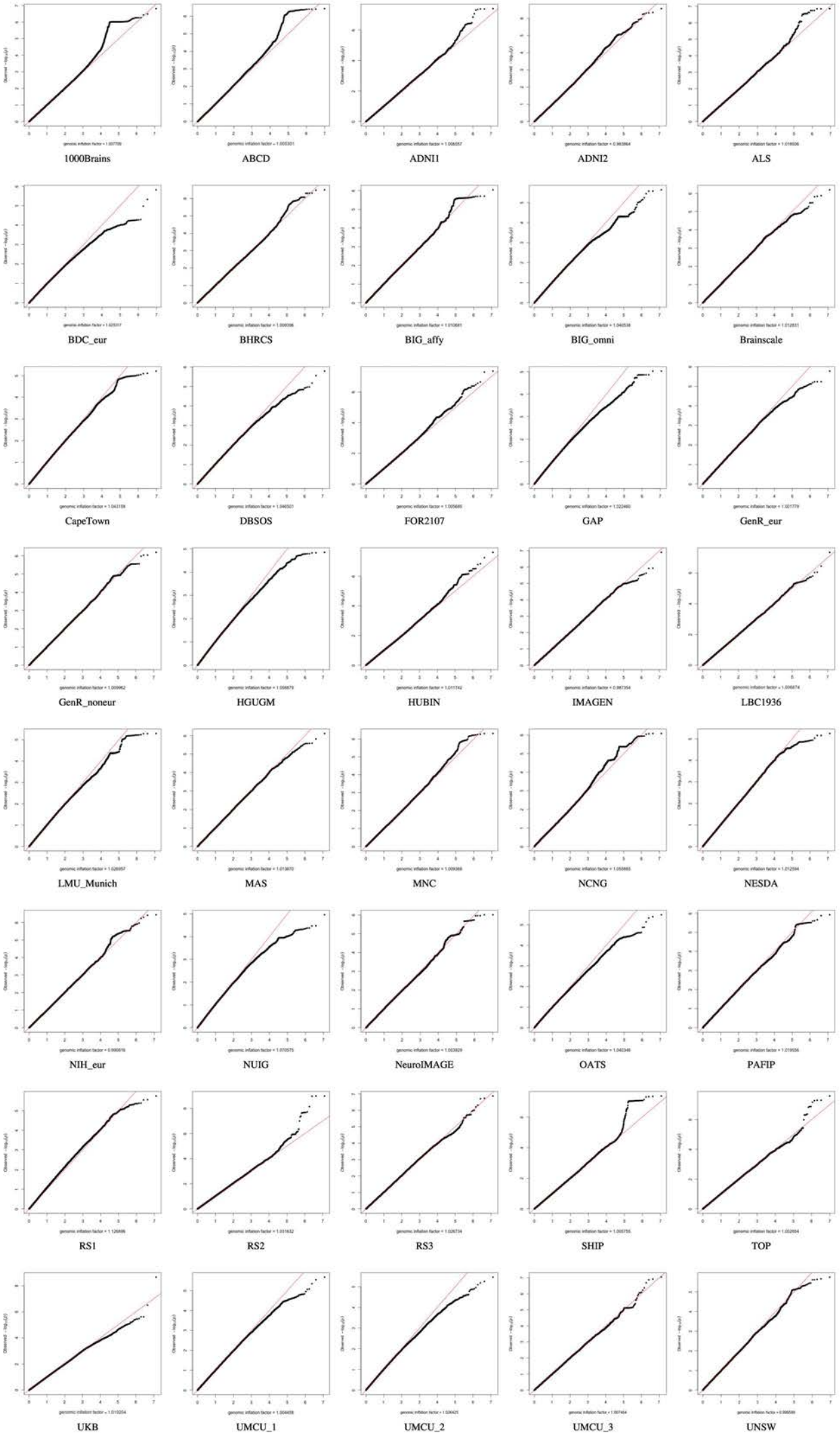

QQ plots Nucleus Accumbens

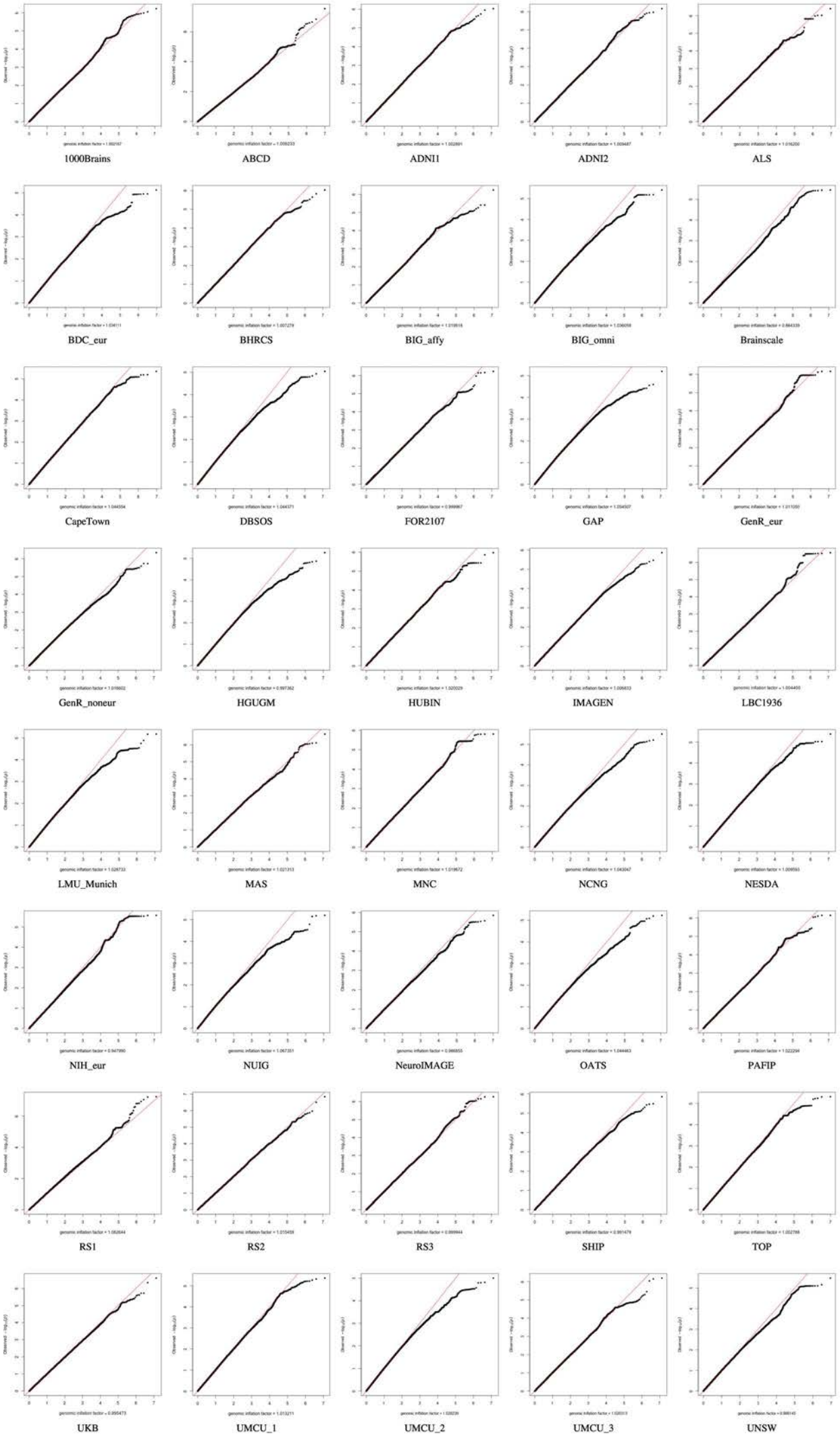

QQ plots Pallidum

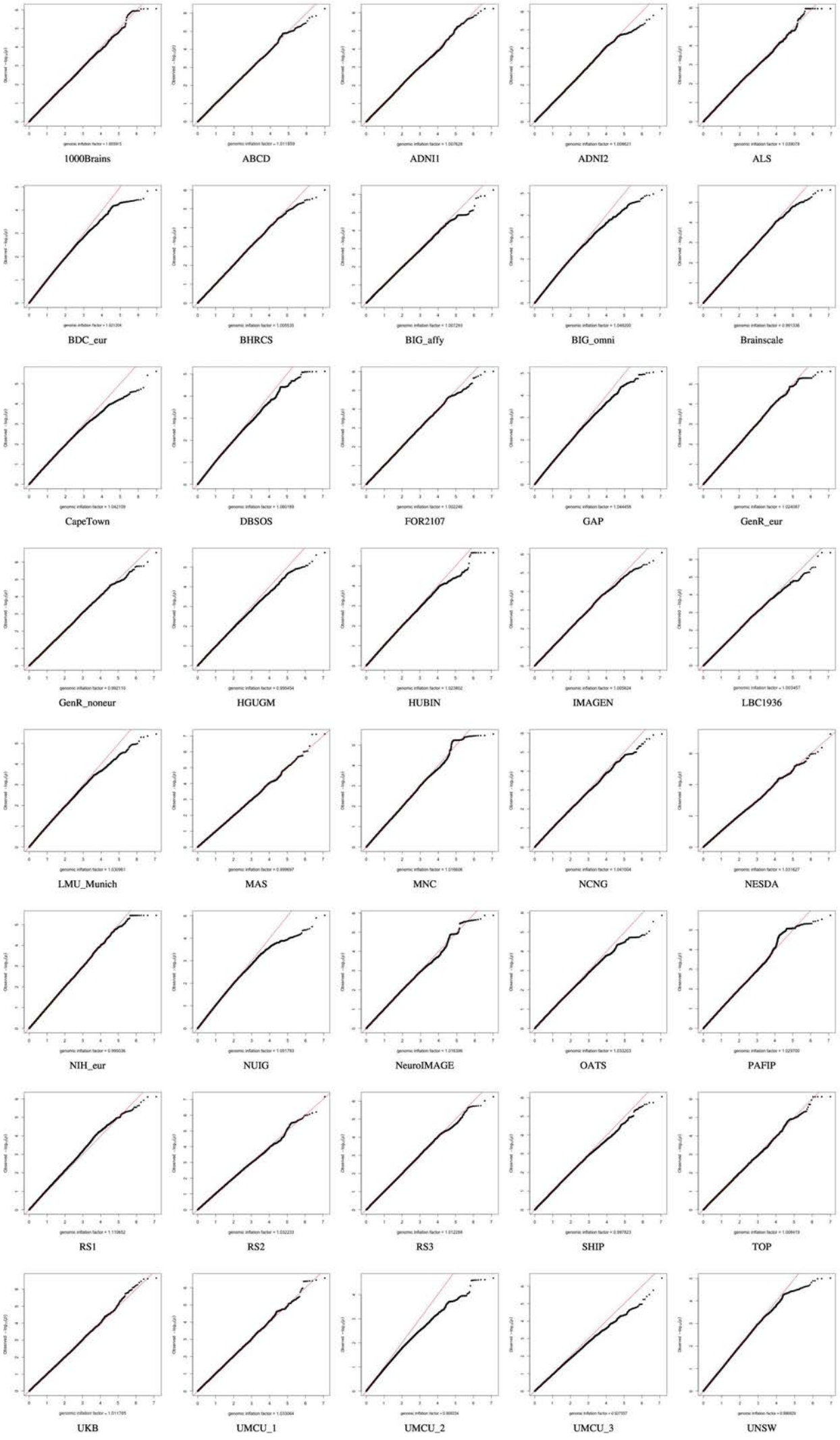

QQ plots Putamen

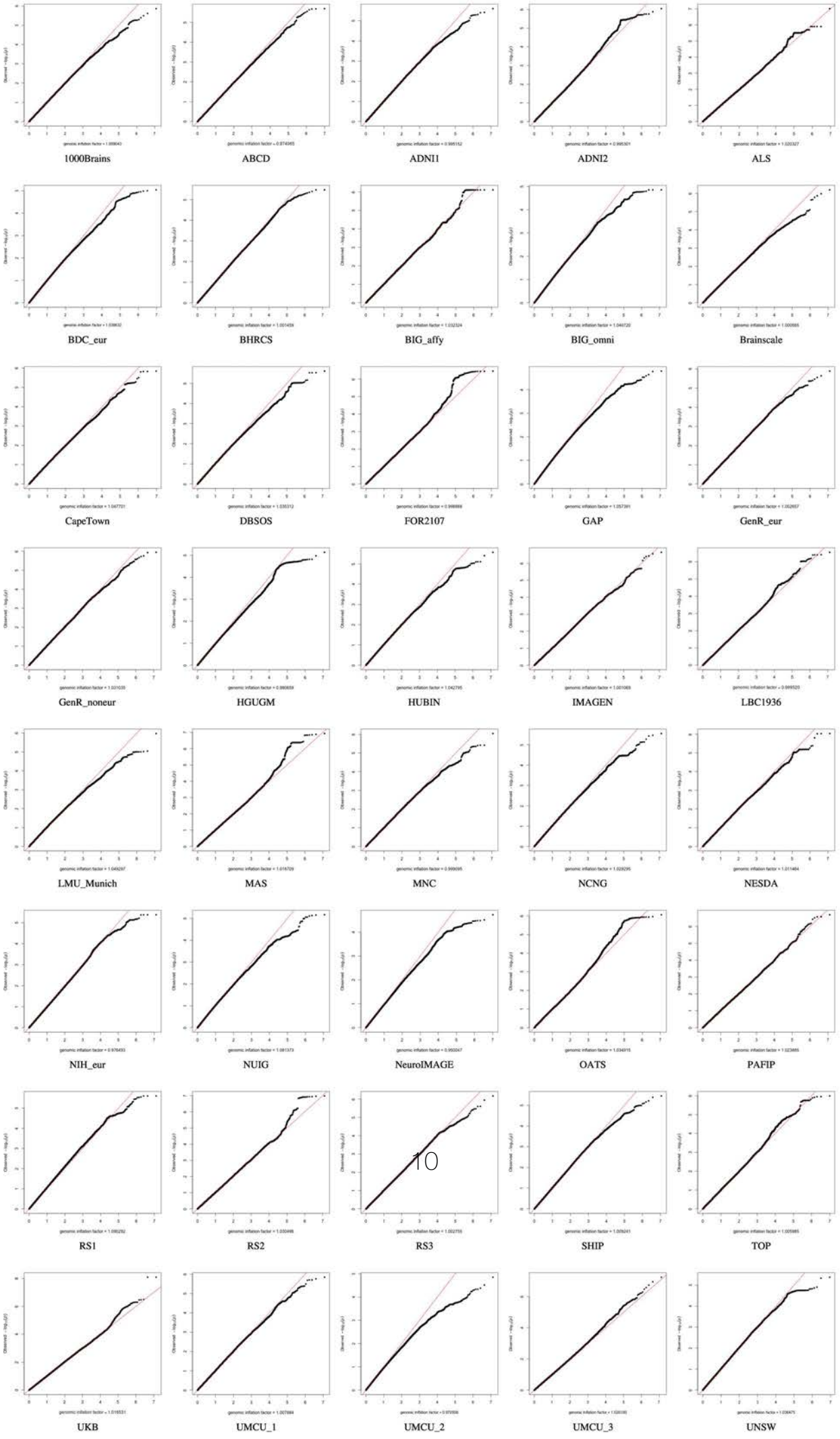

QQ plots Surface Area

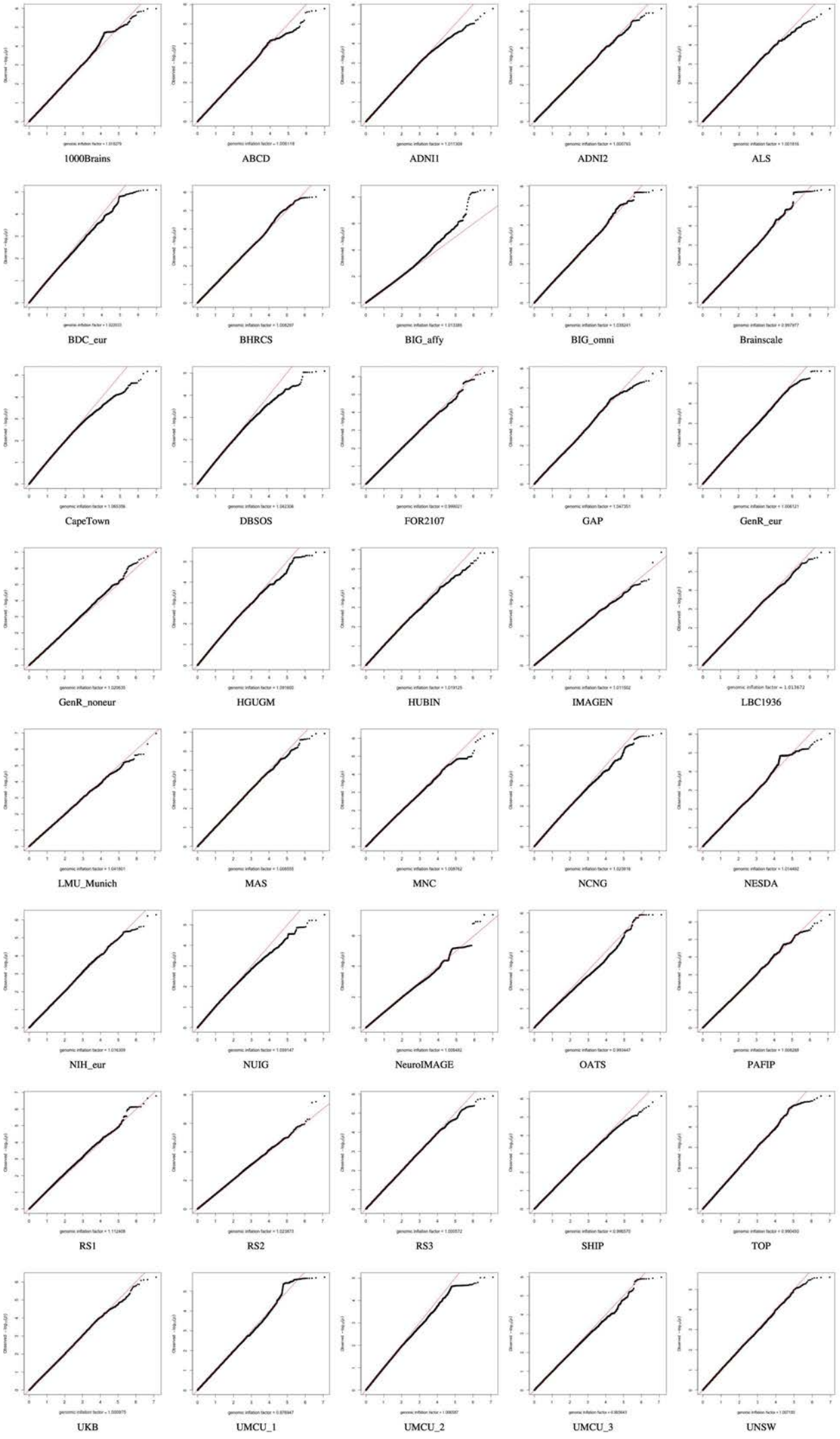

QQ plots Thalamus

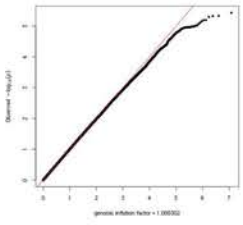
1000Brains

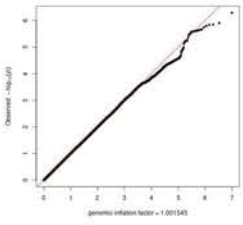
ABCD

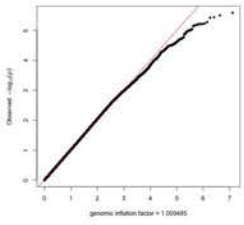
ADNI1

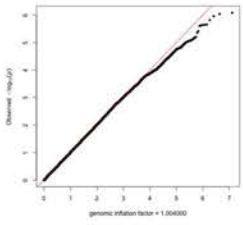
ADNI2

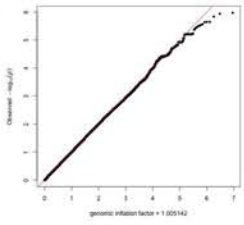
ALS

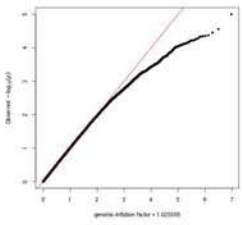
BDC_eur

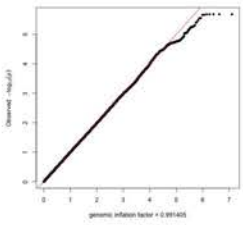
BHRCS

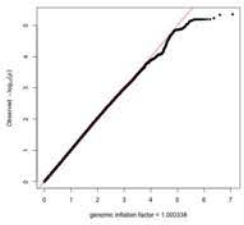
BIG_affy

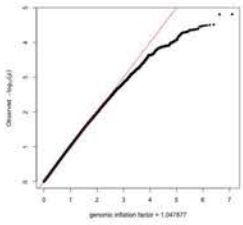
BIG_omni

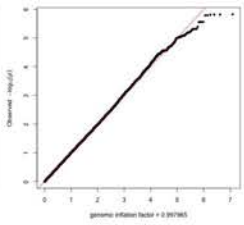
Brainscale

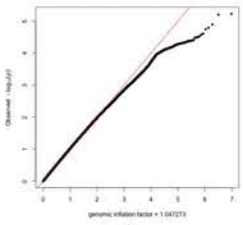
CapeTown

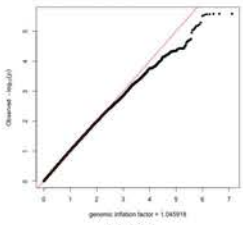
DBSOS

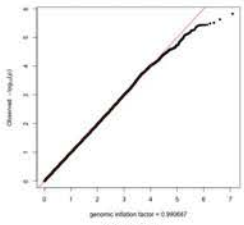
FOR2107

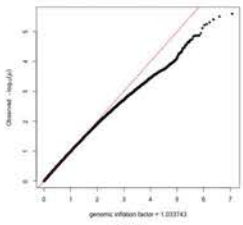
GAP

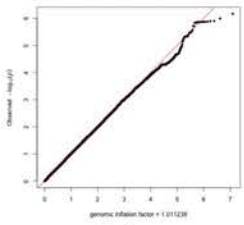
GenR_eur

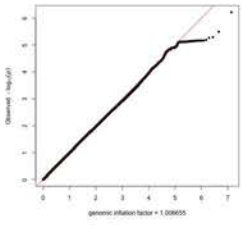
GenR_noneur

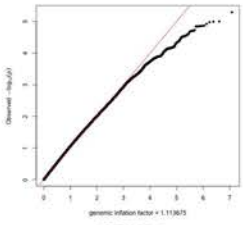
HGUGM

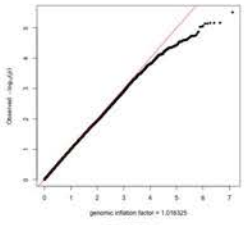
HUBIN

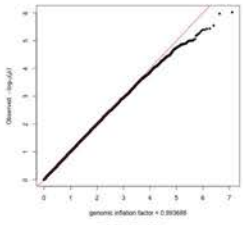
IMAGEN

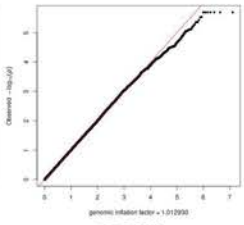
LBC1936

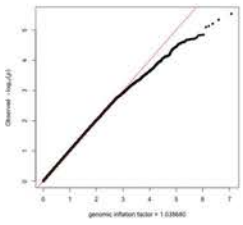
LMU_Munich

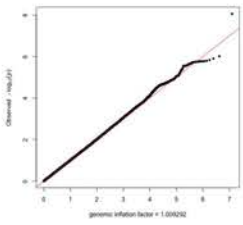
MAS

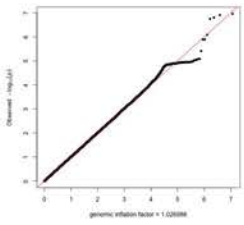
MNC

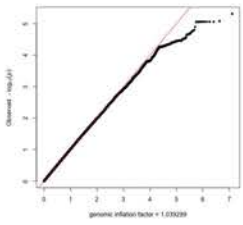
NCNG

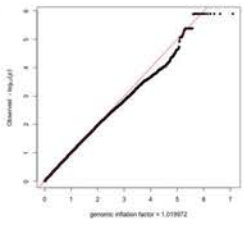
NESDA

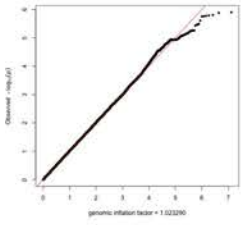
NIH_eur

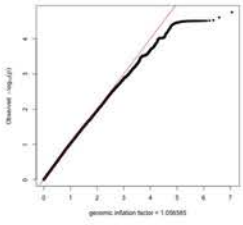
NUIG

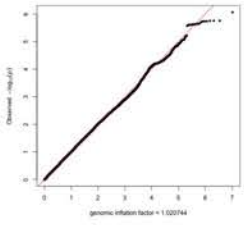
NeuroIMAGE

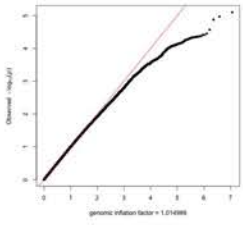
OATS

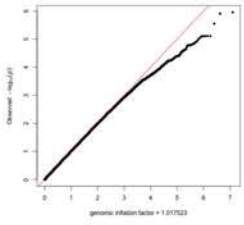
PAFIP

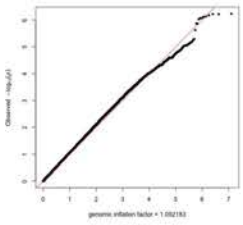
RS1

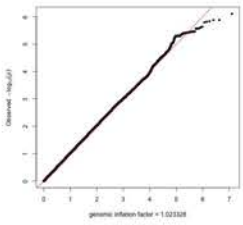
RS2

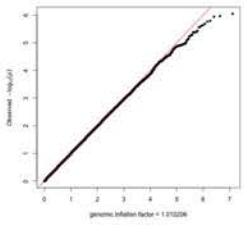
RS3

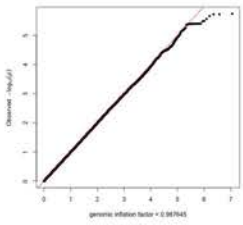
SHIP

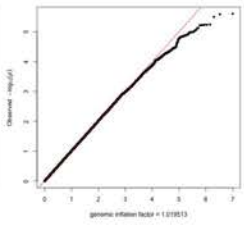
TOP

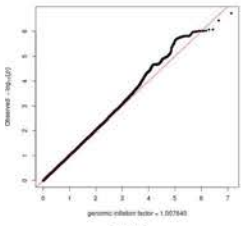
UKB

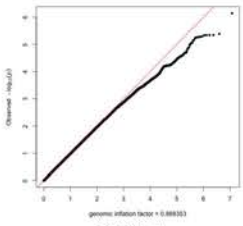
UMCU_1

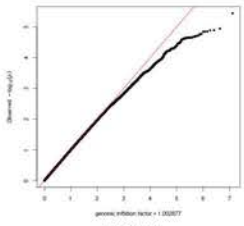
UMCU_2

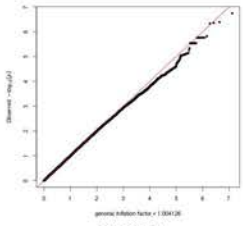
UMCU_3

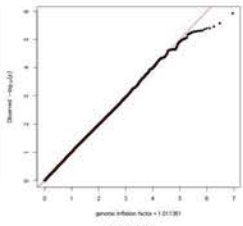
UNSW

QQ plots Total Brain